

NASA CR 166708

(NASA-CR-166708) A MODEL DESCRIBING THE
MICROWAVE EMISSION FROM A MULTI-LAYER
SNOWPACK AT 37 GHz (Kansas Univ. Center for
Research, Inc.) 136 p HC A07/MF A01

N82-11510

Unclas
01605

CSCL 08L G3/43

A MODEL DESCRIBING THE MICROWAVE EMISSION FROM A MULTI-LAYER SNOWPACK AT 37 GHz

Grant NSG 5335

FEBRUARY 1981

1. Report No. NASA CR-	2. Government Accession No.	3. Recipient's Catalog No.	
4. Title and Subtitle A MODEL DESCRIBING THE MICROWAVE EMISSION FROM A MULTI-LAYER SNOWPACK AT 37 GHz		5. Report Date February 1981	
		6. Performing Organization Code	
7. Author(s) M. Abdelrazik, F. Ulaby and H. Stiles		8. Performing Organization Report No. RSL TR 410-2	
9. Performing Organization Name and Address Remote Sensing Laboratory University of Kansas Center for Research, Inc. 2291 Irving Hill Drive - Campus West Lawrence, Kansas 66045		10. Work Unit No.	
		11. Contract or Grant No. NSG-5335	
12. Sponsoring Agency Name and Address NATIONAL AERONAUTICS AND SPACE ADMINISTRATION Goddard Space Flight Center Greenbelt, Maryland 20071		13. Type of Report and Period Covered Technical Report	
		14. Sponsoring Agency Code	
15. Supplementary Notes			
16. Abstract <p>In this study, a multi-layer emission model is described and applied to the measured emission from snow in an attempt to relate the absorption and scattering parameters of the snow medium to its density and wetness.</p> <p>The measured emission and ground-truth data used in this analysis were those collected during a 24-hour diurnal experiment conducted by Stiles and Ulaby (1980) on 2/17-2/18/77 in Steamboat Springs, Colorado. The emission measurements were acquired at 37 GHz and H-polarization using a microwave radiometer mounted atop a truck-mounted boom.</p> <p>The Tinga et al. (1973) mixing formula is used to calculate the dielectric constant of snow at 37 GHz. These values of the dielectric constant of snow along with the multi-layer emission model are used to estimate the absorption and scattering coefficients of snow at 37 GHz and their dependence on wetness. It is found that the scattering coefficient is comparable in value to the absorption coefficient for dry snow. However, the absorption coefficient increases linearly with increasing snow wetness while the scattering (contd.)</p>			
17. Key Words (Selected by Author(s)) Microwave remote sensing Microwave emission - snow Radiative transfer		18. Distribution Statement	
19. Security Classif. (of this report) Unclassified	20. Security Classif. (of this page) Unclassified	21. No. of Pages 133	22. Price

Abstract (contd.)

coefficient decreases linearly with increasing wetness.

The estimated values of the scattering and absorption coefficients are then used to calculate the emission from each layer of the snowpack throughout the diurnal experiment. It is shown that for dry snow, the ground underneath the snowpack contributes about 45% of all measured emission while the rest is due to emission from all the layers within the snowpack. However, when the wetness of the top 5 cm layer of the snowpack increases to 2% by volume, this top 5 cm snowlayer contributes more than 90% of all the measured emission.

TABLE OF CONTENTS

	<u>PAGE</u>
ACKNOWLEDGEMENT	iii
NOMENCLATURE.	iv
LIST OF FIGURES	vii
LIST OF TABLES.	xii
ABSTRACT.	xiii
1.0 INTRODUCTION.	1
2.0 DIELECTRIC PROPERTIES OF SNOW	2
2.1 Dielectric Properties of Water.	2
2.2 Dielectric Properties of Ice.	5
2.3 Dielectric Mixing Formulas.	9
2.4 Dielectric Constant of Dry Snow	18
2.5 Dielectric Constant of Wet Snow	18
2.6 Attenuation Through Snow.	21
3.0 EXPERIMENT DESCRIPTION AND RESULTS.	38
3.1 Description of Microwave Radiometer and Ground Truth Data.	38
3.2 Diurnal Variations of T_{ap} at 37 GHz	39
3.3 Ground Truth Diurnal Variations	41
3.4 Wetness Response.	48
3.5 Depth Response.	52
4.0 MULTILAYER EMISSION MODEL DEVELOPMENT AND TESTING	54
4.1 Development of the Multilayer Emission Model for Snow	54
4.2 Calculations of the Dielectric Constant and the Power Absorption Coefficient of Snow.	59
4.3 Emission Model for a Single Homogenous Snow Layer	65

	<u>PAGE</u>
4.4 Emission Model for a Multilayered Snowpack.	80
4.5 Multilayered Model for Snow with Split Top Layer. . . .	87
5.0 EVALUATION OF THE EMISSION MODELS AND THEIR RESULTS	96
5.1 Evaluation of the Models.	96
5.2 Evaluation of the Values of κ_a and κ_s Estimated by the Multilayered Snowpack Model	107
5.3 Total Emission from Each Snow Layer	110
6.0 CONCLUDING REMARKS.	116
REFERENCES.	118

ACKNOWLEDGMENT

This investigation was supported principally by NASA/Goddard Space Flight Center under Grant NSG-5335. Special thanks are due to the personnel of the Remote Sensing Laboratory for their suggestions and guidance throughout this research.

NOMENCLATURE

c	Velocity of Propagation, m/sec
d	Snow Depth, cm
F	Form Number
f	frequency, HZ
f_0	Relaxation frequency, HZ
K_0	Free Space Permittivity = 8.85×10^{-12} farad/m
K_s	Relative Dielectric Constant of Snow
K'_s	Real Part of the Dielectric Constant of Snow
K''_s	Imaginary Part of the Dielectric Constant of Snow
K_w	Relative Dielectric Constant of Water
K'_w	Real Part of the Dielectric Constant of Water
K''_w	Imaginary Part of the Dielectric Constant of Water
K_i	Relative Dielectric Constant of Ice
K'_i	Real Part of the Dielectric Constant of Ice
K''_i	Imaginary Part of the Dielectric Constant of Ice
K_{ds}	Dielectric Constant of Dry Snow
K_∞	Optical Limit of the Dielectric Constant
K_{dc}	Static Limit of the Dielectric Constant
L	Loss, dB
M_v	Snow Wetness, Percent Liquid Water by Volume
M_w	Weight Percentage of Liquid Water Contained in Snow
R_i	Radius of Ice Particle, mm.
R_w	Radius of Water Covered Ice Particle, mm
R_a	Radius of the Air Space, mm.

T, T_0	Snow Physical Temperature, $^{\circ}\text{K}$
T_B	Brightness Temperature, $^{\circ}\text{K}$
T_{ap}	Apparent Radiometric Temperature of a Target, $^{\circ}\text{K}$
T_{sc}	Scattered Temperature, $^{\circ}\text{K}$, Representing the Downward Emitted Sky Radiation Scattered by the Target in the Direction of the Antenna
T_{sky}	Downward Emitted Sky Radiation, $^{\circ}\text{K}$
T_G	Ground Contribution to T_B , $^{\circ}\text{K}$
T_g	Ground Physical Temperature, $^{\circ}\text{K}$
T_s	Snow Self-Emission Contribution to T_B , $^{\circ}\text{K}$
T_{se}	Snow Self-Emission of a Thin Layer, $^{\circ}\text{K}$
$\tan\delta$	Loss Tangent
W	Snow Water Equivalent, cm
α_a	Attenuation Constant (Field), nepers/cm
κ_1	Damping Coefficient, dB/m
κ_2	Damping Coefficient, dB/m
ϵ	Emissivity
θ	Angle of Incidence, Relative to Nadir, Degrees
θ'	Angle of Propagation, Relative to Nadir, Degrees
κ_e	Snow Extinction Coefficient (Power), nepers/cm
κ_a	Snow Absorption Coefficient (Power), nepers/cm
κ'_a	Snow Mass Absorption Coefficient (Power), nepers g/cm ²
κ'_s	Snow Mass Scattering Coefficient (Power), nepers g/cm ²
κ'_e	Snow Mass Extinction Coefficient (Power), nepers g/cm ²
λ	Wave Length, cm
ρ	Snow Density, g/cm ³
τ_{sa}	Snow-Air Power Transmission Coefficient
τ_{gs}	Ground-Snow Power Transmission Coefficient

τ_{na}	Power Transmission Coefficient from Layer #N, the Uppermost Layer of the Snowpack to Air
$\tau_{i(i+1)}$	Power Transmission Coefficient Across the Boundary Between the i^{th} Snow Layer and the Snow Layer Just Above It
τ_{gl}	Power Transmission Coefficient from the Ground to the Lowermost Snow Layer #1
τ	Relaxation Time of a Dipole, Seconds
r	Linear Correlation Coefficient
Δh	Thin Snow Thickness, cm
σ	Ionic Conductivity, mho/m
Δ	Absolute Fluctuation in Tap Measurement

LIST OF FIGURES

	<u>PAGE</u>
Figure 2-1	Relative Permittivity of Water at $T = 0^{\circ}\text{C}$ and $T = 20^{\circ}\text{C}$ Using Debye Equation. 6
Figure 2-2	Relative Permittivity of Water at $T = 10^{\circ}\text{C}$ and $T = 30^{\circ}\text{C}$ Using Debye Equation. 7
Figure 2-3	Rate of Attenuation in Water 8
Figure 2-4	Dielectric Properties of Ice 10
Figure 2-5	Loss Factor of Fresh Water Ice as a Function of Frequency. 12
Figure 2-6	Attenuation Curve (Tap-Water Ice) at 35.3 GHz. . . . 13
Figure 2-7	Measured and Calculated Brightness Temperatures of a 38-cm Thick Snow Field in the Morning and in the Afternoon. The Density and Temperature of Snow Were Known. The Wetness and Particle Size have Been Selected for Best Fit. 19
Figure 2-8	Variation of Attenuation with Snow Wetness at Selected Frequencies 23
Figure 2-9	Variation of Attenuation with Frequency at Selected Snow Wetness. 23
Figure 2-10	The Rate of Attenuation in Nep/cm as a Function of Snow Wetness and Frequency Calculated Using the Tinga et al. (1973) Mixing Formula for Snow Density of 0.21 g/cm^3 25
Figure 2-11	The Attenuation Through Snow as a Function of its Wetness as Calculated by Linlor's (1980) Empirical Formula and by the Tinga et al. (1973) Mixing Formula at 12 GHz and Snow Density of 0.21 g/cm^3 26
Figure 2-12	Absorption of Radiation by Snow as a Function of Temperature. 27
Figure 2-13	Measured Path Loss as a Function of Snow Thickness for Three Snow Conditions. 31
Figure 2-14	Measured Radiometric Emissivity Response to Dry Snow Water Equivalent at 37 GHz 33
Figure 2-15	Scattering, Absorption and Damping Coefficients for Dry Winter Snow. 36

	<u>PAGE</u>
Figure 2-16	Scattering, Absorption and Damping Coefficients for Dry Spring (Metamorphosed) Snow. 37
Figure 3-1	Apparent Temperature as a Function of Time at 37 GHz, H Polarization and for $\theta = 0^\circ$, 20° and 50°
Figure 3-2	Snow Wetness M_v as a Function of Time in the Top 15 cm of Snow. 42
Figure 3-3	Snow Thermometric Temperature and Wetness at 5:30 AM on 2/17/77. 44
Figure 3-4	Snow Thermometric Temperature and Wetness at 10:00 AM on 2/17/77. 45
Figure 3-5	Snow Thermometric Temperature and Wetness at 1800 Hours on 2/17/77 46
Figure 3-6	Snow Thermometric Temperature and Wetness at 6:45 AM on 2/18/77. 47
Figure 3-7	Tap Response to Snow Wetness M_v , Showing the Hysteresis Effect at $\theta = 0^\circ$ 49
Figure 3-8	Tap Response to Snow Wetness M_v , Showing the Hysteresis Effect at $\theta = 20^\circ$ 50
Figure 3-9	Tap Response to Snow Wetness M_v , Showing the Hysteresis Effect at $\theta = 50^\circ$ 51
Figure 3-10	Radiometric Apparent Temperature Response to Snow Water Equivalent at 37 GHz 53
Figure 4-1	The Real Part of the Dielectric Constant of Snow k'_s , as a Function of M_v , the Percentage Wetness by Volume of Snow as Calculated by Tinga et al. (1973) Mixing Formula. 62
Figure 4-2	The Imaginary Part of the Dielectric Constant of Snow k''_s , as a Function of M_v , the Percentage Wetness by Volume of Snow as Calculated by Tinga et al. (1973) Mixing Formula 63
Figure 4-3	A Linear Fit for the Calculated Loss Factor Using the Tinga et al. (1973) Mixing Formula at 0.1% and 0.2% Wetness by Volume. The Fit is Extended to Predict a Value of k''_s for Dry Snow 64
Figure 4-4	κ_a in Nep/cm as a Function of M_v , the Percentage Wetness by Volume of Snow. 67

	<u>PAGE</u>
Figure 4-5	τ_{sa} , the Power Transmission Coefficient at the Snow-Air Boundary as a Function of M_v , the Percentage Wetness by Volume of Snow at $\theta = 0^\circ$ 72
Figure 4-6	τ_{sa} , the Power Transmission Coefficient at the Snow-Air Boundary as a Function of M_v , the Percentage Wetness by Volume of Snow at $\theta = 20^\circ$ 73
Figure 4-7	τ_{sa} , the Power Transmission Coefficient at the Snow-Air Boundary as a Function of M_v , the Percentage Wetness by Volume of Snow at $\theta = 50^\circ$ 74
Figure 4-8	κ_a , κ_s and κ_e as a Function of Snow Wetness as Predicted by the Single Homogeneous Snowlayer Model . . . 76
Figure 4-9	Observed T_{ap} and T_B Predicted by the Single Homogeneous Snowlayer Model as a Function of Time at $\theta = 0^\circ$ 77
Figure 4-10	Observed T_{ap} and T_B Predicted by the Single Homogeneous Snowlayer Model as a Function of Time at $\theta = 20^\circ$ 78
Figure 4-11	Observed T_{ap} and T_B Predicted by the Single Homogeneous Snowlayer Model as a Function of Time at $\theta = 50^\circ$
Figure 4-12	A Geometrical Presentation of the Snowpack Cross Section During the 2/17/77 - 2/18/77 Diurnal Experiment 81
Figure 4-13	κ_a , κ_s and κ_e for Snow as a Function of Snow Wetness at 37 GHz Estimated by the Multilayered Emission Model. 83
Figure 4-14	Observed T_{ap} and T_B Predicted by the Multilayered Emission Model as a Function of Time at $\theta = 0^\circ$. . . 84
Figure 4-15	Observed T_{ap} and T_B Predicted by the Multilayered Emission Model as a Function of Time at $\theta = 20^\circ$. . . 85
Figure 4-16	Observed T_{ap} and T_B Predicted by the Multilayered Emission Model as a Function of Time at $\theta = 50^\circ$. . . 86
Figure 4-17	A Geometrical Presentation of the Revised Snowpack Cross Section During the 2/17/77 - 2/18/77 Diurnal Experiment. The Top 5 cm Layer is Shown Split into Two 2.5 cm Sublayers 89

Figure 4-18	Percentage Wetness by Volume M_v Curves for the Top 2.5 cm Snow Layers Along With the Original 5 cm Snow Layer Wetness Curve of the 2/17/77 - 2/18/77 Diurnal Experiment. The Top 2.5 cm Layer is Seven Times as Wet as the Original 5 cm Layer in the Melting Stage While the Lower 2.5 cm Layer is Seven Times as Wet as the Original 5 cm Layer in the Refreezing Stage.	91
Figure 4-19	The Observed T_{ap} and the Predicted T_B as Calculated by the Multilayered Emission Model with Split Top Layer at $\theta = 0^\circ$. The Uppermost Sublayer is 2.5 cm Thick and Seven Times as Wet as the Original 5 cm Top Snow Layer.	92
Figure 4-20	The Observed T_{ap} and the Predicted T_B as Calculated by the Multilayered Emission Model with Split Top Layer at $\theta = 20^\circ$. The Uppermost Sublayer is 2.5 cm Thick and Seven Times as Wet as the Original 5 cm Top Snowlayer.	93
Figure 4-21	The Observed T_{ap} and the Predicted T_B as Calculated by the Multilayered Emission Model with Split Top Layer at $\theta = 50^\circ$. The Uppermost Sublayer is 2.5 cm Thick and Seven Times as Wet as the Original 5 cm Top Snowlayer	94
Figure 5-1	Linear Correlation Coefficient Between the Predicted T_B as Calculated by the Single Homogeneous Layer Snowpack Model at $\theta = 0^\circ$ and the T_{ap} Observed	98
Figure 5-2	Linear Correlation Coefficient Between the Predicted T_B as Calculated by the Single Homogeneous Layer Snowpack Model at $\theta = 20^\circ$ and the T_{ap} Observed.	99
Figure 5-3	Linear Correlation Coefficient Between the Predicted T_B as Calculated by the Single Homogeneous Layer Snowpack Model at $\theta = 50^\circ$ and the T_{ap} Observed.	100
Figure 5-4	Linear Correlation Coefficient Between the Predicted T_B as Calculated by the Multilayered Snowpack Model at $\theta = 0^\circ$ and the T_{ap} Observed.	101
Figure 5-5	Linear Correlation Coefficient Between the Predicted T_B as Calculated by the Multilayered Snowpack Model at $\theta = 20^\circ$ and the T_{ap} Observed	102
Figure 5-6	Linear Correlation Coefficient Between the Predicted T_B as Calculated by the Multilayered Snowpack Model at $\theta = 50^\circ$ and the T_{ap} Observed	103

	<u>PAGE</u>
Figure 5-7	Linear Correlation Coefficient Between the Predicted T_B as Calculated by the Multilayered Snowpack with The Split Top Layer and the T_{ap} Observed at $\theta = 0^\circ$. New Uppermost Layer is 2.5 cm in Thickness and Seven Times as Wet as the Original 5 cm Top Snow Layer.104
Figure 5-8	Linear Correlation Coefficient Between the Predicted T_B as Calculated by the Multilayered Snowpack with the Split Top Layer and the T_{ap} Observed at $\theta = 20^\circ$. New Uppermost Layer is 2.5 cm in Thickness and Seven Times as Wet as the Original 5 cm Top Snow Layer.105
Figure 5-9	Linear Correlation Coefficient Between the Predicted T_B as Calculated by the Multilayered Snowpack with the Split Top Layer and the T_{ap} Observed at $\theta = 50^\circ$. New Uppermost Layer is 2.5 cm in Thickness and Seven Times as Wet as the Original 5 cm Top Snow Layer . . .106
Figure 5-10	T_B Calculated From an Undisturbed Snowpack as a Function of W for One Layered Snowpack at $\theta = 27^\circ$ Using the κ_a , κ_s and κ_e Calculated in This Study . . .111
Figure 5-11	T_B Calculated From an Undisturbed Snowpack as a Function of W for a Single Layer Snowpack at $\theta = 57^\circ$ Using the κ_a , κ_s and κ_e Calculated in the Study. .112
Figure 5-12	T_B as a Function of κ_e' for a Snowpack of One Homogeneous Layer at Nadir. The Snow Depth is 30 cm and Snow Temperature is 262.33°K113
Figure 5-13	The Percentage Contribution of Each Layer Within the Snowpack as a Function of Time115

LIST OF TABLES

		<u>PAGE</u>
Table 2-1	Relaxation Frequency of Water f_0 at Different Temperatures.	4
Table 2-2	Relative Dielectric Constants of Ice at 35.3 GHz as Reported by Perry and Straiton (1972).	11
Table 2-3	Mixing Formulas	15
Table 2-4	Dielectric Constant at Dry Snow at 37 GHz as Reported by Edgerton et al. (1971)	20
Table 2-5	Loss Caused by Snow and Ice at 35.26 GHz.	28
Table 2-6	Loss Measurements at 35 GHz	29
Table 2-7	Values of A, B, κ_e , κ_a and κ_s Generated by Fitting the Experimental Values of ϵ at 37 GHz to Equation 2-11.	34
Table 3-1	Snow Thermometric Temperature in $^{\circ}\text{K}$ for Different Depths Within the Snowpack on 2/17/77 - 2/18/77	43
Table 4-1	The Dielectric Constant of Snow as a Function of the Percentage Wetness by Volume of Snow at 37 GHz Calculated by the Tinga et al. (1973) Mixing Formula. .	61
Table 4-2	Values of κ_a in Nep/cm as a Function of Snow Wetness. .	66
Table 5-1	The Residual Sum of Squares Analyses Conducted for all the Models Developed and at $\theta = 0^{\circ}$, 20° and 50° . .	97
Table 5-2	Values of κ_a , κ_s and κ_e for Dry Snow as a Function of θ Calculated Using Stiles and Ulaby (1980) Model, the Multilayered Snowpack Emission Model and the Hofer and Matzler (1980) Model.	109

**A MODEL DESCRIBING THE MICROWAVE EMISSION
FROM A MULTI-LAYER SNOWPACK AT 37 GHz**

**M. Abdelrazik
Remote Sensing Laboratory
University of Kansas Center for Research, Inc.
Lawrence, Kansas 66045**

ABSTRACT

In this study a multi-layer emission model is described and applied to the measured emission from snow in an attempt to relate the absorption and scattering parameters of the snow medium to its density and wetness.

The measured emission and ground truth data used in this analysis were those collected during a 24-hour diurnal experiment conducted by Stiles and Ulaby (1980) on 2/17 - 2/18/77 in Steamboat Springs, Colorado. The emission measurements were acquired at 37 GHz and H-polarization using a microwave radiometer mounted atop a truck-mounted boom.

The Tinga et al. (1973) mixing formula is used to calculate the dielectric constant of snow at 37 GHz. These values of the dielectric constant of snow along with the multi-layer emission model are used to estimate the absorption and scattering coefficients of snow at 37 GHz and their dependence on wetness. It is found that the scattering coefficient is comparable in value to the absorption coefficient for dry snow. However, the absorption coefficient increases linearly with increasing snow wetness while the scattering coefficient decreases linearly with increasing wetness.

The estimated values of the scattering and absorption coefficients are then used to calculate the emission from each layer of the snowpack throughout the diurnal experiment. It is shown that for dry snow, the ground underneath the snowpack contributes about 45% of all measured emission while the rest is due to emission from all the layers within the snowpack. However, when the wetness of the top 5 cm layer of the snowpack increases to 2% by volume, this top 5 cm snowlayer contributes more than 90% of all the measured emission.

1.0 INTRODUCTION

During the Winter of 1977, an experimental program was conducted at a test site near Steamboat Springs, Colorado involving microwave measurements of snowpacks (Stiles and Ulaby, 1980). Among the investigations conducted was an experiment consisting of a 37 GHz passive microwave measurement over a 24 hour diurnal period. In conjunction with the microwave measurements, several snow parameters were recorded which include snow wetness, snow thermometric temperature and snow density at several depths in the snowpack.

The purpose of this study is to apply a multi-layer emission model to the measured emission from snow in an attempt to relate the absorption and scattering parameters of the snow medium to density and wetness.

Chapter ³~~2~~ covers a brief description of the diurnal experiment reported by Stiles and Ulaby (1980) and reviews relevant results obtained in other parts of the same investigation.

The development and applications of the microwave emission model are given in Chapter 4. Results estimated by the different models for the scattering and absorption coefficients of snow at 37 GHz are shown.

In Chapter 5, an evaluation of the different models which were developed is shown. A comparison between scattering and absorption coefficients estimated in this study and those reported in the literature is also provided.

Finally Chapter 6 summarizes the findings of this study and the errors involved in the development and application of the model.

2.0 DIELECTRIC PROPERTIES OF SNOW

Snow is a mixture of ice, water and air. The absorption, emission and scattering of an electromagnetic wave by snow are governed by the geometrical and electrical (dielectric) properties of the snow medium. The relative dielectric constant of snow, K_s , is in general a function of:

- (a) Microwave frequency;
- (b) Percentage volume of ice;
- (c) Percentage volume of air;
- (d) Percentage volume of free water;
- (e) Snow thermometric temperature;
- (f) Crystal size and structure of the snow medium; and
- (g) Presence of impurities.

As will be seen in the next sections, the percentage of free water in a volume of snow has the strongest effect of all of the above parameters on the value of K_s . The dielectric properties of water and ice which constitute, along with air, the snow medium will be examined first, followed by an examination of the dielectric and attenuation properties of dry and wet snow at 37 GHz.

2.1 Dielectric Properties of Water

The dielectric constant of water in the microwave region is governed by the Debye equation:

$$K_w = K_\infty + \frac{K_{dc} - K_\infty}{1 - j2\pi\tau f} + j \frac{\sigma}{2\pi K_0 f} \quad (2-1)$$

where

K_w = Complex relative dielectric constant of water, $K_w =$

$$K'_w - jK''_w$$

K_∞ = Optical limit of dielectric constant

K_{dc} = Static limit of dielectric constant

τ = Relaxation time of the water molecule dipole

K_0 = Permittivity of free space

σ = Ionic conductivity

f = frequency in Hertz

The real and imaginary parts resulting from the previous equation are

$$K'_w = K_\infty + \frac{K_{dc} - K_\infty}{1 + (2\pi f\tau)^2} \quad (2-2a)$$

$$K''_w = \frac{(2\pi f\tau)(K_{dc} - K_\infty)}{1 + (2\pi f\tau)^2} + \frac{\sigma}{2\pi K_0 f} \quad (2-2b)$$

The Debye equation shows a single resonance phenomena at the relaxation frequency f_0 given by:

$$f_0 = \frac{1}{2\pi\tau} \quad (2-3)$$

The relaxation frequency is temperature dependent as shown in Table 2-1 and is located in the microwave region. The limiting values on the equations for dielectric constant are

TABLE 2-1

Relaxation Frequency of Water f_0 at
Different Temperatures (Royer, 1973)

$T(^{\circ}\text{C})$	$f_0(\text{GHz})$
0	8.5
10	11.7
20	15.8
30	21.2
40	27.0
50	33.9

$$K'_W \approx K_{dc} \quad \text{for } f \ll f_0 \quad (2-4a)$$

$$K''_W \approx (K_{dc} - K_{\infty}) / (2\pi\tau f) \quad \text{for } f \ll f_0 \quad (2-4b)$$

$$K'_W \approx K_{\infty} \quad \text{for } f \gg f_0 \quad (2-5a)$$

$$K''_W \approx (K_{dc} - K_{\infty}) / (2\pi\tau f) \quad \text{for } f \gg f_0 \quad (2-5b)$$

Figures 2.1 and 2.2 show the real and imaginary parts of the dielectric constant of water as a function of frequency and for different water temperatures. These curves were calculated by Royer (1973) using regression fits to obtain the values of K'_W and K''_W for several experimenters' data. The rate of attenuation in water is shown in Figure 2-3. It is seen that water is a very lossy medium throughout the microwave region. This loss is due to the fact that the relaxation frequency (f_0) is located in the microwave region. The attenuation of water at 37 GHz is between 1.5×10^4 dB/meter and 2.0×10^4 dB/meter depending on the temperature of the water. Because the dielectric constant of water is much larger than those of ice and air, small amounts of free water appearing in a snow medium can drastically alter the real and imaginary parts of the dielectric constant of snow and therefore change its emission, scatter and attenuation behavior.

2.2 Dielectric Properties of Ice

The dielectric constant of ice, like water, is governed by the Debye Equation 2-1. However the water molecules in ice are bound, and therefore not as mobile as those of free water. This results in a relaxation frequency for ice that is much lower than that of water

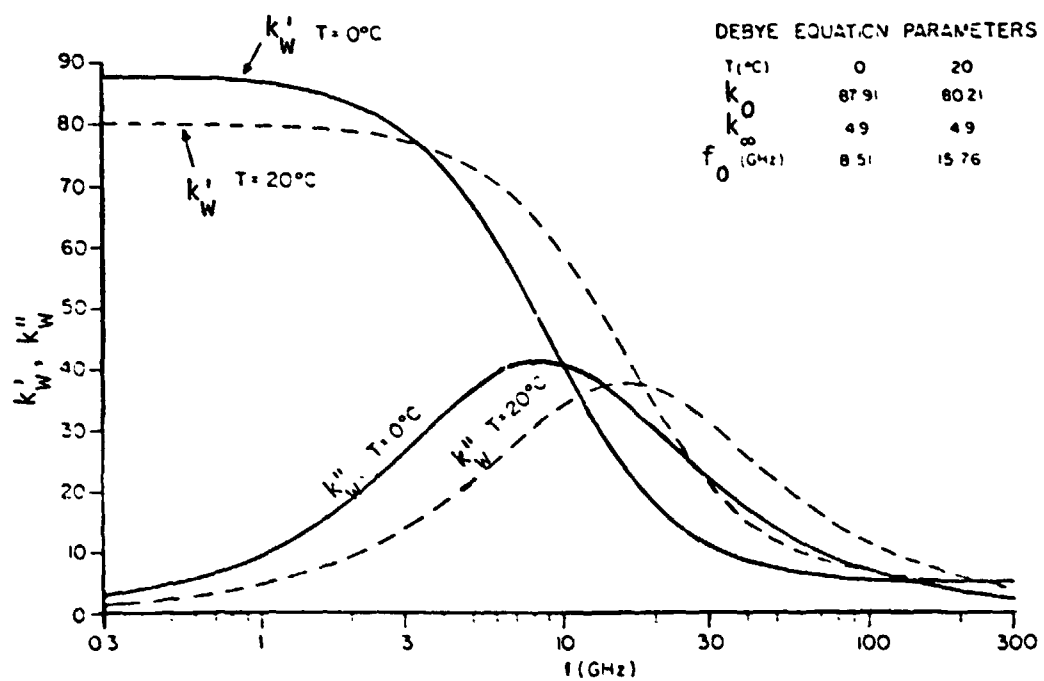


Figure 2-1 Relative Permittivity of Water at $T = 0^\circ \text{C}$ and $T = 20^\circ \text{C}$ Using Debye Equation (Royer, 1973).

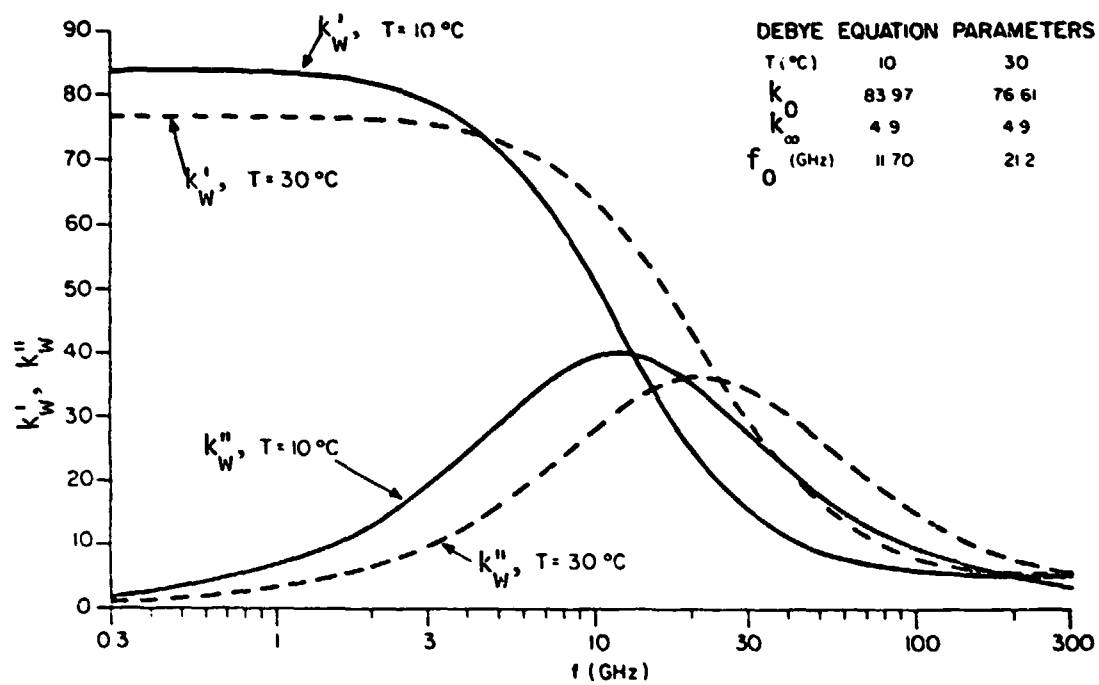


Figure 2-2 Relative Permittivity of Water at $T = 10^\circ \text{C}$ and $T = 30^\circ \text{C}$ Using Debye Equation (Royer, 1973).

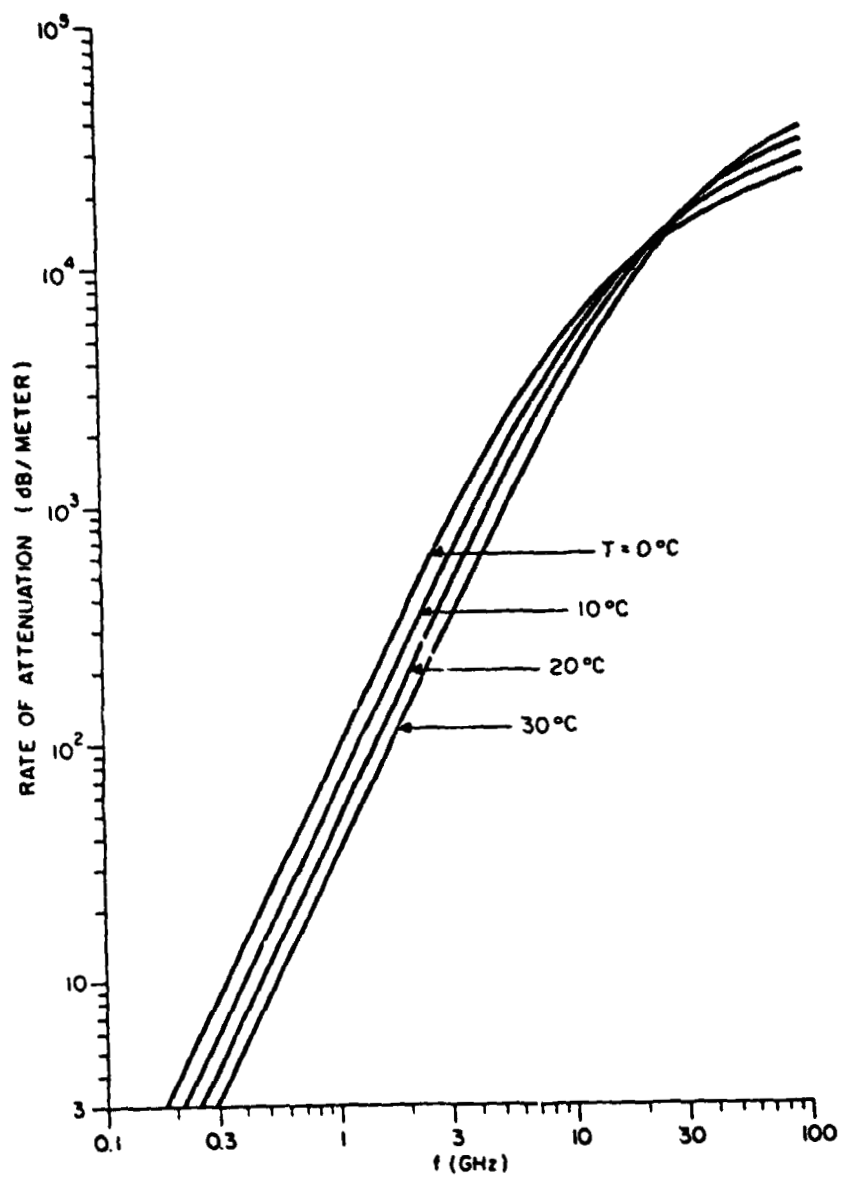


Figure 2-3 Rate of Attenuation in Water (Royer, 1973).

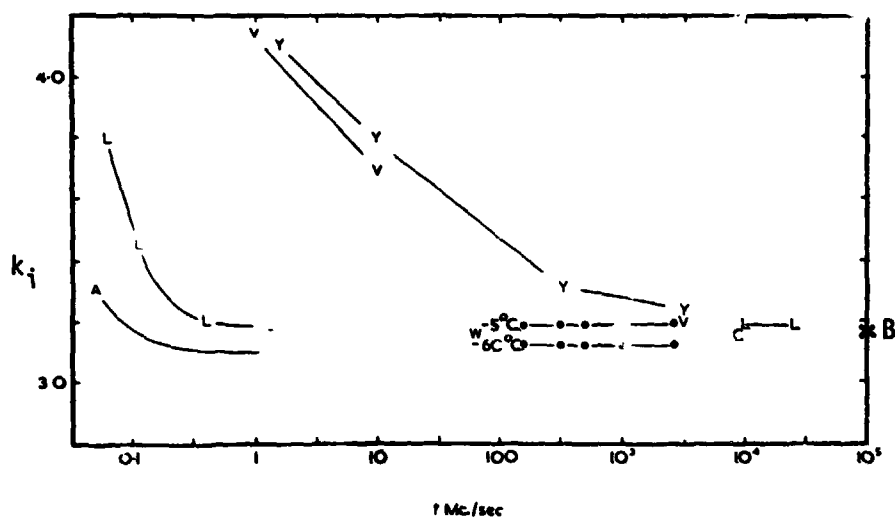
and is of the order of 10 KHz (Evans, 1965). The optical limit is therefore easily satisfied for the Debye equation and the real and imaginary parts of the dielectric constant of ice are given by equations (2-5a) and (2-5b).

Measurements up to 183 GHz indicate that the real part of the dielectric constant of ice is approximately 3.17 in the microwave region and is independent of frequency and temperature as shown in Figure 2-4 (Evans, 1965). The imaginary part was found to be temperature dependent at a frequency of 10 GHz showing a sharp increase near 0°C (Lamb and Turney, 1949). Measurements of the dielectric constant of ice are shown in Figure 2-4. Above 24 GHz, the dielectric constant measurements for ice are limited to the results of Perry and Straiton (1972). Table 2-2 shows their results at 35.3 GHz. These data are suspected to be in error (Gough, 1972) since they are anomalously different from both lower and higher frequency data. However Hallikainen (1977) used the results shown for the loss tangent in Figure 2-4 to calculate an average value for the loss factor of ice as a function of frequency. His results are shown in Figure 2-5.

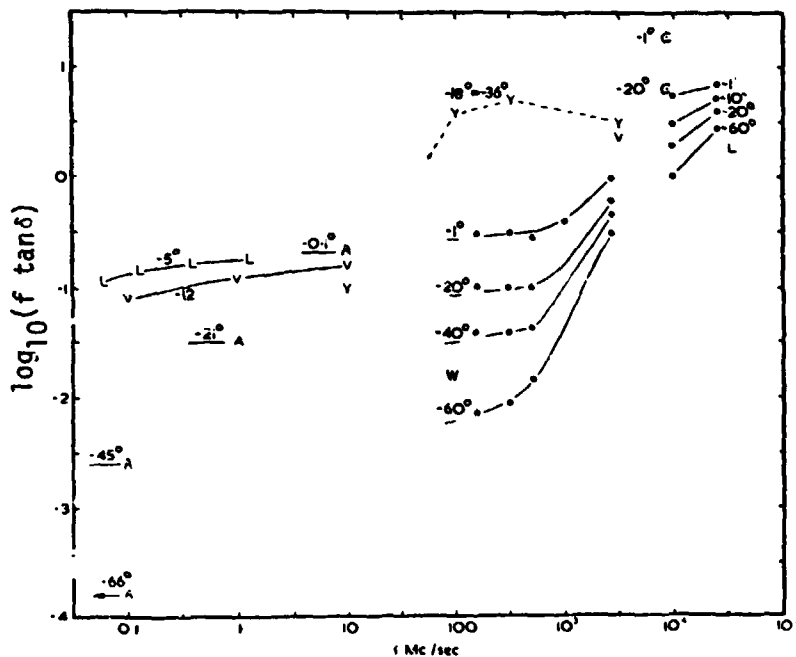
The rate of attenuation of tap-water ice in dB for different ice thickness at 35.3 GHz was also reported by Perry and Straiton (1972) and is shown in Figure 2-6.

2.3 Dielectric Mixing Formulas

Since snow is a mixture of ice, water and air, the varying volumetric properties of these components in snow make the dielectric properties of snow difficult to examine. In addition, the structure of snow is a significant factor in determining its dielectric properties.



Relative permittivity of ice (ordinates) versus logarithm of radio-frequency (abscissae).



Loss tangent of ice versus radio frequency. The quantity plotted vertically is $\log_{10}(f \tan \delta)$ where f is the frequency in mc/sec. On the high-frequency tail of a relaxation spectrum this quantity is constant: it has the further useful property that the attenuation of a radio wave (measured in dB/m) passing through the medium is directly proportional to $f \tan \delta$. Temperatures are marked in $^{\circ}\text{C}$.

- L: Lamb (1946) and Lamb and Turney (1949) -5°C at low frequencies, 0° to -190°C at high frequencies: distilled water.
- C: Cumming (1952) Distilled water, tap water, and melted snow (no observable difference)
- A: Auty and Cole (1952) Conductivity water, ice free from stress. Limiting values plotted arbitrarily at 1,000 times the relaxation frequency.
- V: Von Hippel (1954) Conductivity water, ice not available.
- Y: Yashino (1961) Antarctic ice core samples, not annealed, density 0.91g/cm^3 .
- W: Westphal (private communication) Greenland ice, annealed, density 0.90g/cm^3 .
- B: Blue (1979)

Figure 2-4 Dielectric Properties of Ice (Evans, 1965).

TABLE 2-2
Relative Dielectric Constants of Ice at 35.3 GHz
as Reported by Perry and Straiton, (1972)

k'_i	k''_i	$\tan \delta$	Ice Source
1.91 ± 0.03	$<4 \times 10^{-3}$	$<2.1 \times 10^{-3}$	Deionized H ₂ O
1.89 ± 0.03	1.14×10^{-1}	6.03×10^{-2}	T _{ap} H ₂ O

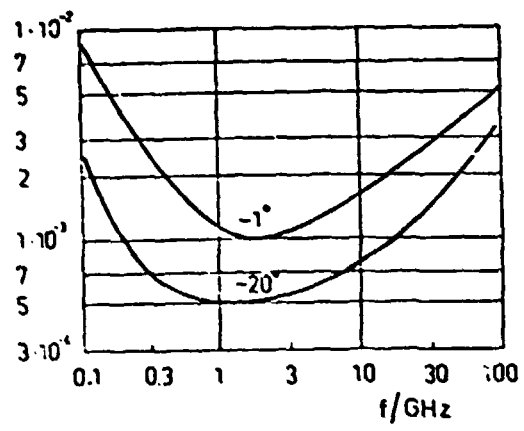


Figure 2-5 Loss Factor of Fresh Water Ice as a Function of Frequency (Hallikainen, 1977).

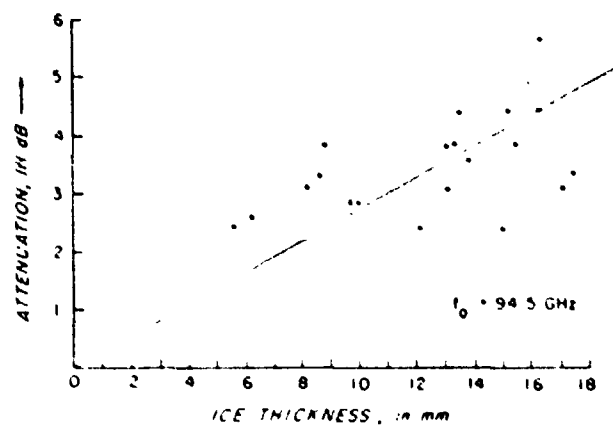


Figure 2-6 Attenuation Curve (Tap-Water Ice) at 35.3 GHz (Perry and Straiton, 1972).

Table 2-3 shows several mixing formulas that have been proposed to calculate the dielectric constant of a mixture consisting of two components (Poe, 1971; Sweeny and Colbeck, 1974; Tinga et al., 1973). The form number F , used in the first five formulas accounts for structure in the dielectric medium. The numerical values of the form number can vary from $F = 0$ (vertical particles), to $F = 2$ (spherical particles), to infinity (for elongated horizontal particles). Values of F for freshly fallen snow are normally between 2 and 10 (Evans, 1965). Edgerton et al. (1971) used a form number of $F = 32$ to get the best fit for their data for wet snow using the Weiner mixing formula.

The mixing formulas generally show no dependence on frequency; however, as the wavelength of interest approaches the order of the snow crystal size, scattering effects may become significant and the form number may require different values as a function of frequency. The wavelength at the desired frequency of 37 GHz is 0.81 cm which is of the order of snow crystal size; scattering, therefore, may become significant.

The first five mixing formulas were used to fit dielectric constant data for snow below 10 GHz (Evans, 1965) and were reported to have worked satisfactorily. However, since few measurements of snow dielectric constant were conducted above 10 GHz, the mixing formulas were never used to fit any data for wet or dry snow at or near the desired frequency of 37 GHz.

The Tinga et al. mixing formula was used to determine the dielectric constant of snow from the dielectric properties of ice and water at 5 GHz and 37 GHz (Tiuri and Schultz, 1980). The calculated values

TABLE 2-3
Mixing Formulas

Weiner (Poe, 1971)

$$\frac{k_{ds} - 1}{k_{ds} + F} = \rho_i \frac{k_i - 1}{k_i + F} + (1 - \rho_i) \frac{k_o - 1}{k_o + F}$$

where

ρ_i = Volumetric Fraction of Ice

k_o = Dielectric constant of air

k_i = Dielectric constant of ice

k_{ds} = Dielectric constant of dry snow

F = Form number

Böttcher (Poe, 1971)

$$\frac{k_{ds} - k_o}{3 k_{ds}} = \rho_i \frac{k_i - k_o}{k_i + 2 k_{ds}}$$

Wet Snow (Weiner) (Poe, 1971)

$$k_{ws} = \frac{k_w \rho_w U + k_{ds} (1 - \rho_w)}{\rho_w U + (1 - \rho_w)}$$

where

$$U = \frac{k_{ds} + F}{k_w + F}$$

k_{ws} = Dielectric constant of wet snow

k_w = Dielectric constant of bulk water

ρ_w = Volumetric fraction of water

Pierce (Poe, 1971)

$$k_{ds} = k_i + \frac{(1 - \rho_i)(1 - F)}{1 - (1 - \rho_i)F} (k_o - k_i)$$

deLoor (Sweeny and Colbeck, 1974)

$$k_{ws} = k_{ds} + \frac{\rho_w}{3} (k_w - k_{ds}) \sum_{j=1}^3 \frac{1}{1 + \left[\left(\frac{k_w}{k_n} \right) - 1 \right] A_j}$$

where

k_n = Dielectric constant of bound water

A_j = Particle Depolarization factor for each of the three major axes (Sweeney and Colbeck, 1974)

Tinga et al. (1973)

$$k_s = \frac{3 \left[\left(\frac{R_w}{R_a} \right)^3 (k_w - 1)(2k_w + k_i) \right]}{(2 + k_w)(2k_w + k_i) - 2 \left(\frac{R_i}{R_w} \right)^3 (k_w - 1)(k_w - k_i) - \left(\frac{R_w}{R_a} \right)^3} \\ - \frac{\left(\frac{R_i}{R_a} \right)^3 (k_w - k_i)(2k_w + 1)}{(k_w - k_i)(2k_w + k_i) + \left(\frac{R_i}{R_a} \right)^3 (k_w - k_i)(2k_w + 1)} + 1$$

but

$$R_w = R_i \left(1 + \frac{0.92 M_w}{1 - M_w} \right)^{1/3}$$

$$R_a = R_i \left(\frac{0.92}{\rho_s} \right)^{1/3} \left(1 + \frac{M_w}{1 - M_w} \right)^{1/3}$$

where

k_w = Dielectric constant of water

k_i = Dielectric constant of ice

R_i = Radius of ice particle

R_w = Radius of water covered ice particle

M_w = Weight percentage of liquid water contained
in snow

ρ_s = Density of snow

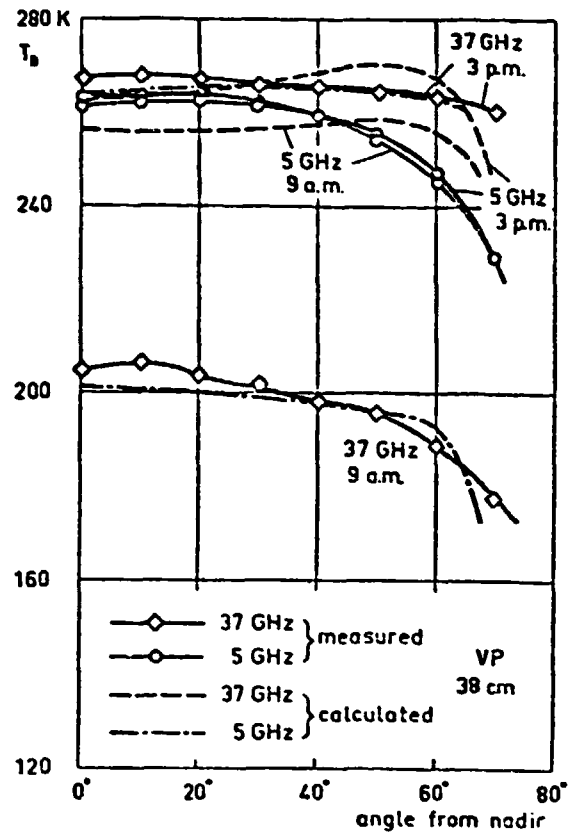
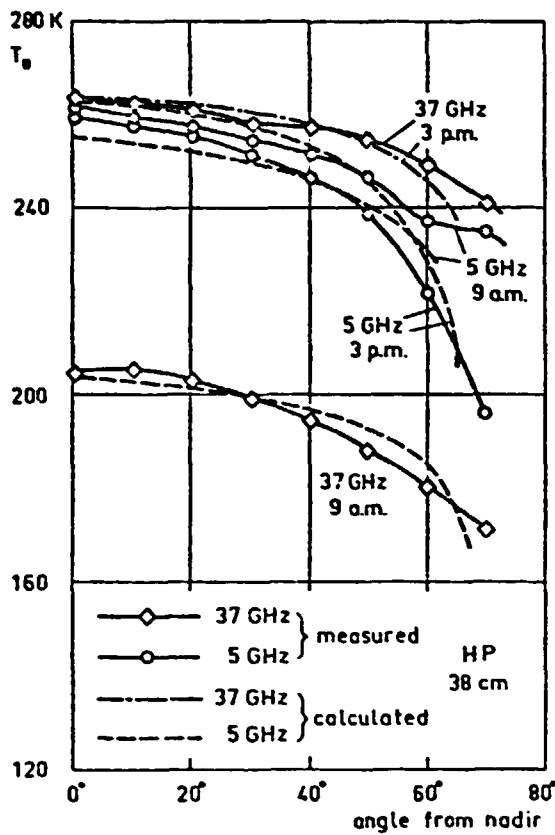
of the dielectric constant of snow were used to calculate the brightness temperature of snow using a radiative transfer model and assuming the snow to consist of spherical ice particles in air for dry snow. Wet snow was assumed to consist of the same ice spheres with a thin water shell surrounding them. Figure 2-7 shows the calculated dielectric constants of snow for the different snow wetnesses. The density and temperature of the snow were measured but the wetness and particle size have been selected for best calculated fit. It can be seen that a relatively good fit has been achieved for all cases.

2.4 Dielectric Constant of Dry Snow

Dry snow is a mixture of ice and air. Therefore, its response to temperature and frequency is similar to that of ice. However if the wavelength is of the order of the snow crystal size, scattering may cause a frequency dependence in snow. Due to the difficulty associated with measuring the dielectric constant of snow while maintaining the environment constant during the measurement, only one set of dielectric constant measurements of snow above 10 GHz is reported. Table 2-4 shows the results of the experiments conducted by Edgerton et al. (1971) at 37 GHz for dry snow. These measurements were made using an ellipsometer to measure the reflection coefficient.

2.5 Dielectric Constant of Wet Snow

Due to the high values of the dielectric constant of water, small amounts of water can significantly change the dielectric constant of snow. The lack of a good method to measure the wetness of snow along with the difficulty in keeping the environment constant during measurements



Thickness (m)	Density (kg/m ³)	Wetness (%)	Temperature (C)	Particle radius (mm)	Optical depth 4.8/36.8	Diel.Re. 4.8/36.8	Diel.Im. 4.8/36.8	Albedo 4.8/36.8
0.2	350	0.28	-0.1	0.5	0.17/6.30	1.59/1.57	0.011/0.0064	0.010/0.37
0.18	410	1.1	-0.3	0.6	0.66/13.1	1.78/1.70	0.048/0.029	0.0050/0.76

Thickness (m)	Density (kg/m ³)	Wetness (%)	Temperature (C)	Particle radius (mm)	Optical depth 4.8/36.8	Diel.Re. 4.8/36.8	Diel.Im. 4.8/36.8	Albedo 4.8/36.8
0.01	350	10	0	0.5	0.10/1.50	2.07/1.67	0.15/0.19	0.0027/0.26
0.19	350	6	0	0.5	1.74/19.9	1.92/1.62	0.13/0.12	0.0023/0.51
0.18	410	2	-0.3	0.6	1.07/15.8	1.36/1.71	0.090/0.052	0.0044/0.65

Figure 2-7 Measured and Calculated Brightness Temperatures of a 38 cm Thick Snow Field in the Morning and in the Afternoon. The Density and Temperature of Snow Were Known. The Wetness and Particle Size have been Selected for Best Fit (Tiuri and Schultz, 1980).

TABLE 2-4

Dielectric Constant of Dry Snow at
37 GHz as Reported by
Edgerton et al. (1971)

k'_s	k''_s	Temperature ° C	Density Units	Grain Size (mm)
2.77*	< 0.03	-2	0.5	1.2
1.9	< 0.03	-10	0.5	0.5

*The high values were explained as resulting from difficulty in sample preparation.

make dielectric constant measurements of wet snow difficult to obtain. Measurements of dielectric constant of wet snow above 10 GHz are nonexistent. Therefore, there is no data for the dielectric constant of snow of any wetness at or near the desired frequency of 37 GHz.

2.6 Attenuation Through Snow

The absorption coefficient for a lossy medium is given by:

$$\alpha_a = \frac{2\pi}{\lambda} \left\{ \frac{K'_S}{2} \left[\left(1 + \left(\frac{K''_S}{K'_S} \right)^2 \right)^{1/2} - 1 \right] \right\}^{1/2} \quad (2-6)$$

However, experimental evidence indicates that for wet and dry snow:

$$K''_S \ll K'_S \quad (2-7)$$

This reduces equation (2-6) to:

$$\alpha_a = \frac{\pi K''_S}{\lambda \sqrt{K'_S}} \quad (2-8)$$

where

α_a = Field absorption coefficient, nep/m

λ = Wavelength (meters)

$$K_S = K'_S - j K''_S$$

= Complex dielectric constant of snow

Attenuation rates in dB/m are given by:

$$L = 20 \log_{10} \left(e^{-\alpha_a} \right) = -8.68\alpha_a \quad (2-9)$$

Power loss measurements made through a layer of snow are composed of two parts, mismatch loss and attenuation loss. If the power loss measurements are conducted with coherent transmission, the two types of loss cannot be separated because of the interference effects caused by multiple reflections.

Linlor (1980) measured the rate of attenuation in dB/cm as a function of snow wetness and at selected frequencies between 4 and 12 GHz using phase shift and transmission loss measurements through two identical containers. One of the containers was empty and used as the reference unit and the other was filled with the snow sample. Figures 2-8 and 2-9 show the results of his experiment. These attenuation curves were plotted using an empirical relation derived by Linlor (1980) and given as:

$$\text{Attenuation(dB/cm)} = M_V \left[0.045(f-4) + 0.066 \right] \quad (2-10)$$

where

M_V = Percentage wetness by volume

f = frequency in GHz

Notice the increase in attenuation with increasing snow wetness and increasing frequency. Figure 2-8 shows that the attenuation through dry snow (zero wetness) is zero. This, according to the author, is not the case but the attenuation was less than 1 dB and so could not be measured using the available measuring instruments.

The Tinga et al. (1973) mixing formula along with Equation (2-8) are used to calculate the attenuation through snow as a function of its wetness at 37 GHz, 18 GHz and 12 GHz, for snow with a density of 0.21 g/cm^3 ,

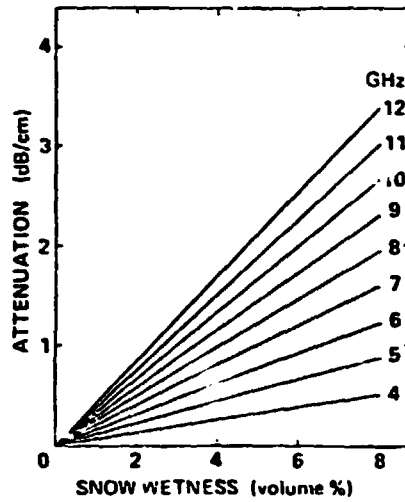


Figure 2-8 Variation of Attenuation with Snow Wetness at Selected Frequencies (Linlor, 1980).

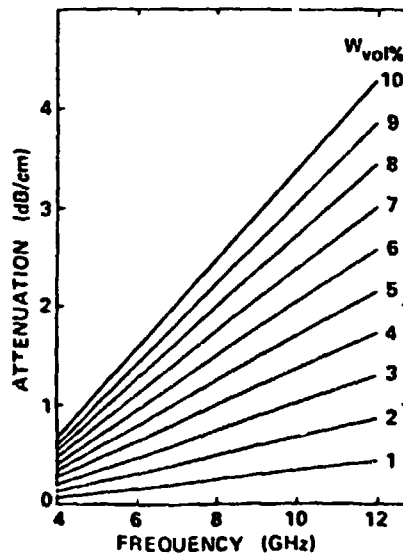


Figure 2-9 Variation of Attenuation with Frequency at Selected Snow Wetness (Linlor, 1980).

Figure 2-10 shows the results of this calculation. As seen by the figure, there is an increase in attenuation with increasing wetness of the snow and with increasing frequency. However, at 12 GHz, the attenuation starts to saturate at a percentage wetness, M_v , of 3%. In Figure 2-11, the attenuation in Nep/cm is plotted as a function of M_v at 12 GHz using both Equation (2-10) of Linlor (1980) and the Tinga et al. (1973) mixing formula. It is seen that the attenuation values obtained by the mixing formula are higher in value than those obtained by Linlor's empirical formula for percentage wetness by volume of snow that are less than $M_v = 2.75$.

Battles and Crane (1965, 1966) used interferometry techniques to measure loss from artificially created snow. Figure 2-12 shows their results in dB/ft as a function of snow temperature at 35.2 GHz. The loss shows a slow increase with increasing temperature until the temperature nears the melting point. Near 32° F, the melting point of ice, a sharp increase in loss through snow is seen which is due to the appearance of moisture in the snow. Table 2-5 shows the results of another experiment reported by Battles and Crane (1966), in which loss from different types of snow is reported at 35.26 GHz. The higher losses for locally packed and ice crystal cases were explained to be the result of scattering of the wave by the snow crystals.

Currie et al. (1977) made measurements using a pulsed radar operating at 35 GHz. Their loss measurements were calculated by comparing the return from a corner reflector placed below the snow layer with the return measured from the same corner reflector placed above the snowlayer. Table 2-6 shows their results. The loss measure-

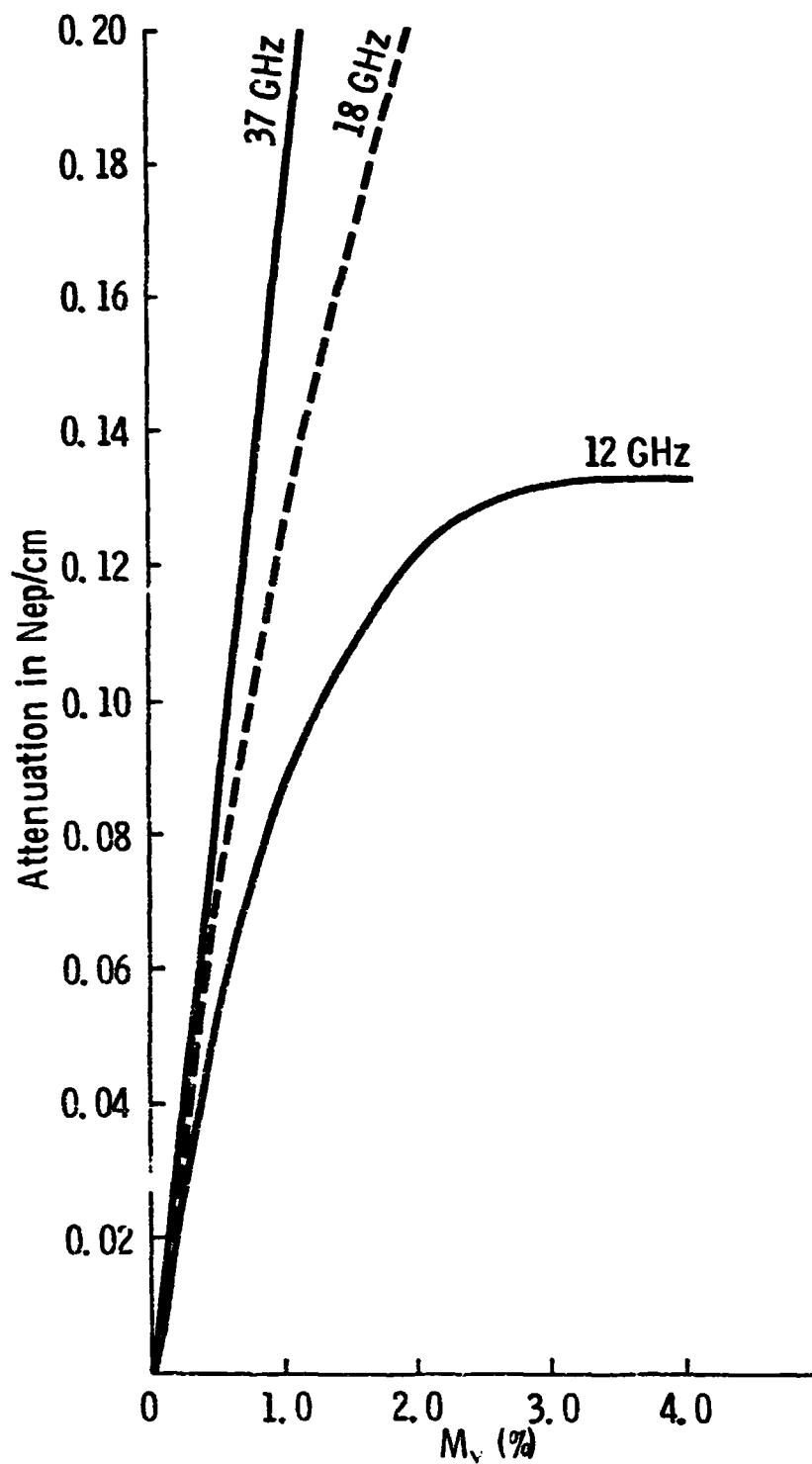


Figure 2-10 The Rate of Attenuation in Nep/cm as a Function of Snow Wetness and Frequency Calculated Using the Tinga et al. (1973) Mixing Formula for a Snow Density of 0.21 g/cm^3 .

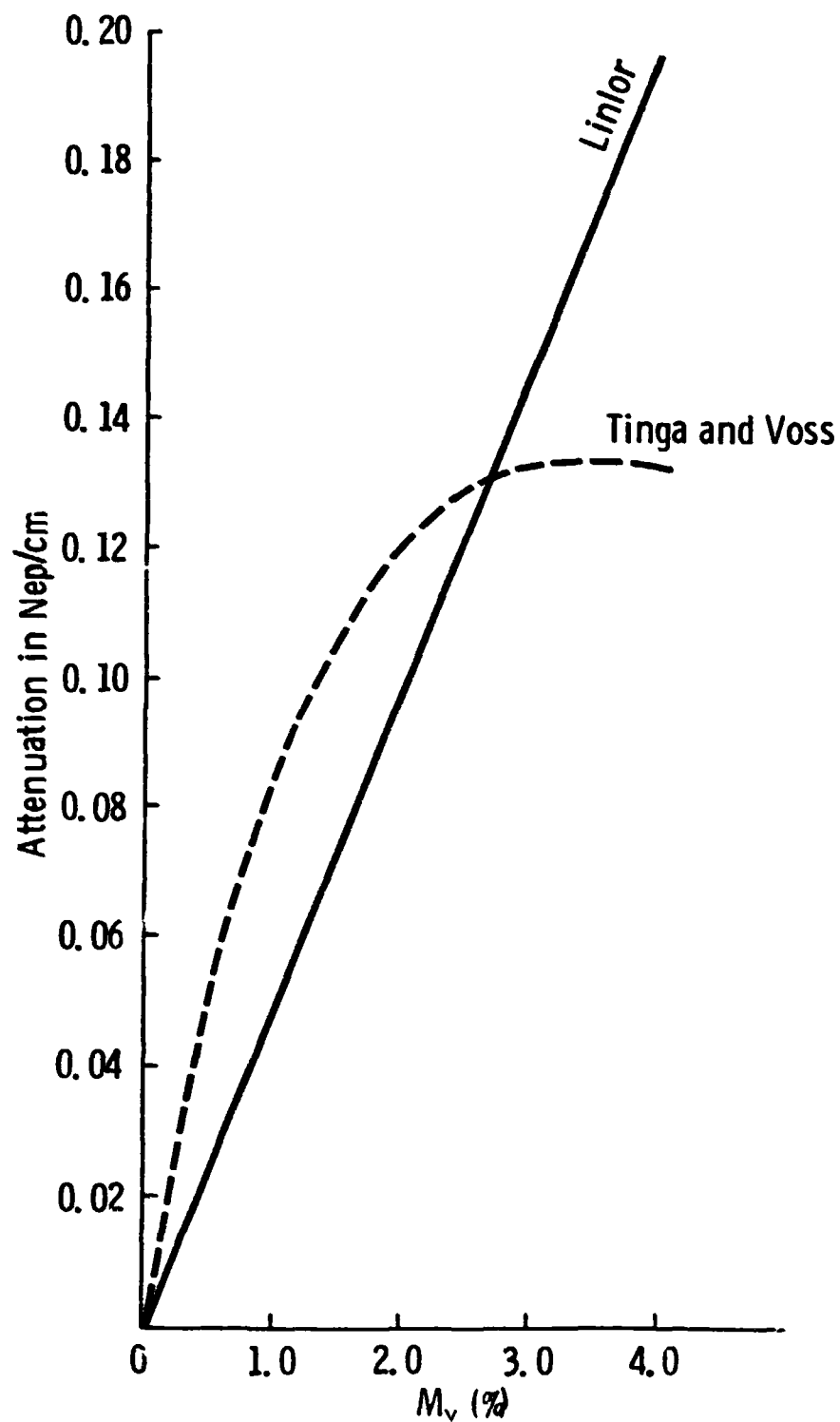


Figure 2-11 The Attenuation Through Snow as a Function of its Wetness as Calculated by Linlor's (1980) Empirical Formula and by the Tinga et al. (1973) Mixing Formula at 12 GHz and Snow Density of 0.21 g/cm^3 .

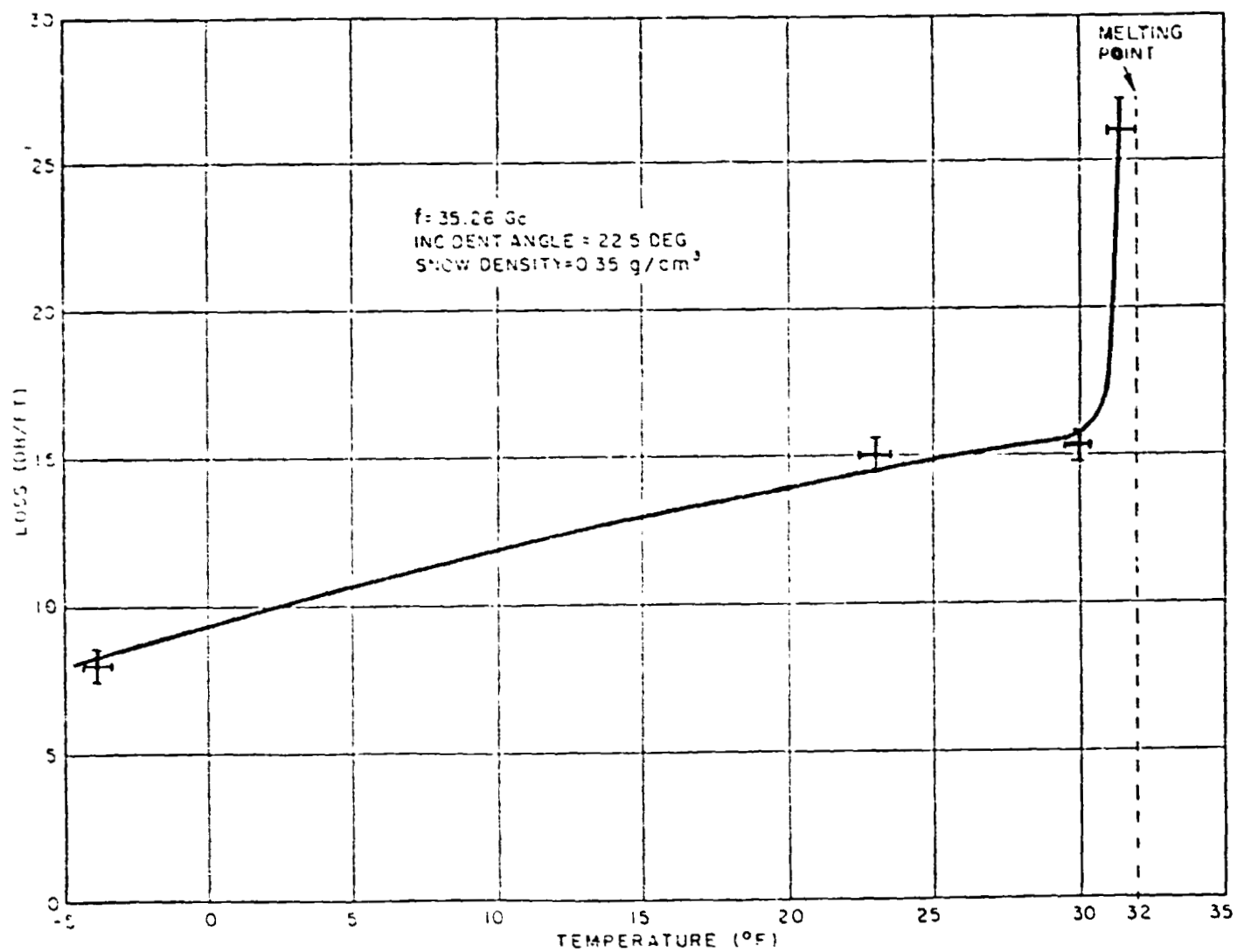


Figure 2-12 Absorption of Radiation by Snow as a Function of Temperature (Battles and Crane, 1965).

TABLE 2-5

Loss Caused by Snow and Ice at 35.26 GHz
(Battles and Crane, 1966)

Type	Thickness (cm)	Density g/cm ³	Loss (dB)
Fine, loose snow	14.0	0.2	2.5
Locally packed loose snow	14.0	0.33	7.2
Large ice crystals	14.0	0.39	9.2
Packed snow	14.0	0.47	1.4
Ice	5.1	0.92	1.2

TABLE 2-6
Loss Measurements at 35 GHz
(Currie et al., 1977)

Snow Condition	Layer Thickness (cm)	Loss (dB)
Wet Snow Crust	3.5	11
Dry Snow Crust	4.6	21
Dry Snow Crust	5.0	5
Dry Snow Crust	3.5	3

ments are due to both mismatch and attenuation losses and, therefore, an attenuation coefficient cannot be calculated.

Stiles and Ulaby (1980) measured path loss at 35 GHz as a function of depth for three snow conditions using transmission techniques. Figure 2-13 shows their results in dB as a function of snow depth.

Stiles and Ulaby (1980) also calculated the emissivity of snow at 37 GHz as a function of the angle of incidence of the radiometer relative to nadir. The emissivity $\epsilon(\theta)$ was calculated using the equation below

$$\epsilon(\theta) = \frac{T_{ap}(\theta) - T_{sky}(\theta)}{T_o - T_{sky}(\theta)} \quad (2-11)$$

where

T_{ap} = Apparent temperature of snow measured by radiometer;
°K

T_{sky} = Sky brightness temperature; °K

T_o = Physical temperature of snow; °K

Stiles and Ulaby (1980) developed a simple emission model for a homogeneous layer of snow and the ground underneath it, and were able to fit their emissivity data calculated using the previous equation to the following equation developed by their model for emissivity as a function of the angle of incidence θ :

$$\begin{aligned} \epsilon(\theta) &= \left(\tau_{sa} \frac{\kappa_a}{\kappa_e} \right) + \left(\tau_{sa} \tau_{gs} - \tau_{sa} \frac{\kappa_a}{\kappa_e} \right) \text{Exp} \left(-\kappa'_e \text{Sec } \theta W \right) \\ &= A + B \text{Exp} \left(-\kappa'_e \text{Sec } \theta W \right) \end{aligned} \quad (2-12)$$

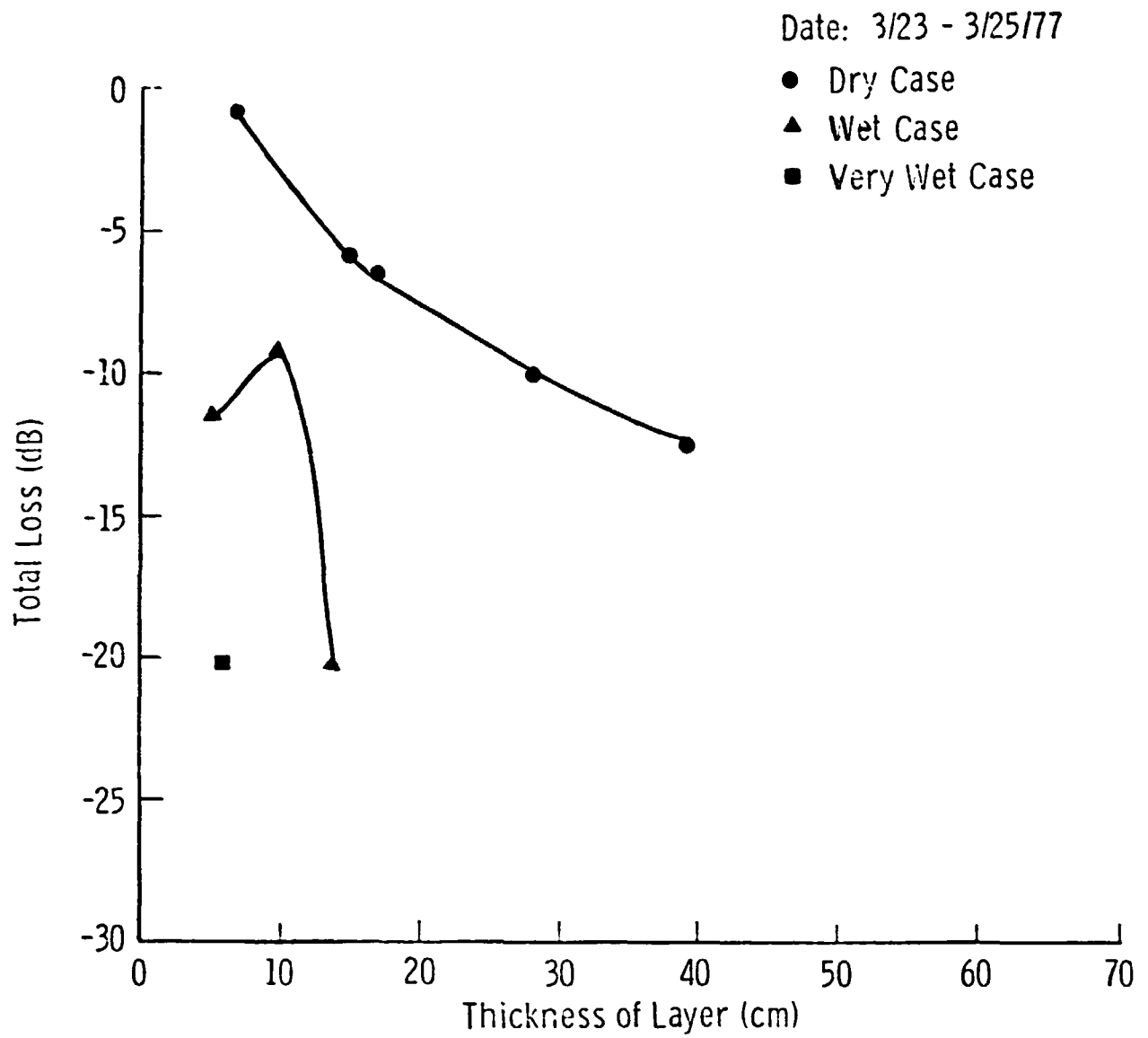


Figure 2-13 Measured Path Loss as a Function of Snow Thickness for Three Snow Conditions (Stiles and Ulaby, 1980).

where A and B represent the constant terms inside the parenthesis and

τ_{sa} = Snow-air power transmission coefficient

τ_{gs} = Ground-snow power transmission coefficient

κ_a = Snow absorption coefficient (nep/cm)

κ_e = Snow extinction coefficient (nep/cm)

$$= (\kappa_a + \kappa_s)$$

κ'_e = Mass extinction coefficient of snow (nep g⁻¹ cm²)

κ_s = Snow scattering coefficient (nep/cm)

W = Snow water equivalent, cm

θ = Angle of incidence, relative to nadir (degrees).

Figure 2-14 shows a plot of measured radiometric emissivity for dry snow at 37 GHz and for $\theta = 27^\circ$ and 57° as a function of the water equivalent W of snow. The best fit curves obtained using Equation (2-12) to fit the emissivity data are also shown. The values of A and B estimated by regression analysis to produce the best fits are shown in Figure 2-14 and Table 2-7. From these values it is seen that at $\theta = 27^\circ$:

$$\tau_{sa} \frac{\kappa_a}{\kappa_e} = 0.517 \quad (2-13a)$$

$$\tau_{sa} \tau_{gs} - \tau_{sa} \frac{\kappa_a}{\kappa_e} = 0.481 \quad (2-13b)$$

$$\kappa'_e \sec 27^\circ = 0.0235 \quad (2-13c)$$

Assuming $\tau_{sa} = 0.99$, for the snow density measured during the experiment (0.41 g/cm³), the above three equations are used to calculate κ_a .

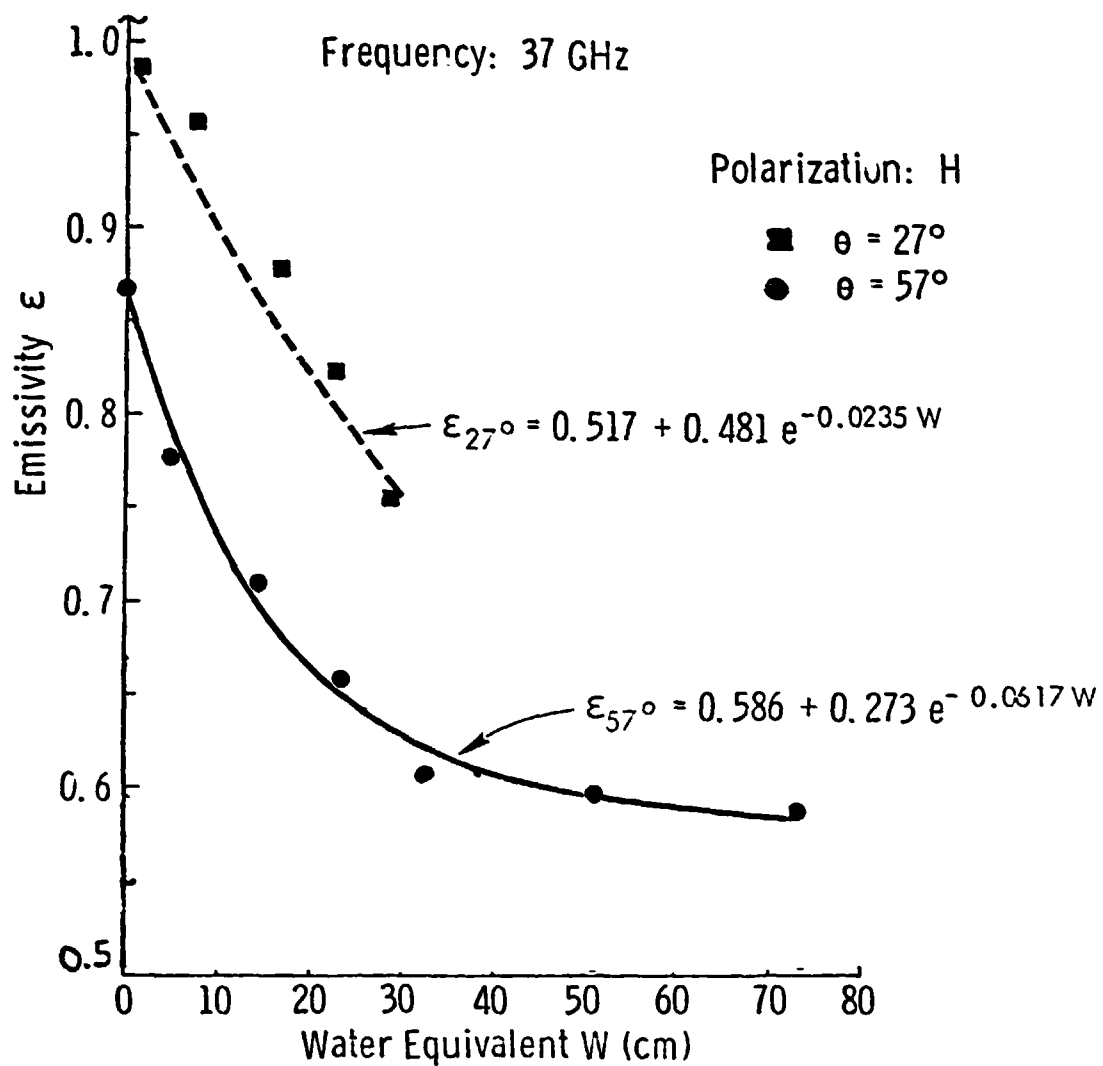


Figure 2-14 Measured Radiometric Emissivity Response to Dry Snow Water Equivalent at 37 GHz (Stiles and Ulaby, 1980).

TABLE 2-7

Values of A, B, κ_e , κ_a and κ_s Generated by Fitting
the Experimental Values of ϵ at 37 GHz to Equation 2-11:
(Stiles and Ulaby, 1980)

θ°	A	B	κ_e nep/cm	κ_a nep/cm	κ_s nep/cm	Maximum Error*
27°	0.517	0.481	8.60×10^{-3}	4.50×10^{-3}	4.10×10^{-3}	0.02
57°	0.586	0.273	1.38×10^{-2}	8.17×10^{-3}	5.63×10^{-3}	0.02

*Maximum Error = $|\epsilon_C - \epsilon_M|$; ϵ_C = Calculated from best fit eq. 2-12.
 ϵ_M = Measured (equation 2-11).

κ_s and κ_e for snow at $\theta = 27^\circ$. The results of the calculations are shown in Table 2-7. Similar calculations are carried out for $\theta = 57^\circ$ and the values obtained are also shown in Table 2-7.

Attenuation rates for snow were calculated using the temperature measurements of a snow layer of known thickness over a metal plate (Hofer and Matzler, 1980). The attenuation rates were calculated using two simple models proposed by Hofer and Matzler (1980). The first model included the effects of multiple reflections but neglected interference effects, whereas the second model was a radiative transfer model which included volume scattering κ_s and absorption κ_a . Figure 2-15 and 2-16 show the results. κ_2 is the power damping coefficient which combines the effects of absorption and scattering and is given by (Hofer and Matzler, 1980):

$$\kappa_2 = \sqrt{\kappa_a^2 + 2\kappa_a\kappa_s} \quad (2-14)$$

κ_1 is the power attenuation coefficient calculated using the first model. Hofer and Matzler (1980) reported moist snow with wetness of 1 to 3 percent by volume exhibited power damping coefficients greater than 30 dB/meter at 36 GHz.

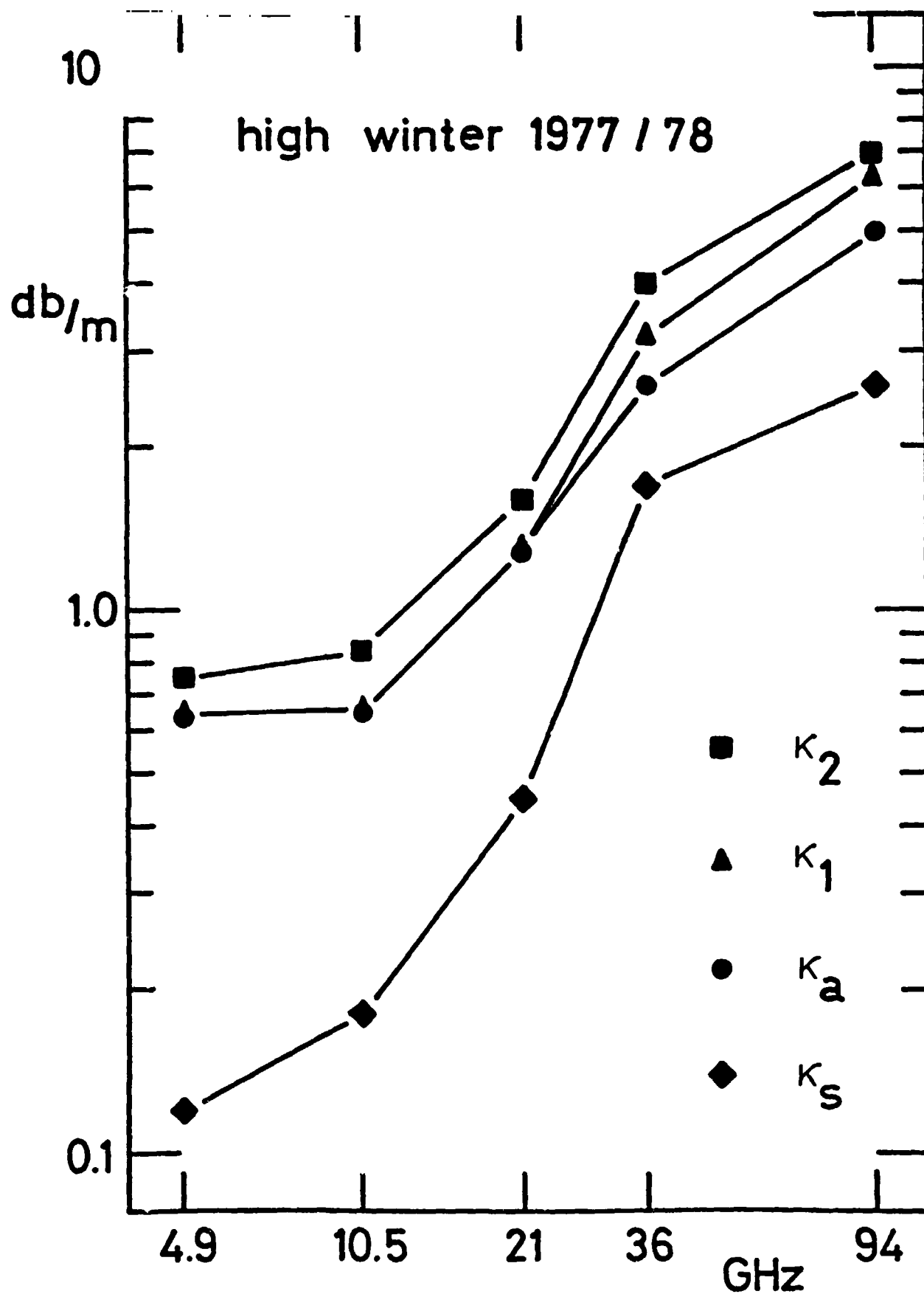


Figure 2-15 Scattering, Absorption and Damping Coefficients for Dry Winter Snow (Hofer and Matzler, 1980).

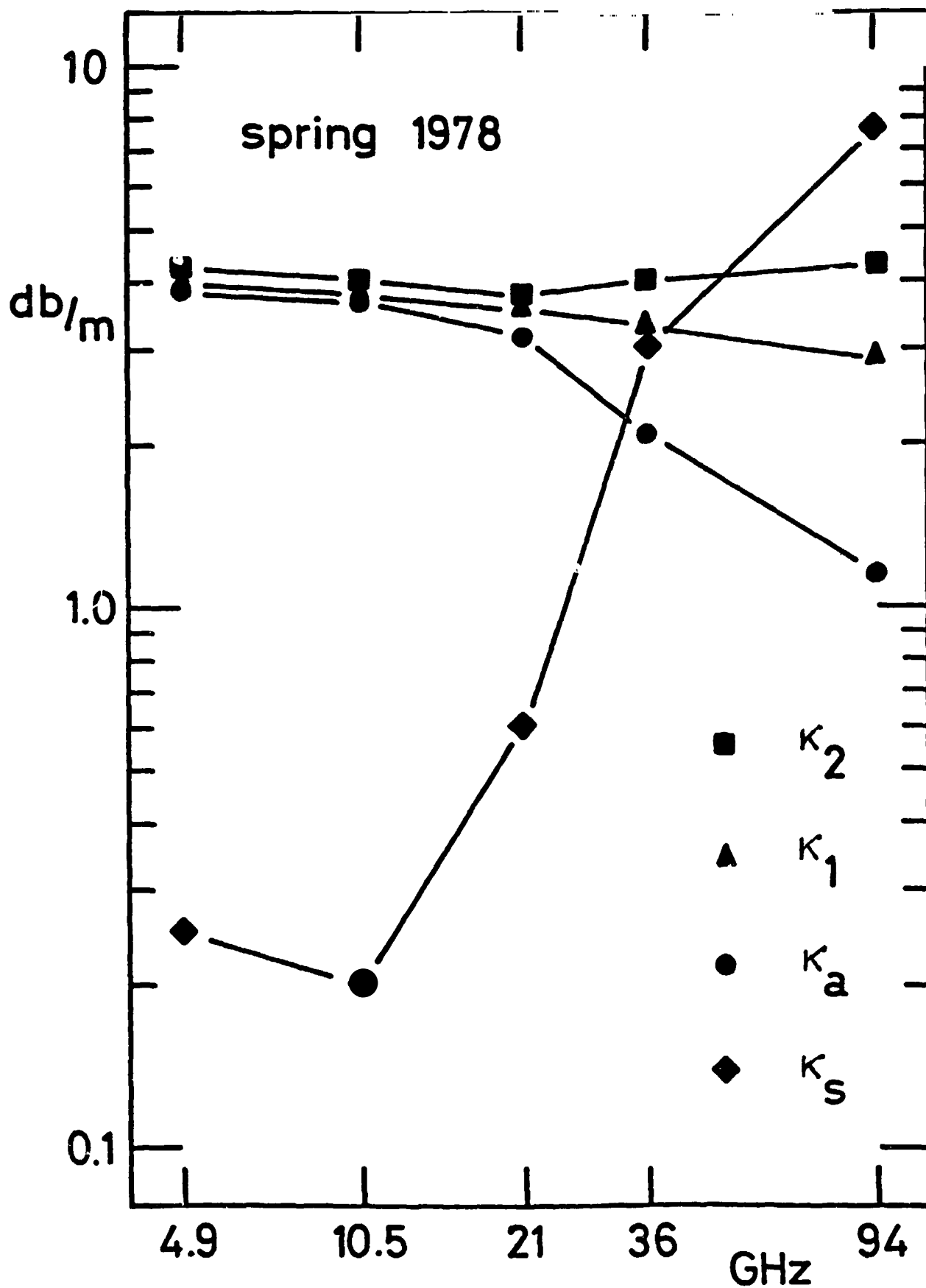


Figure 2-16 Scattering, Absorption and Damping Coefficients for Dry Spring (Metamorphosed) Snow (Hofer and Matzler, 1980).

3.0 EXPERIMENT DESCRIPTION AND RESULTS

This chapter provides a description of the microwave diurnal experiment conducted by Stiles and Ulaby (1980) on 2/17 - 2/18/77 and on which this study is based. The first section gives a brief description of the sensor used, test site and the different microwave and ground truth experiments conducted. Later sections of the chapter illustrate the results of the experiment.

3.1 Description of the Microwave Radiometer and Ground Truth Data

A microwave radiometer was mounted atop a truck-mounted boom and used to acquire ~~apparent~~^{surface} temperature (T_{ap}) data at a test site near Steamboat Springs, Colorado. The radiometer used during the experiment was a dual-polarized Dicke type manufactured by Aerojet General Corporation. It operated at 37 GHz, had a bandwidth of 300 MHz, a sensitivity of 0.5°K , an accuracy of 1°K and operated over a temperature range of $0-500^{\circ}\text{K}$. The radiometer had an approximate gain of 0.010 volts/K and used an automatic gain control mechanism. Calibration of the radiometer was conducted at the University of Kansas after completion of the experiment (Stiles and Ulaby, 1980).

The test site chosen for the experiment was a 40-acre hayfield near Steamboat Springs. The surface of the field was very flat and was covered with close-cut hay, approximately 6 cm in height. A snow-pack approximately 30 cm in depth lay on the surface of the field during the 2/17 - 2/18/77 diurnal experiment.

The diurnal experiment consisted of continuous data acquisition over a 28-hour period commencing at 6:00 AM on 2/17/77. T_{ap} data

was acquired at 37 GHz at both the horizontal and vertical polarizations and at 0° , 20° and 50° angles of incidence. Ground truth data were gathered in a snow pit on the test site and included measurements of snow density profiles, snow wetness profiles, snow temperature profiles along with soil moisture samples and soil temperature in the top 5 cm of the soil. These measurements were obtained at hourly intervals except for the snow wetness measurements which required a slightly longer duration. Snow density profiles were obtained by taking horizontal cores from each layer in the snowpack. Snow wetness was measured with a freezing calorimeter at 5 cm intervals vertically throughout the snowpack. Snow temperature was measured using a digital thermometer and was monitored at 2 cm intervals vertically throughout the snowpack. Since water equivalent is the total amount of water contained in the form of snow per unit area, it is calculated as the product of density and depth of each snow layer. Results of T_{ap} and ground truth measurements are discussed below (Stiles and Ulaby, 1980).

3.2 Diurnal Variation of T_{ap} at 37 GHz

Since the model developed later in this paper uses only the T_{ap} data obtained at 37 GHz in the horizontal polarization mode, only the horizontal polarization data are illustrated here. Figure 3-1 shows the apparent temperature T_{ap} response at $\theta = 0^\circ$, 20° and 50° throughout the diurnal experiment. Notice the increase in T_{ap} starting at 1000 hours and ending at 2200 hours. This increase in T_{ap} is due to the appearance of water in the snowpack as a result of warmer snow

(Stiles and Ulaby, 1980)

Date: 2/17 - 2/18/77

Polarization: H

Frequency: 37 GHz

Snow Depth: 30 cm

Water Equivalent: 6.3 cm

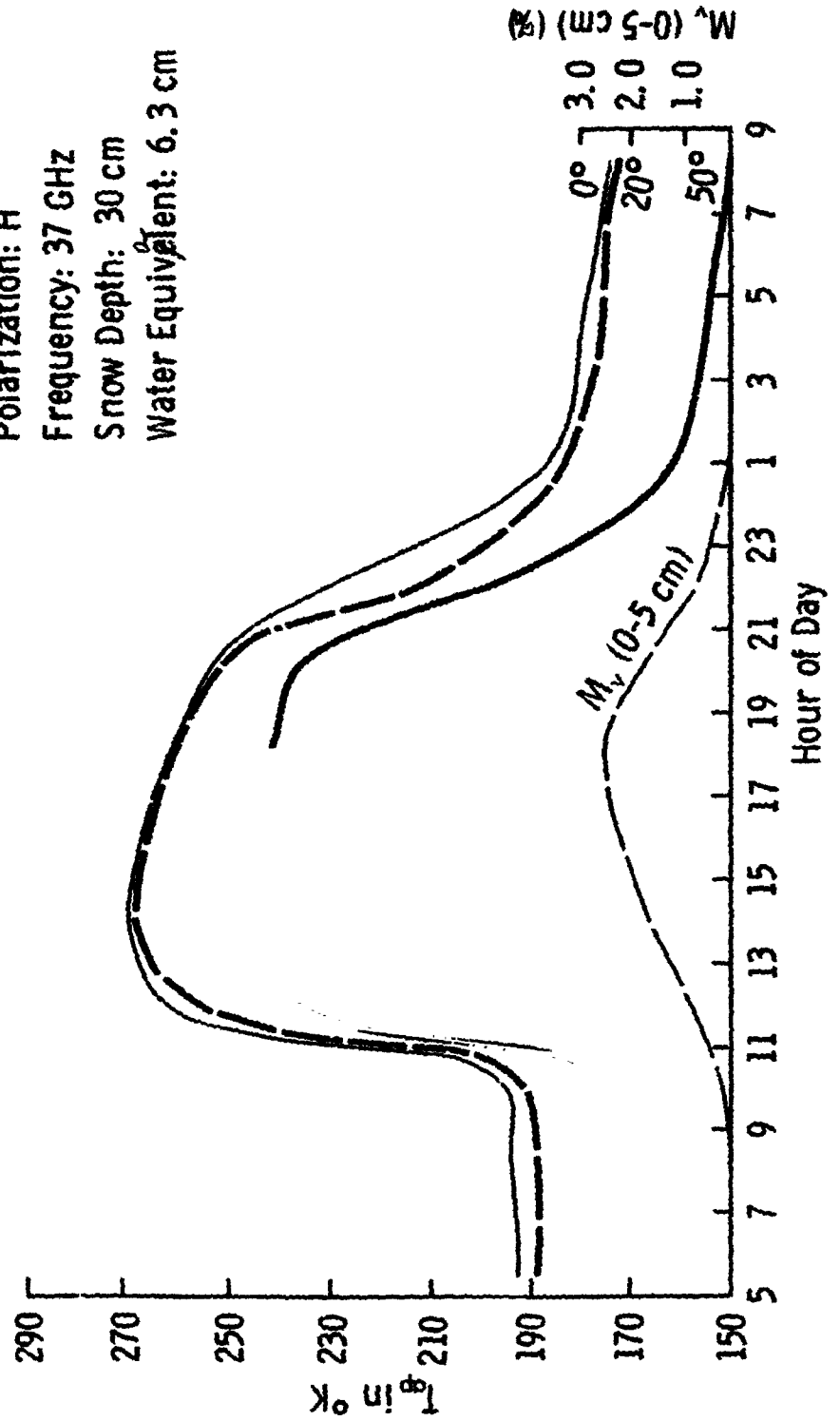


Figure 3-1 Apparent Temperature as a Function of Time at 37 GHz, H Polarization and for $\theta = 0^\circ, 20^\circ$ and 50° (Stiles and Ulaby, 1980).

temperatures. Notice also the little difference between the T_{ap} response at $\theta = 0^\circ$ and 20° . Figure 3.2 shows the snow wetness in individual 5 cm layers in the top 15 cm of snow as a function of time. By comparing Figures 3-1 and 3-2 one notices that T_{ap} is shown to lag behind $M_v(0-5 \text{ cm})$, the percentage wetness by volume of the snow in the top 5 cm of the snowpack, by about two hours. T_{ap} exhibits sharp increases and decreases as the snow starts to melt and refreeze respectively.

3.3 Ground Truth Diurnal Variations

As mentioned in the section above, Figure 3-2 shows the wetness M_v of the snowpack at the depths of 0-5 cm, 5-10 cm and 10-15 cm from the snow surface. The snowpack at depths lower than 15 cm was frozen throughout the experiment and showed no wetness. M_v is defined as the volume percentage of liquid water contained in a unit volume of snow.

Snow thermometric temperatures measured every 2 cm from the top of the snowpack to a depth of 5 cm below the soil surface were used to generate the average values shown in Table 3-1. In this table, the snow thermometric temperatures are averaged to give an average temperature for the snow every 5 cm from the snow surface. Table 3-1 shows 21 different data sets representing snow thermometric temperatures throughout the diurnal experiment. Figures 3-3, 3-4, 3-5 and 3-6 show the snow thermometric temperature along with the snow wetness at intervals of 5 cm of snow and at the hours of 5:30, 10:00, 18:00 and 6:45 respectively. Notice that as the snow starts getting warm and starts melting, it warms up first at the surface layer of snow and then the lower layers of the snow begin to warm up. Later in

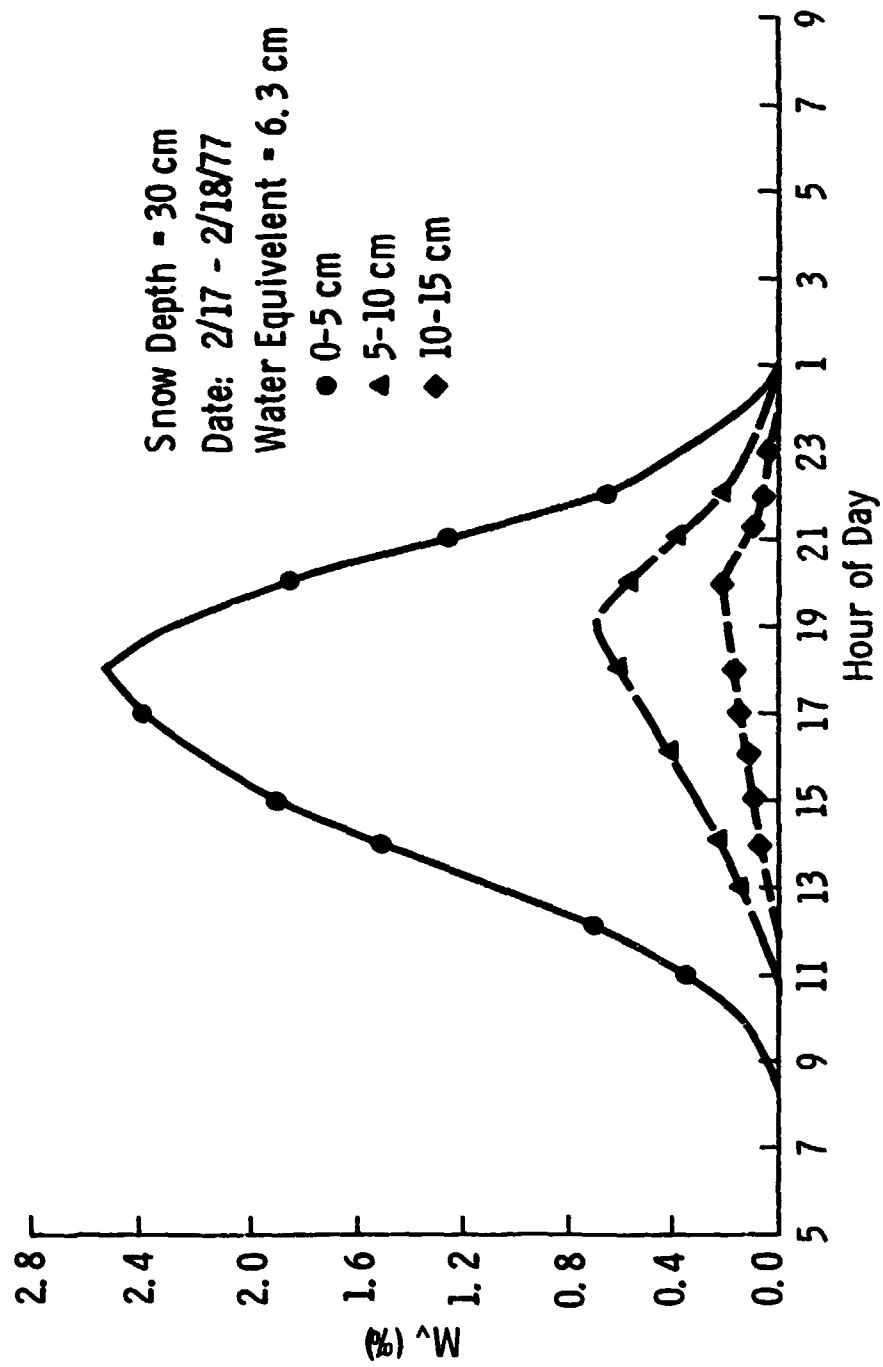


Figure 3-2 Snow Wetness M_v as a Function of Time in the Top 15 cm of Snow (Stiles and Ulaby, 1980).

TABLE 3-1

Snow Thermometric Temperature in $^{\circ}\text{K}$ for Different Depths
 Within the Snowpack on 2/17/77 - 2/18/77.
 (Liles and Ulaby, 1980)

Time	0-5 cm	5-10 cm	10-15 cm	15-30 cm
0530	267.9	267.2	268.1	269.3
0830	270.8	269.5	269.5	270.8
1000	273.8	272.5	271.4	272.0
1100	274.0	272.3	271.8	272.3
1200	274.0	273.3	272.6	272.6
1300	274.0	273.3	272.8	272.8
1400	274.1	273.4	273.2	272.9
1500	274.0	273.4	273.3	272.8
1600	274.0	273.4	273.3	273.0
1700	273.7	273.4	273.2	273.0
1800	273.4	273.3	273.2	273.0
1900	273.2	273.2	273.1	273.0
2000	273.1	273.1	273.1	273.0
2100	272.0	273.0	273.0	273.0
2200	271.1	273.0	273.0	272.9
0100	267.8	270.1	271.9	272.6
0400	262.3	264.4	268.0	271.2
0615	260.0	263.6	267.3	270.5
0645	259.8	263.5	267.3	270.4
0745	262.9	262.7	265.9	269.9
0820	266.1	264.4	266.9	269.7

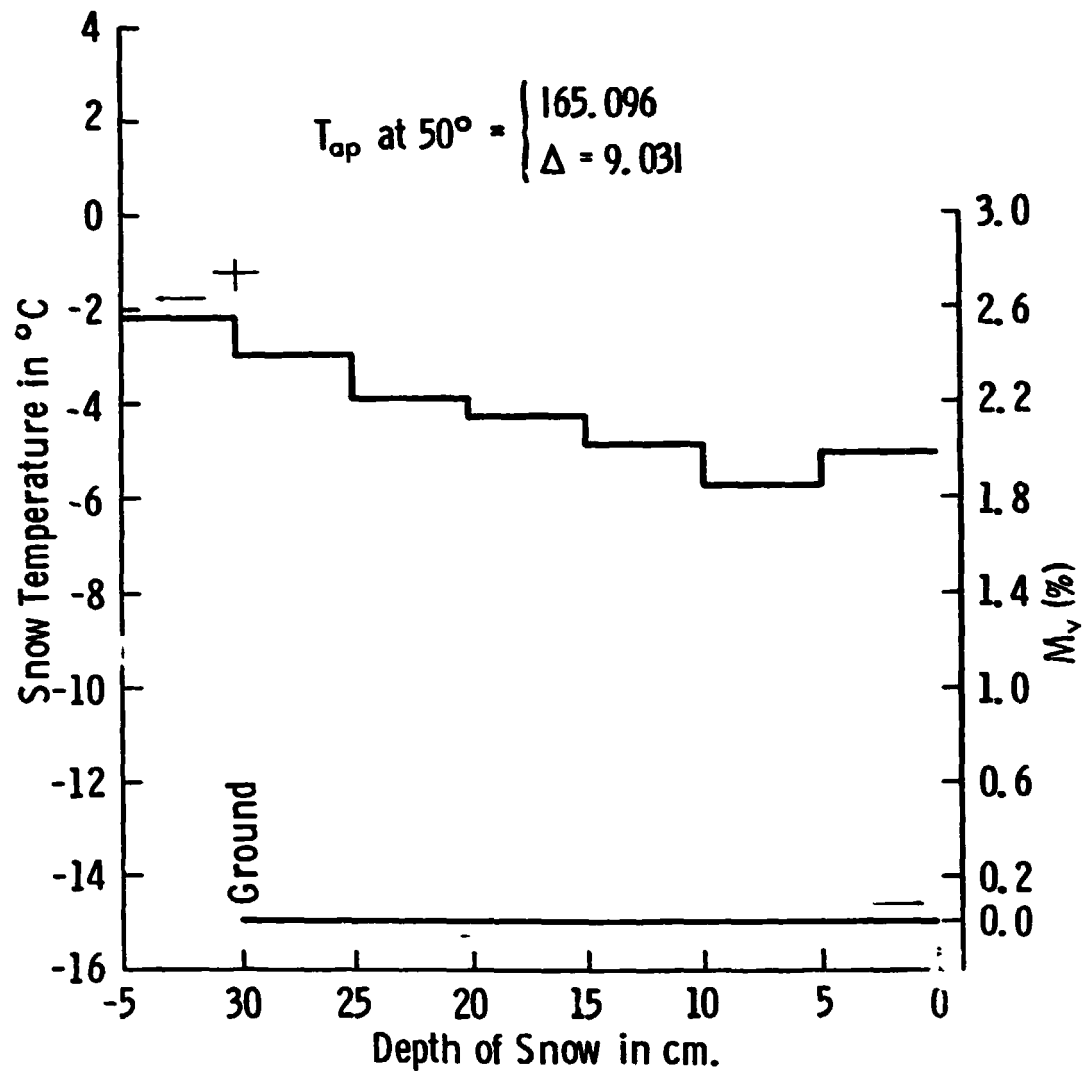


Figure 3-3 Snow Thermometric Temperature and Wetness at 5:30 AM on 2/17/77.

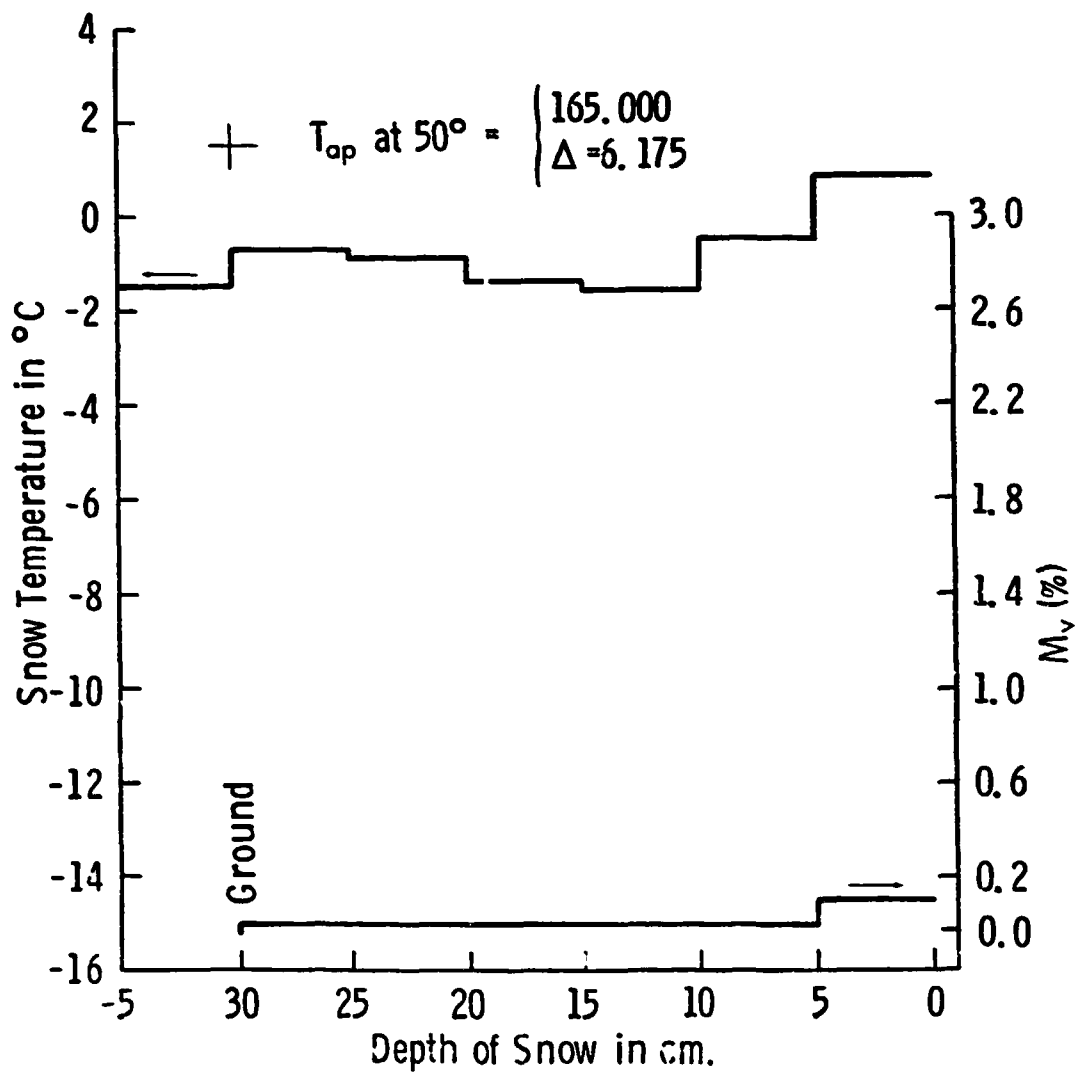


Figure 3-4 Snow Thermometric Temperature and Wetness at 10:00 AM on 2/17/77.

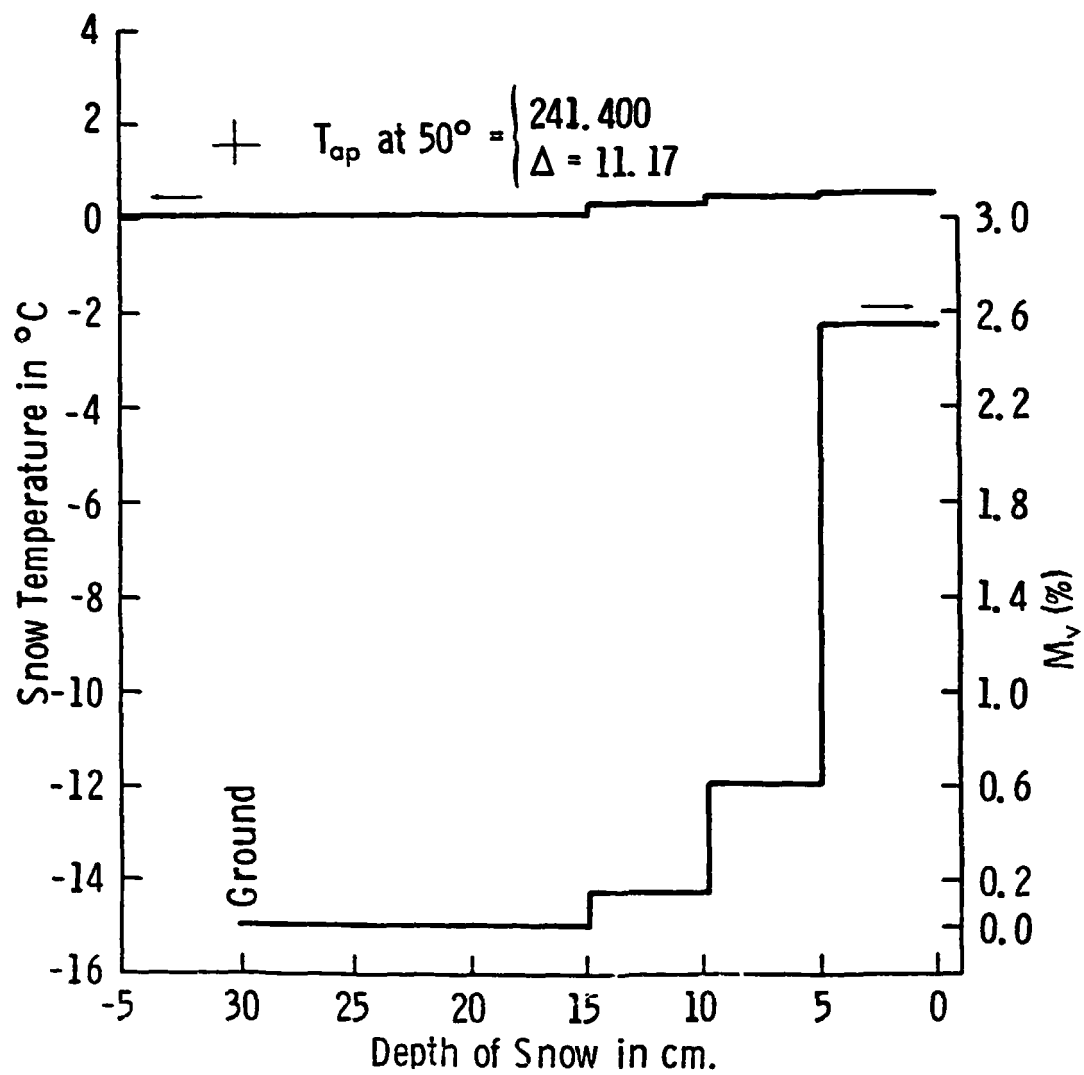


Figure 3-5 Snow Thermometric Temperature and Wetness at 1800 Hours on 2/17/77.

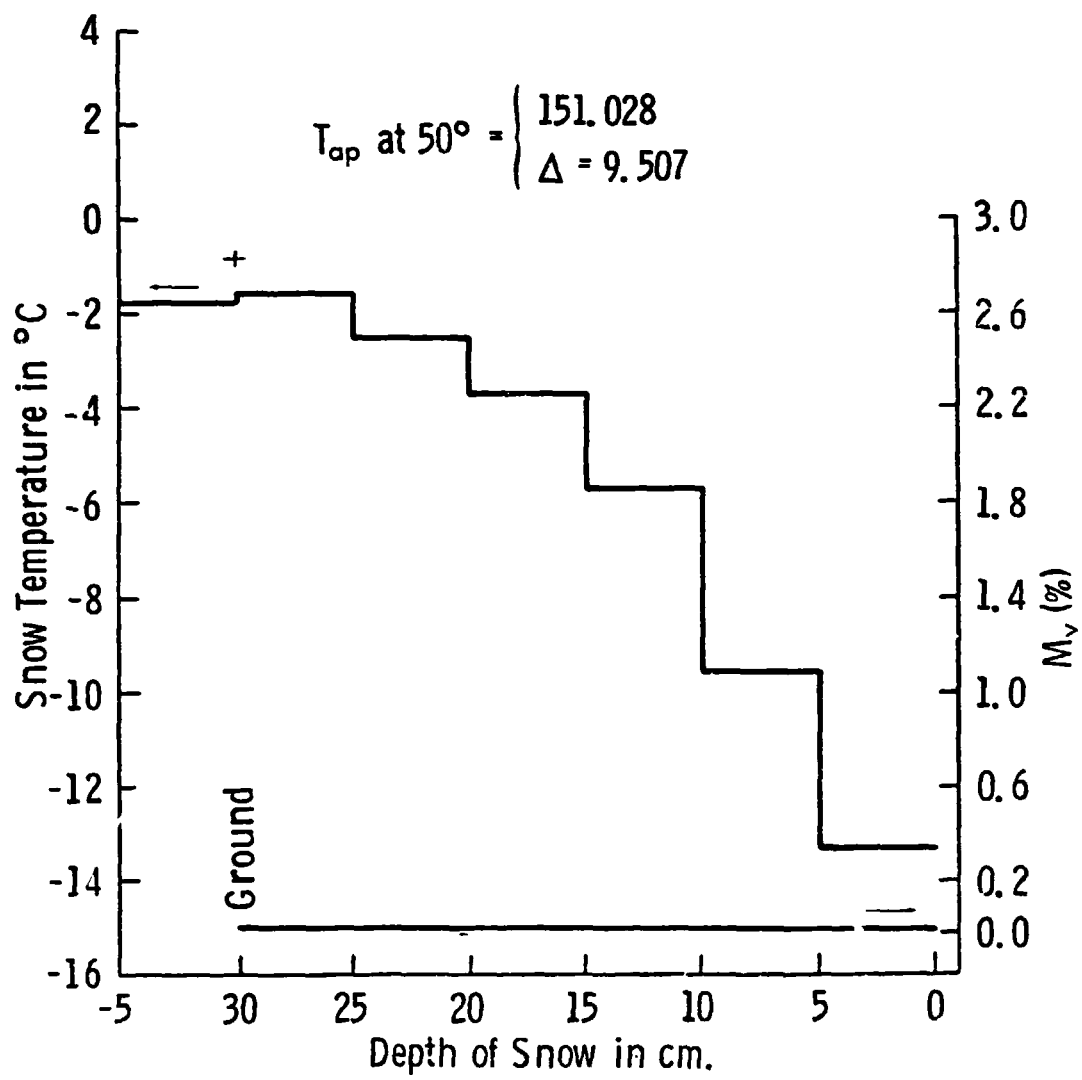


Figure 3-6 Snow Thermometric Temperature and Wetness at 6:45 AM on 2/18/77.

the day as the surface layer becomes very wet, the lower layers warm up to almost the same temperature as the top 5 cm snow layer as shown in Figure 3-5. Similarly at the refreezing stage after the sun goes down and the snow starts drying up in moisture, the top 5 cm layer starts decreasing in temperature first followed by the lower snow layers. Therefore, the refreezing process starts, like the melting process, from the snow surface down to the lower layers of snow.

Snow density was measured for each physical layer from the top of the snowpack down to the soil surface. The average density was found to be 0.21 g/cm^3 and did not change significantly at different depths in the snowpack or with time throughout the diurnal experiment. Therefore, the water equivalent of the total snowpack did not change and was measured to be 6.3 cm throughout the entire experiment. Also, the snow depth remained constant at 30 cm.

3.4 Wetness Response

Figures 3-7, 3-8 and 3-9 illustrate the response of T_{ad} to snow wetness of the top 5 cm layer at $\theta = 0^\circ$, 20° and 50° respectively. T_{ap} is shown to exhibit a hysteresis-like pattern. This hysteresis-like pattern is due to the fact that as the snow gets wet, the microwave radiometer operating at 37 GHz becomes sensitive to a snow depth that is smaller than the top 5 cm layer of the snow from which the snow wetness measurement was obtained. The snow depth to which the sensor is sensitive when the snow is wet depends on the penetration depth of the wave in the wet snow layer. In other words, the snow wetness actually measured is the average wetness of the top 5 cm of snow. The wetness values for

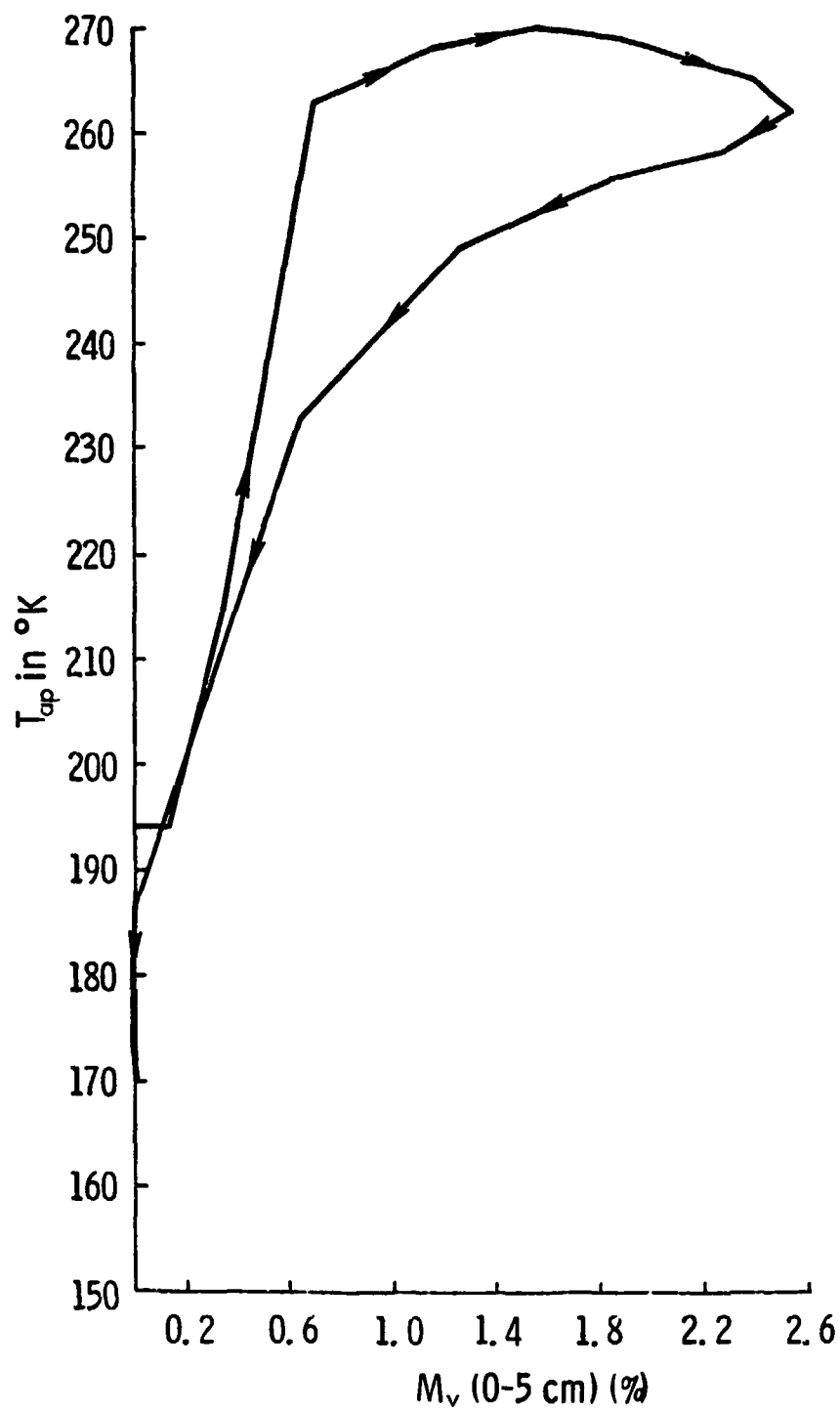


Figure 3-7 T_{ap} Response to Snow Wetness M_v , Showing the Hysteresis Effect at $\theta = 0^\circ$.

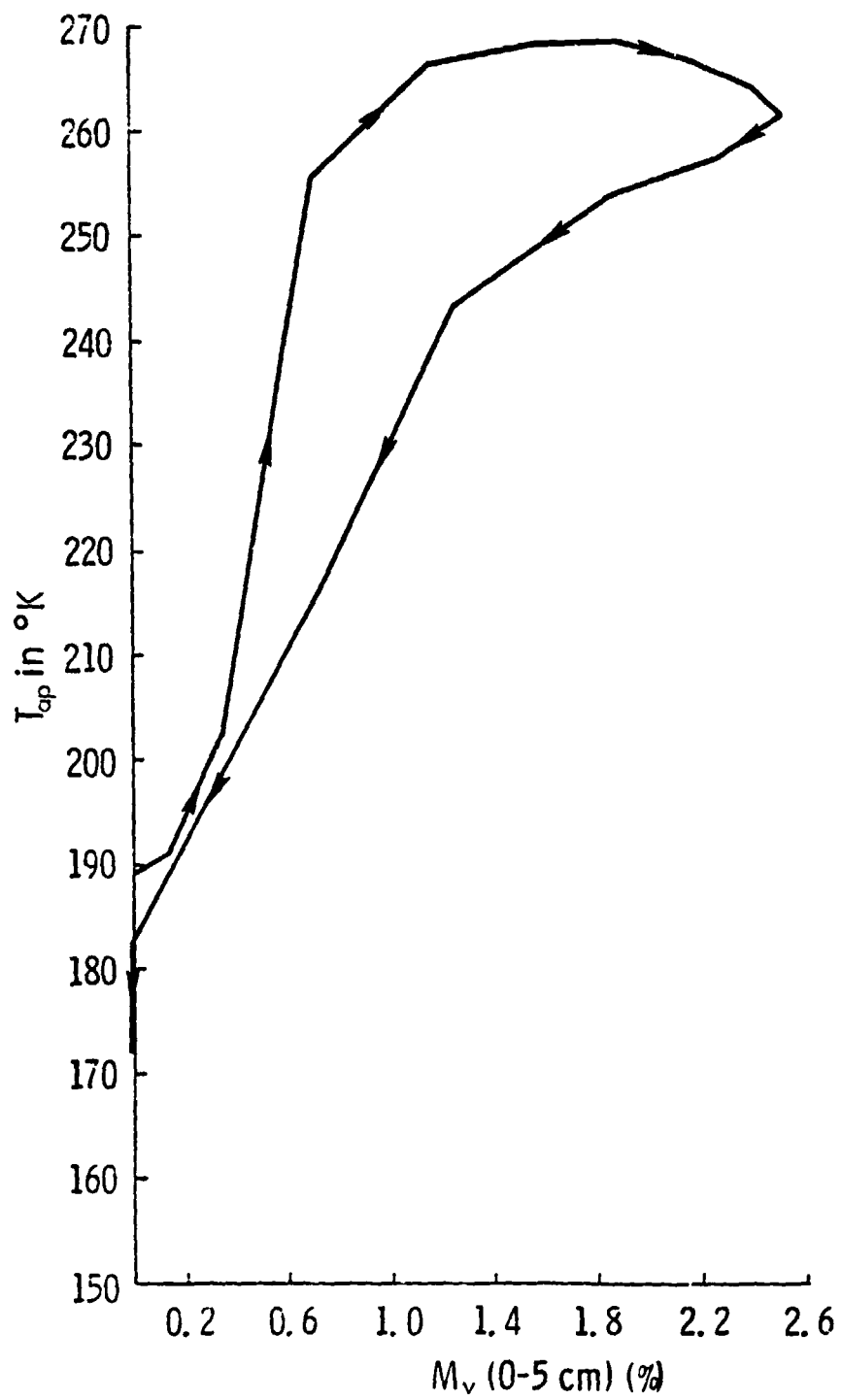


Figure 3-8 T_{ap} Response to Snow Wetness M_v . Showing the Hysteresis Effect at $\theta = 20^\circ$.

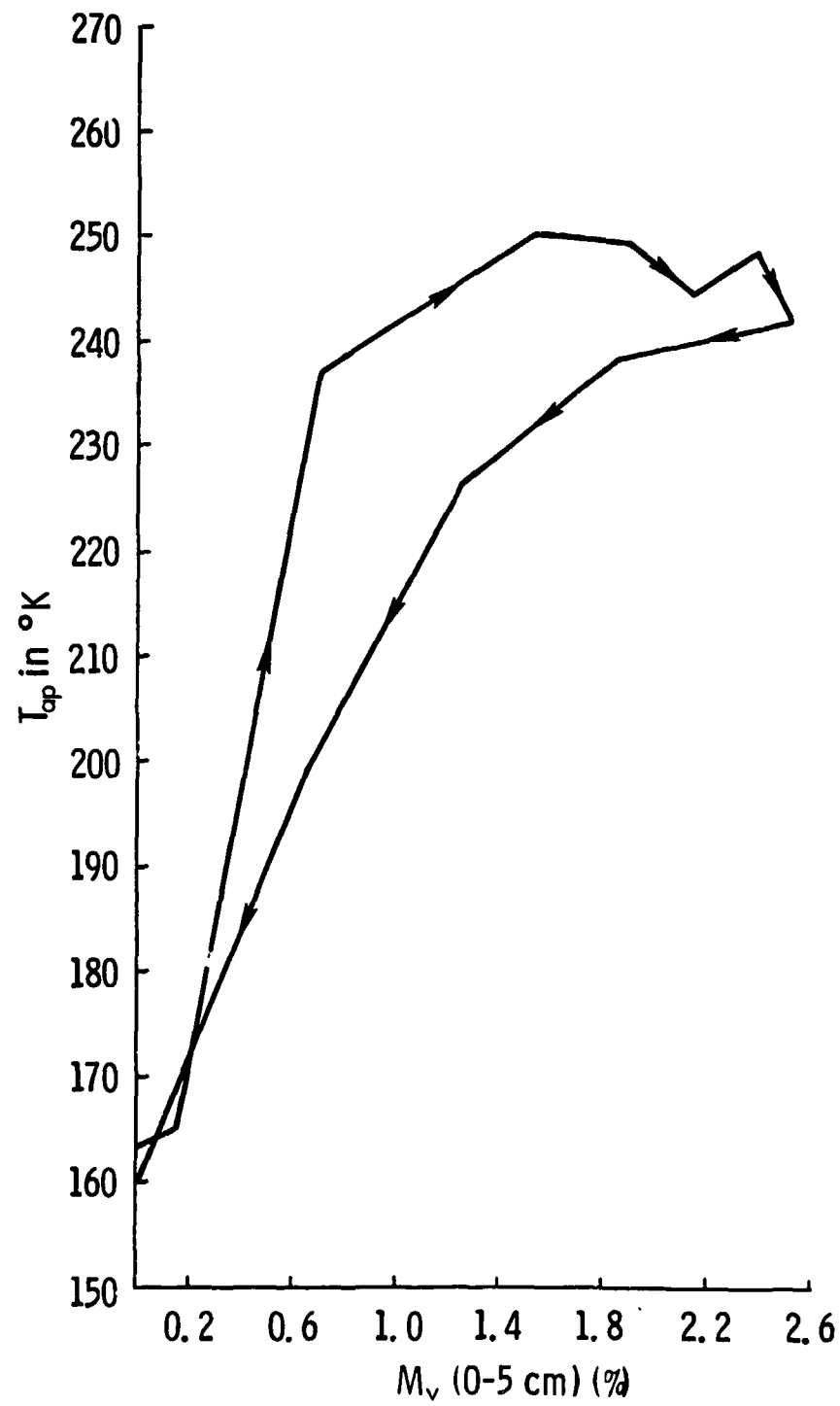


Figure 3-9 T_{ap} Response to Snow Wetness M_v , Showing the Hysteresis Effect at $\theta = 50^\circ$.

the top 5 cm snow layer therefore gives a value of wetness that is smaller than the actual wetness of the snow depth z which the sensor is sensitive at the melting stage and a larger value of wetness at the refreezing stage. This causes the T_{ap} response to lead M_v in the melting stage and to lag behind it in the refreezing stage which is shown in Figure 3-1 and is the cause of the hysteresis effect.

3.5 Depth Response

Stiles and Ulaby (1980) conducted an experiment in which they measured T_{ap} at 37 GHz for different snow depths and different angles of incidence. The depth of snow was varied by piling dry snow to a depth of 170 cm. Apparent temperature T_{ap} shows an exponential-like decrease with increasing water equivalence, as shown in Figure 3-10.

Data collected from an adjacent undisturbed snowpack shows values of T_{ap} that are considerably lower than those from the snow pile. This is due to the presence of ice layers in the natural snow and to differences in layering and in the distribution of crystal sizes which contribute to a larger scattering loss at 37 GHz and, therefore, lower emission.

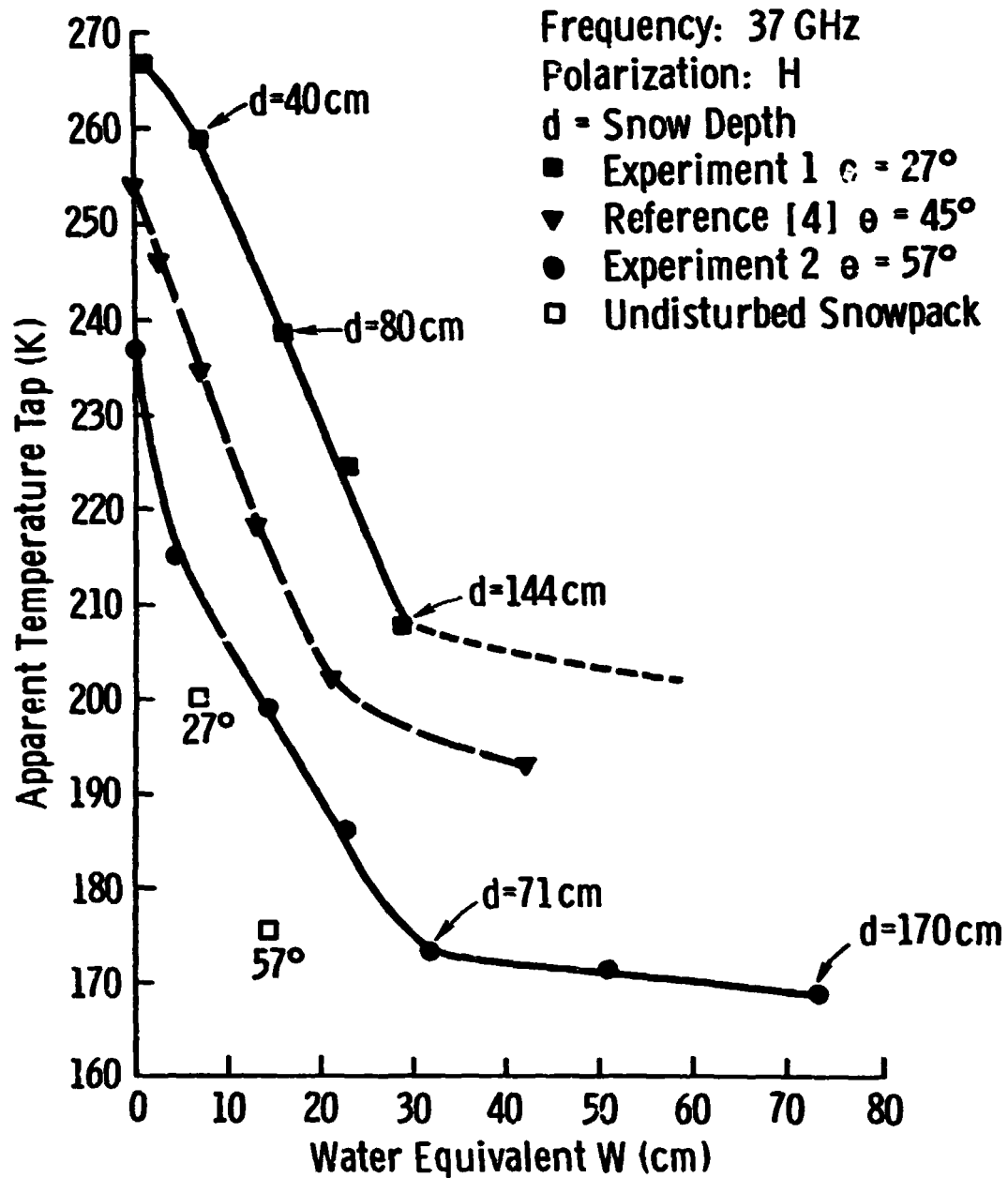


Figure 3-10 Radiometric Apparent Temperature Response to Snow Water Equivalent at 37 GHz (Stiles and Wiley, 1980).

4.0 MULTILAYER EMISSION MODEL DEVELOPMENT AND TESTING

The relationship between the measured microwave data (T_{ap}) from a snowpack and the physical and dielectric parameters of the snowpack can be examined through the development of models to explain this relationship. In the first section of this chapter, an emission model for snow is developed in a more general form. Later sections of this chapter show the use of a mixing formula to calculate the complex dielectric constant of snow at 37 GHz for different snow wetness. The calculated complex dielectric constant of snow is used along with the different forms of the emission model developed to estimate the absorption and scattering coefficients of snow at 37 GHz and their dependence on snow wetness. These coefficients are then used along with the snow model to estimate the values of T_{ap} measured throughout the diurnal experiment.

4.1 Development of the Multilayer Emission Model for Snow

Consider a snowpack of height d above the ground and consisting of N different snow layers. It is assumed that:

- (a) Each snow layer in the snowpack has a uniform thickness d_i cm, where i stands for the snow layer number from the soil surface up to the snow surface. Dielectric and thermal properties of each snow layer are assumed to be constant within the layer, at a given time.
- (b) The surface of the snow and the soil underneath the snowpack are smooth.
- (c) Multiple reflections at layer boundaries are ignored.
- (d) The radiation received by the radiometer is incoherent.

(e) Since the radiometer used in the experiment was a ground based system, there is neither attenuation nor emission between the surface of the snowpack and the radiometer.

(f) The snowpack is a layered scattering volume with κ_{ai} and κ_{si} taken to be the absorption and scattering coefficients of the i^{th} snow layer respectively. κ_{ei} is the sum of κ_{ai} and κ_{si} and is the extinction coefficient of the i^{th} snow layer. Explicitly, diffuse scatter is ignored; however it is understood that the above coefficients are effective values that at least partially compensate for this approximation.

The apparent temperature measured by the radiometer at different angles of incidence θ is given by:

$$T_{ap}(\theta) = T_B(\theta) + T_{sc}(\theta) \quad (4-1)$$

where T_B is the brightness temperature due to emission from the snowpack and the ground underneath it, and T_{sc} is the component of the downward emitted sky radiation scattered by the scene in the direction of the radiometer. The brightness temperature of the scene measured at an angle of incidence θ is given by:

$$T_B(N^+) = \tau_{na} T_B(N^-) \quad (4-2)$$

where

$T_B(N^+)$ = The brightness temperature measured directly
above the snow-air boundary, $^{\circ}\text{K}$

τ_{na} = The power transmission coefficient from layer N,
the uppermost layer of the snowpack to air

$T_B(N^-)$ = The brightness temperature measured directly below
the snow-air boundary

$T_B(N^-)$ is the sum of the components due to emission by all the layers within the snowpack $T_S(\text{SUM})$, and the component due to the emission by the ground T_G , therefore

$$T_B(N^-) = T_S(\text{SUM}) + T_G \quad (4-3)$$

Self-emission by a thin layer of snow of thickness Δh within the i^{th} layer of snow is given by:

$$T_{\text{sei}} = T_i \left[1 - \text{EXP} \left(-\kappa'_{ai} \rho_i \text{Sec } \theta'_i \Delta h \right) \right] \cong T_i \kappa'_{ai} \rho_i \text{Sec } \theta'_i \quad (4-4)$$

The letter i above is an indication of the position of the snow layer considered within the snowpack, starting with $i = 1$ for the snow layer on the bottom of the snowpack directly above the ground surface, and $i = N$ for the snow layer at the top of the snowpack directly below the snow-air boundary. T_i is the physical temperature of the i^{th} layer of snow, ρ_i is its density, κ'_{ai} is its absorption coefficient and θ'_i is the angle of propagation in the i^{th} snow layer relative to nadir.

The total emission by the i^{th} snow layer thickness d_i is

(Stiles and Ulaby, 1980):

$$T_{\text{si}} = T_i \int_0^{d_i} \rho_i \kappa'_{ai} \text{Sec } \theta'_i \text{Exp} \left[-(\kappa'_{ai} + \kappa'_{si}) \rho_i (d_i - h) \text{Sec } \theta'_i \right] dh \quad (4-5)$$

where κ'_{si} is the scattering coefficient of the i^{th} layer of snow.

After integration, Equation (4-5) reduces to:

$$T_{si} = T_i \left(\frac{\kappa_{ai}}{\kappa_{ai} + \kappa_{si}} \right) \left\{ 1 - \exp \left[-(\kappa'_{ai} + \kappa'_{si}) \rho_i d_i \sec \theta'_i \right] \right\} \quad (4-6)$$

The radiation emitted by the i^{th} snowlayer travels through the snow layers above it before it is seen directly below the air-snow boundary. The radiation emitted by the i^{th} layer of snow is, therefore, attenuated by the factor

$$\exp \left\{ \sum_{j=i+1}^N \left[-(\kappa'_{aj} + \kappa'_{sj}) \rho_j d_j \sec \theta'_j \right] \right\} \quad (4-7)$$

The above factor is the loss due to the propagation of the radiation emitted by the i^{th} snow layer through the $(N-i)$ snow layers above it.

Therefore

$$T_s(\text{SUM}) = \sum_{i=1}^N \left(\prod_i^{N-1} \tau_{i(i+1)} \right) \cdot T_{si} \exp \left\{ \sum_{j=i+1}^N \left[-(\kappa'_{aj} + \kappa'_{sj}) \rho_j d_j \sec \theta'_j \right] \right\} \quad (4-8)$$

$\tau_{i(i+1)}$ is the power transmission coefficient across the boundary between the i^{th} snow layer and the snow layer just above it. Similarly if T_g is the ground thermometric temperature underneath the snowpack and τ_{g1} is the power transmission coefficient at the ground-snow interface, the ground contribution measured directly below the snow-air boundary is:

$$T_G = \tau_{q1} \cdot T_g \cdot \prod_{i=1}^{N-1} \tau_i(i+1) \cdot \exp \left\{ \sum_{i=1}^N \left[-(\kappa'_{ai} + \kappa'_{si}) \rho_i d_i \sec \theta'_i \right] \right\} \quad (4-9)$$

τ_{q1} is the power transmission coefficient at the boundary between the ground and the lowermost snow layer (layer =1).

The value of T_{si} given by Equation (4-6) is substituted into Equation (4-8), and this later equation giving an expression for T_s (SUM) along with Equation (4-9) giving an expression for T_G , are substituted into Equation (4-3) producing a complete expression for $T_B(N^-)$. The final expression for $T_B(N^-)$ is substituted into equation (4-2) to give:

$$T_B(N^+) = \tau_{na} \sum_{i=1}^N \left(\prod_{i=1}^{N-1} \tau_i(i+1) \right) T_i \left(\frac{\kappa_{ai}}{\kappa_{ai} + \kappa_{si}} \right) \left\{ 1 - \exp \left[-(\kappa'_{ai} + \kappa'_{si}) \rho_i d_i \sec \theta'_i \right] \right\} \cdot \exp \left\{ \sum_{j=i+1}^N \left[-(\kappa'_{aj} + \kappa'_{sj}) \rho_j d_j \sec \theta'_j \right] \right\} + \tau_{na} \tau_{q1} T_g \left(\prod_{i=1}^{N-1} \tau_i(i+1) \right) \exp \left\{ \sum_{i=1}^N \left[-(\kappa'_{ai} + \kappa'_{si}) \rho_i d_i \sec \theta'_i \right] \right\} \quad (4-10)$$

The above equation describes the emission from a snowpack of N different layers above the ground and the emission from the ground underneath the snowpack. This equation when substituted into equation (4-1) gives the general expression of the model developed.

T_{sc} , the component of the downward emitted sky radiation scattered by the scene in the direction of the radiometer, shown in equation (4-1) is given as:

$$T_{sc}(\epsilon) = (1 - \tau_{na}) T_{sky} \quad (4-11)$$

T_{sky} is the downward emitted sky radiation. Equation (4-11) when added to Equation (4-10) produces an expression for the apparent temperature, T_{ap} , measured by the radiometer.

4.2 Calculations of the Dielectric Constant and the Power Absor., on Coefficient of Snow

In order to apply the emission model developed in the previous section and described by Equation (4-1), calculations of the power transmission coefficients at every boundary connecting two different snow layers and at the snow-air interface and the ground-snow interface are needed. In addition, values of the propagation angle in every snow layer and the absorption and scattering coefficients of every snow layer need to be calculated. To obtain all these values, the complex dielectric constant of snow at 37 GHz is needed as a function of snow wetness and snow density. Since measurements of the dielectric constant of snow at 37 GHz do not exist, one of the mixing formulas shown in Table 2-3 will be used. The Tinga et al. (1973) mixing formula is used to obtain the dielectric constant of snow as a function of its wetness and density at 37 GHz. The Tinga et al., mixing formula is used here because it was shown to yield good results by Tiuri and Schultz (1980) when used at 37 GHz. The radius of the ice particle R_i is taken to be 0.5 mm. ρ_s , the density of snow, was measured during the ground truth experiment, and previously reported in Section 3-3, equal to 0.21 g/cm³. The value of k_w , the dielectric constant of water

at 37 GHz, is obtained from Figure 2-1 and is $k_w = 9.55 - j 19.10$.

The value of k_i , the dielectric constant of ice at 37 GHz, is obtained from Figure 2-5 and is equal to $k_i = 3.15 - j 0.003$. The values of the dielectric constant of snow, obtained from the mixing formula, as a function of the percentage wetness by volume of the snow is shown in Table 4-1 and Figures 4.1 and 4.2.

The imaginary part of the dielectric constant of snow, k_s'' , shows a very small value when the snow is of zero wetness. However, this value increases substantially as the snow wetness increases by a very small amount, as shown in Table 4-1 for a percentage of snow wetness by volume of 0.1%. The difference in wetness between completely dry snow and that of 0.1% wetness by volume cannot be detected by any available experimental methods. This leads us to suspect that the value of the loss factor calculated for completely dry snow is unrealistic and, therefore, should be replaced by a value comparable to that calculated for a snow wetness of 0.1% by volume. If a linear fit is used to fit the values of k_s'' at percentages of snow wetness by volume of 0.1% and 0.2% and then the fit is extended to predict the value of k_s'' for snow of zero wetness, the value of k_s'' predicted is 0.0015 as shown in Figure 4-3. This value is very close to that reported by Sweeny and Colbeck (1974) who experimentally measured the loss factor for dry snow at a frequency of 6 GHz and found it to be 0.003. Hence, the value $k_s'' = 0.003$ is the one chosen in the investigation for $M_v = 0$.

The values of k_s' and k_s'' obtained by the mixing formula of Tinga et al. (1973) and modified at one value of k_s'' for dry snow are sub-

TABLE 4-1

The Dielectric Constant of Snow
as a Function of the Percentage Wetness by Volume of Snow
at 37 GHz, Calculated by the Tinga et al. Mixing Formula.

M_v	k'_s	k''_s
0.0	1.317	0.2844×10^{-3}
0.1	1.319	0.5852×10^{-2}
0.2	1.321	0.0113
0.3	1.323	0.0168
0.4	1.326	0.0221
0.5	1.328	0.0273
0.6	1.331	0.0325
0.7	1.334	0.0376
0.8	1.337	0.0426
0.9	1.339	0.0475
1.0	1.342	0.0523
1.1	1.344	0.0547
1.2	1.345	0.0571
1.3	1.348	0.0617
1.4	1.351	0.0662
1.5	1.355	0.0707
1.6	1.358	0.0751
1.7	1.361	0.0793
1.8	1.364	0.0835
1.9	1.368	0.0876
2.0	1.371	0.0916
2.1	1.375	0.0954
2.2	1.378	0.0992
2.3	1.382	0.1029
2.4	1.385	0.1065
2.5	1.389	0.1101
2.6	1.392	0.1135
2.7	1.395	0.1168
2.8	1.400	0.1200
2.9	1.403	0.1232

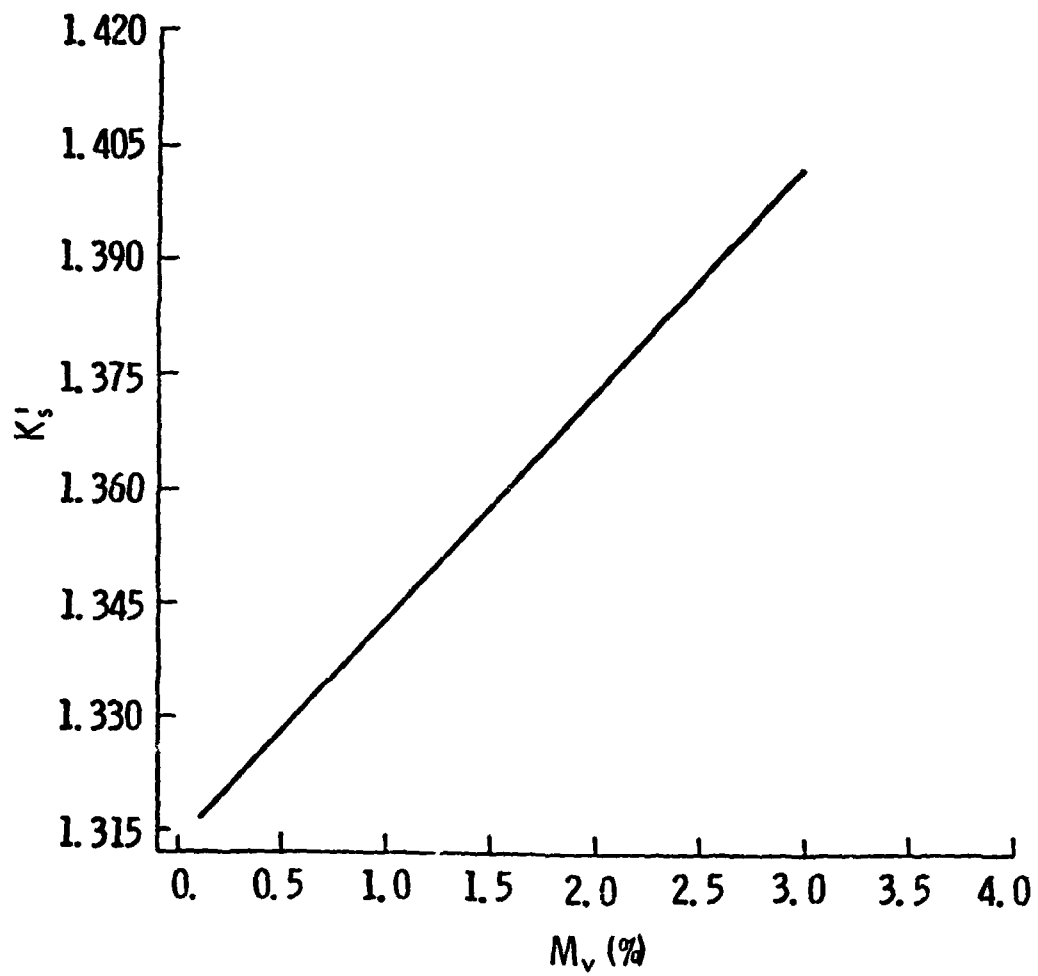


Figure 4-1 The real Part of the Dielectric Constant of Snow k'_s , as a Function of M_v , the Percentage Wetness by Volume of Snow as Calculated by Tinga et al. (1973) Mixing Formula.

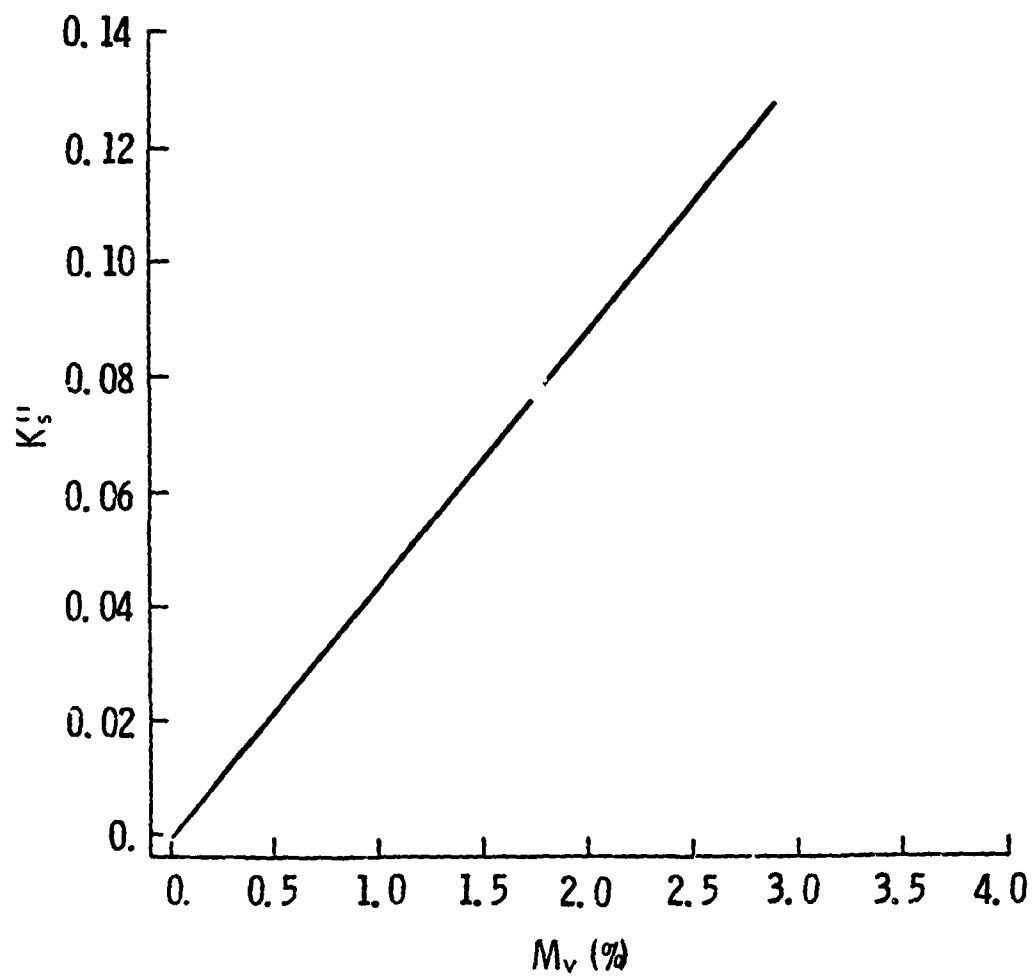


Figure 4-2 The Imaginary Part of the Dielectric Constant of Snow k''_s , as a Function of M_v , the Percentage Wetness by Volume of Snow as Calculated by Tinga et al. (1973) Mixing Formula.

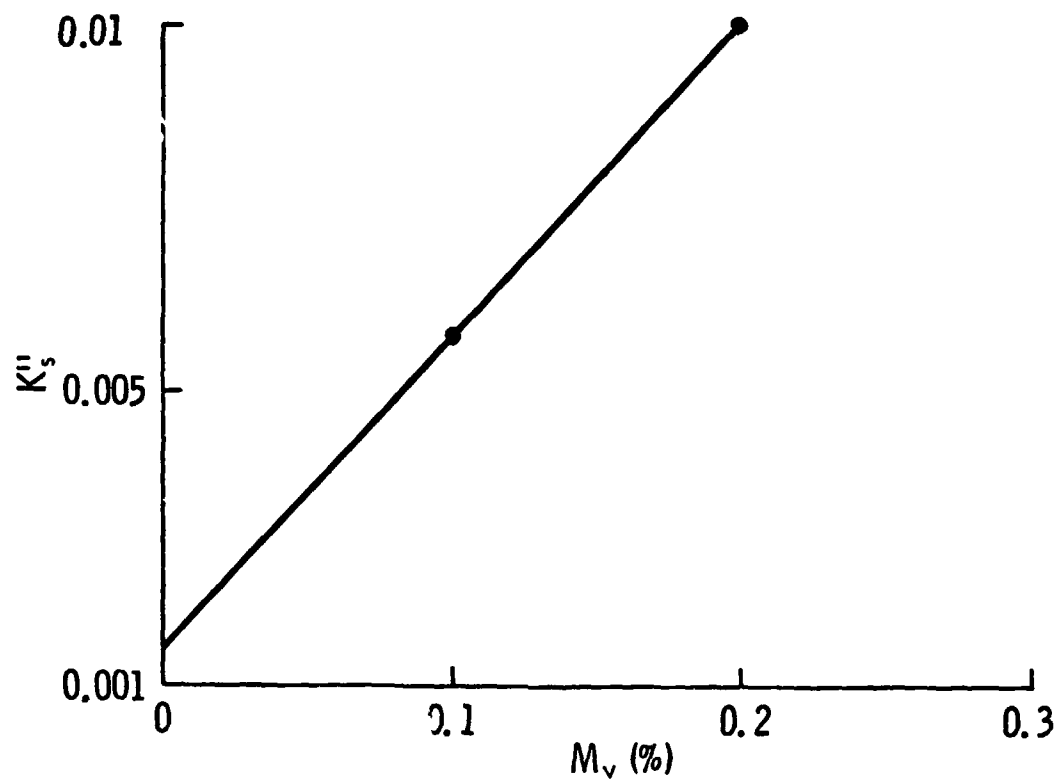


Figure 4-3 A Linear Fit for the Calculated Loss Factor Using the Tinga et al. (1973) Mixing Formula at 0.1% and 0.2% Wetness by Volume. The Fit is Extended to Predict a Value of K''_s for Dry Snow.

stituted in equation (2-8) to give the values of α_a , the field absorption coefficient of snow as a function of the snow wetness. The corresponding values of κ_a ,

$$\kappa_a = 2\alpha_a \quad (4-12)$$

where κ_a is the power absorption coefficient in Nep/cm, are shown in Table 4-2. Figure 4-4 shows a plot of κ_a in Nep/cm versus the percentage wetness by volume of snow, M_v . This figure shows that the dependence of κ_a on wetness is linear and its linear best fit is given by:

$$\kappa_a = 0.0203 + 0.2741 M_v, \text{ Nep/cm} \quad (4-13)$$

The equation above is used throughout the rest of this investigation to describe the power absorption coefficient of snow at 37 GHz.

4.3 Emission Model for a Single Homogeneous Snow Layer:

During the diurnal experiment conducted on 2/17 - 2/18/77 by Stiles and Ulaby (1980) the total depth of the snowpack above the ground was 30 cm. The snowpack was divided into four layers. The thermometric temperatures of each snow layer were measured throughout the experiment and are shown in Table 3-1. The percentage wetness by volume, M_v , of each snow layer ~~were~~^{was} measured throughout the experiment and ~~are~~^{is} shown in Figure 3-2. T_{ap} measurements for $\theta = 0^\circ$, 20° and 50° , as measured by the radiometer are reported in Figure 3-1. Combining the results shown in Table 3-1 and Figure 3-2, produces 21 complete

TABLE 4-2

Values of κ_a in Nep/cm as a Function of Snow Wetness

M_v (%)	κ_a in Nep/cm
0.0	0.2030×10^{-1}
0.11	0.3949×10^{-1}
0.21	0.7649×10^{-1}
0.32	0.1129
0.42	0.1487
0.53	0.1839
0.63	0.2184
0.74	0.2523
0.84	0.2855
0.95	0.3181
1.05	0.3500
1.15	0.3812
1.26	0.4117
1.36	0.4416
1.47	0.4707
1.58	0.4992
1.68	0.5269
1.78	0.5539
1.89	0.5803
1.99	0.6059
2.10	0.6309
2.20	0.6551
2.31	0.6787
2.41	0.7016
2.52	0.7237
2.62	0.7453

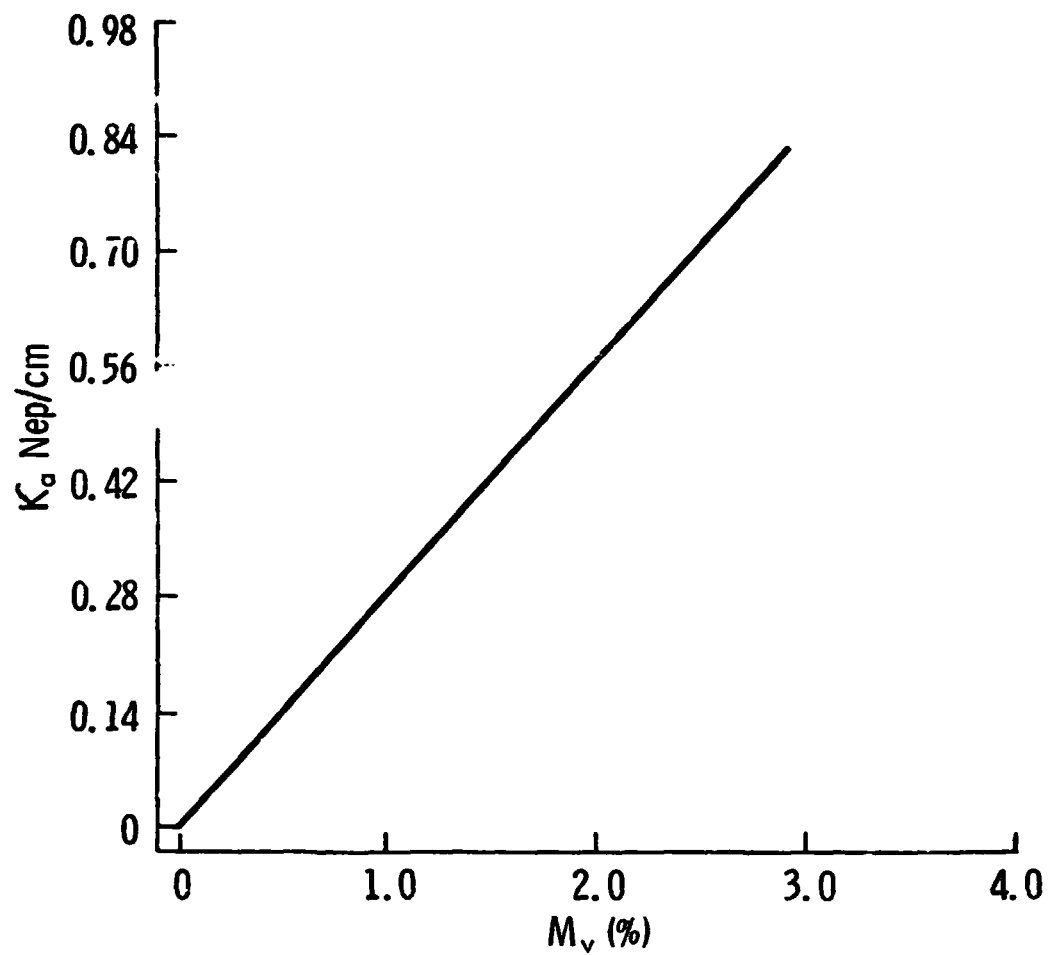


Figure 4-4 κ_a in Nep/cm as a function of M_v , the Percentage Wetness by Volume of Snow.

ground truth and microwave measurements at different times in the diurnal experiment. For eight out of the 21 different measurements, the snow was totally dry in all its layers within the snowpack.

In this first application of the model described by equations (4-10) and (4-11), the snowpack is assumed to be made up of one homogeneous snow layer that is 30 cm thick. The thermometric temperature of this homogeneous snow layer, its density and its wetness are assumed similar to those measured for the top 5 cm snow layer of the snowpack. In other words, an attempt will be made in this section to see whether the temperature, wetness and density of the top 5 cm layer of snow can be used to represent the whole snowpack.

When Equation (4-10) is used to describe the emission from one layer of snow above the ground it reduces to:

$$T_B = \tau_{sa} T_1 \left(\frac{\kappa_{a1}}{\kappa_{a1} + \kappa_{s1}} \right) \left\{ 1 - \exp \left[-(\kappa'_{a1} + \kappa'_{s1}) \rho_1 d_1 \sec \theta'_1 \right] \right\} + \tau_{gs} \tau_{sa} T_g \exp \left[-(\kappa'_{a1} + \kappa'_{s1}) \rho_1 d_1 \sec \theta'_1 \right] \quad (4-14)$$

where

- τ_{sa} = Power transmission coefficient at the snow-air boundary,
- τ_{gs} = Power transmission coefficient at the ground-snow boundary,
- T_1 = The snow thermometric temperature in $^{\circ}\text{K}$.

The equation above is solved in the following way:

(a) T_1 , the snow thermometric temperature values were shown in Table 3-1. T_1 values used are those reported for the top 5 cm snowlayer. These temperatures are assumed indicative of the whole snowpack.

(b) ρ_1 , the density of snow was measured during the ground truth experiment and reported equal to 0.21 g/cm^3 . This value did not change throughout the diurnal experiment.

(c) d_1 , the total depth of the snowpack was measured throughout the experiment and was equal to 30 cm. The depth of the snowpack did not change throughout the diurnal experiment.

(d) T_g , the thermometric temperature of the ground underneath the snow was measured for the top few centimeters of the ground and was equal to 273^0K . That is the ground was frozen throughout the diurnal experiment.

(e) The relative dielectric constant of frozen ground k_g is assumed equal to 3.

(f) The power transmission coefficient τ_{sa} at the snow-air boundary is calculated for each of the 21 measurements considered using.

$$\tau_{sa} = 1.0 - \left| \frac{\cos \theta - \sqrt{k_s - \sin^2 \theta}}{\cos \theta + \sqrt{k_s + \sin^2 \theta}} \right|^2 \quad (4-15)$$

where

θ = The look angle of the radiometer, 0^0 , 20^0 and 50^0 .

$k_s = k'_s - jk''_s$ = The complex dielectric constant of snow.

τ_{sa} is a function of the radiometer's look angle and the snow dielectric constant. The snow dielectric constant is calculated using the Tinga et al. (1973) mixing formula shown in Table 2-3, for each of the 21 different measurements considered. τ_{sa} is calculated as shown above for the different k_s values and are shown as a function of the percentage wetness by volume of snow in Figures 4-5, 4-6 and 4-7 for $\theta = 0^\circ, 20^\circ$ and 50° respectively.

(g) The propagation angles in the snow layer are calculated using Snell's law given below as:

$$\sec \theta'_s = \frac{\sqrt{k_s}}{\sqrt{k_s - \sin^2 \theta}} \quad (4-16)$$

The propagation angle, θ'_s , is a function of the snow dielectric constant and, therefore, is a function of the snow wetness.

(h) The power transmission coefficient τ_{gs} at the ground-snow boundary is calculated using a similar expression to that shown by Equation (4-15), that is:

$$\tau_{gs} = 1.0 - \left| \frac{\cos \theta'_s - \sqrt{k_g/k_s - \sin^2 \theta'_s}}{\cos \theta'_s + \sqrt{k_g/k_s - \sin^2 \theta'_s}} \right|^2 \quad (4-17)$$

k_g is the dielectric constant of ground. τ_{gs} is calculated for each of the 21 different measurements considered and for the different propagation angles in the snow layer.

(i) The value of κ_a is taken equal to that previously shown by equation (4-13).

(j) The scattering coefficient κ_s , is assumed to have the form:

$$\kappa_s = A + BM_v \quad (4-18)$$

That is κ_s is assumed to have a linear dependence on the snow wetness M_v , similar to κ_a . A and B are constants to be determined.

(k) T_{sc} , the downward emitted sky radiation scattered by the snowpack in the direction of the radiometer and previously shown by Equation (4-11), is assumed to be small in value and is neglected in this analysis. That is T_B , the brightness temperature of the snow and the ground underneath as described by Equation (4-10) is taken equal to T_{ap} , the apparent temperature measured by the radiometer at $\theta = 0^\circ$, 20° and 50° . This is because as shown in Figures 4-5, 4-6 and 4-7 for τ_{sa} as a function of M_v at $\theta = 0^\circ$, 20° and 50° respectively, the minimum value of τ_{sa} calculated is 0.9715 for $\theta = 50^\circ$ and $M_v(\%) = 2.53$. This value when substituted into Equation (4-11) and T_{sky} is taken equal to 300°K , the maximum possible value for T_{sky} , T_{sc} is only equal to 8.55°K . This value is small enough to be neglected. T_{ap} values measured are shown in Figure 3-1.

The values calculated by steps (a) - (k) above are substituted into Equation (4-14). This produces 21 equations, each describing the emission from the homogeneous layer of snow at a particular time throughout the diurnal^o experiment. These equations are solved using non-linear regression analysis (BMDP, UCLA: 1977) to estimate the values of the constants A and B. This is done by solving Equation (4-14) for the eight measurements in which snow was totally dry in all its layers. In this case Equations (4-13) and (4-18) reduce to:

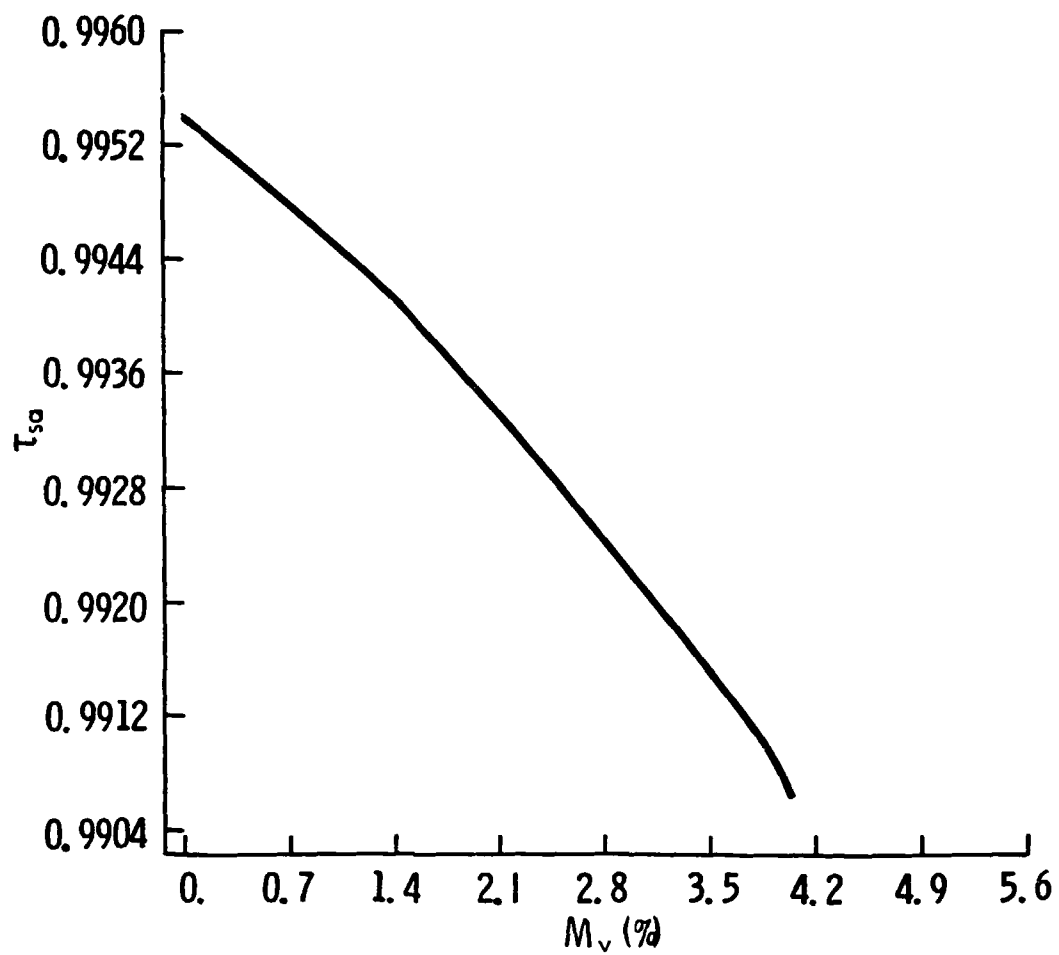


Figure 4-5 τ_{sa} , the Power Transmission Coefficient at the Snow-Air Boundary as a Function of M_v , the Percentage Wetness by Volume of Snow at $\theta = 0^\circ$.

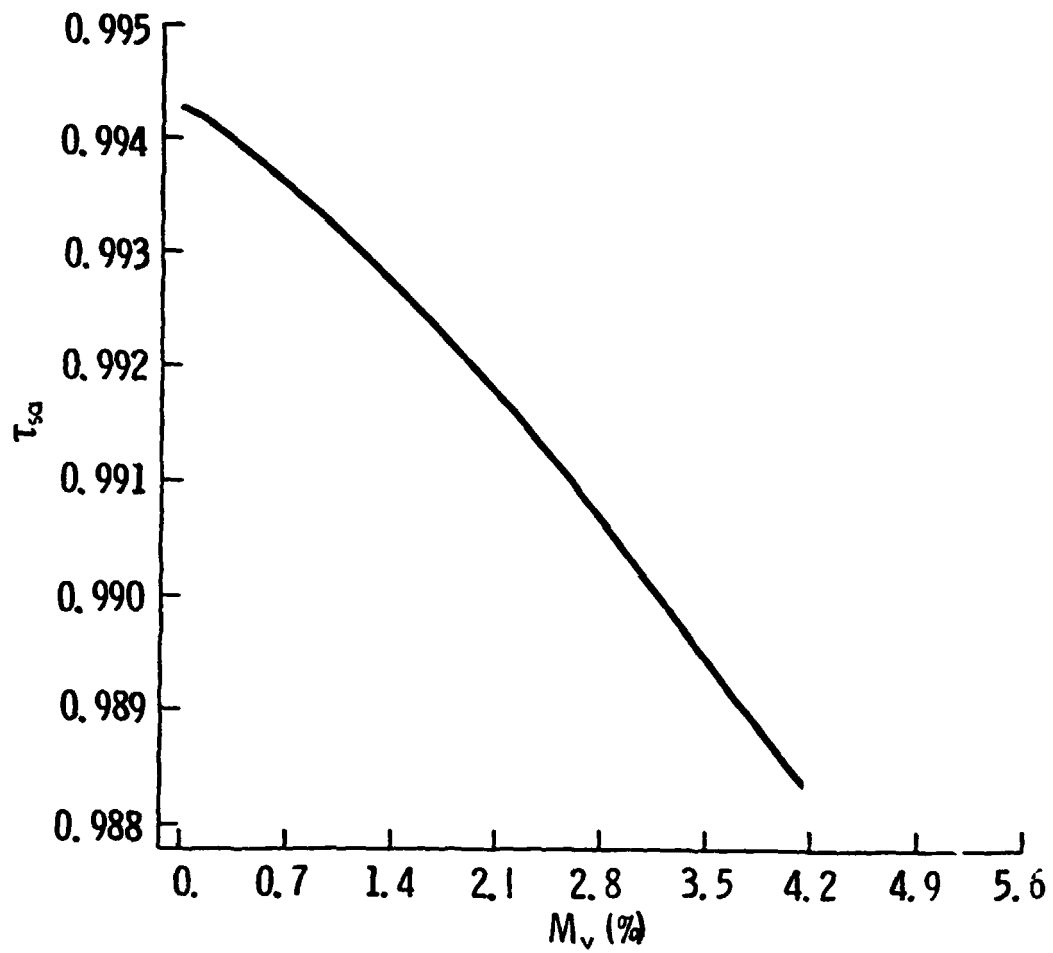


Figure 4-6 τ_{sa} , the Power Transmission Coefficient at the Snow-Air Boundary as a Function of M_v , the Percentage Wetness by Volume of Snow at $\theta = 20^\circ$.

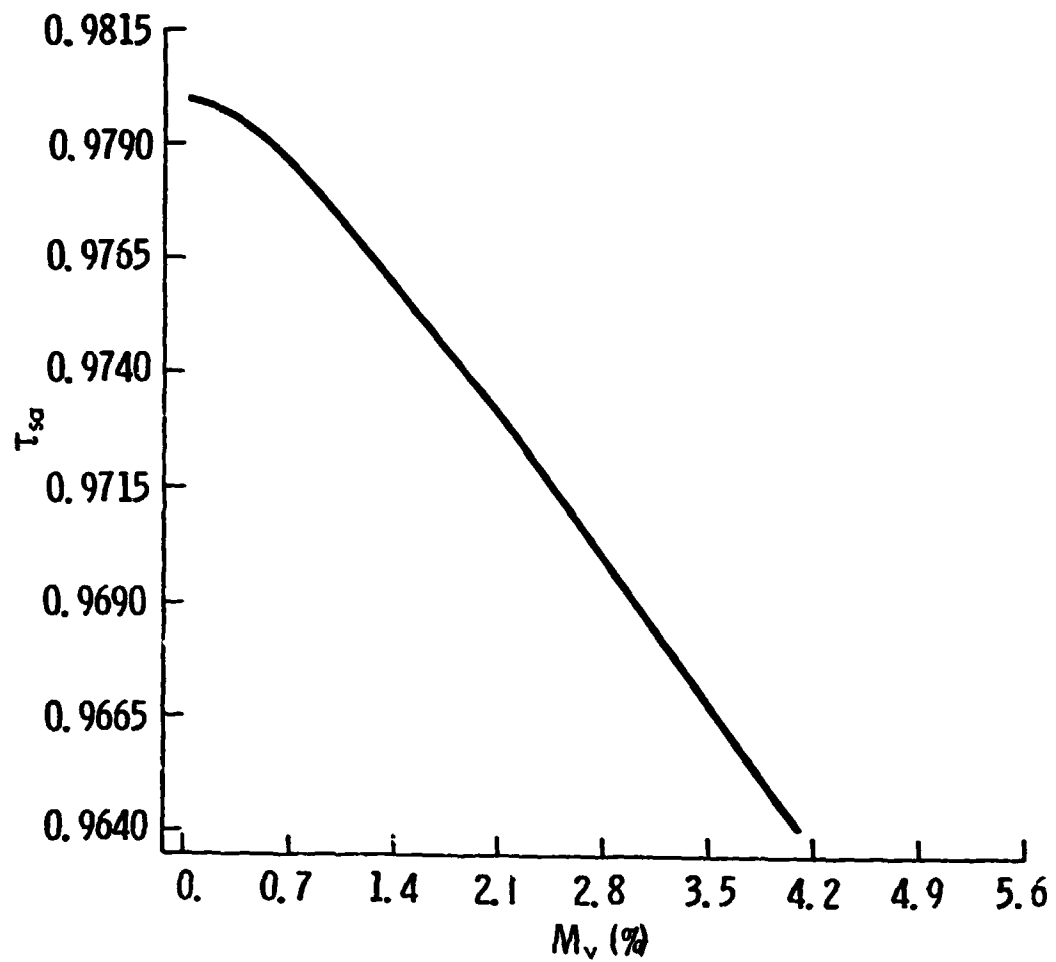


Figure 4. τ_{sa} , the Power Transmission Coefficient at the Snow-Air Boundary as a Function of M_v , the Percentage Wetness by Volume of Snow at $\theta = 50^\circ$.

$$\kappa_a = 0.0203 \quad , \text{ Nep/cm} \quad (4-19)$$

and

$$\kappa_s = A \quad , \text{ Nep/cm} \quad (4-20a)$$

Once the value of A has been estimated, it is substituted into Equation (4-18) and the expression for κ_s with only constant B unknown is substituted into Equation (4-14). Non-linear regression analyses are carried out for both the dry and wet snow conditions to estimate the value of the Constant B. The results of these analyses show that:

$$A = 0.0171 \quad \text{Nep/cm} \quad (4-20b)$$

$$B = 0$$

The above equation gives a value for the scattering coefficient of snow at 37 GHz. κ_s predicted shows no dependence on snow wetness. Figure 4-8 shows a plot of κ_a , κ_s and κ_e as predicted by this model as a function of M_v , the percentage wetness by volume of the snow layer.

The values of κ_a and κ_s shown by Equations (4-13) and (4-20b) respectively are now substituted into Equation (4-10) and this equation is solved for the 21 different measurements to produce estimates of T_B at different times throughout the diurnal experiment. Figures 4-9, 4-10 and 4-11 show the observed T_{ap} measurement along with the calculated T_B values as a function of time along the diurnal for $\theta = 0^\circ$, 20° and 50° respectively. For all the three angles considered, the predicted

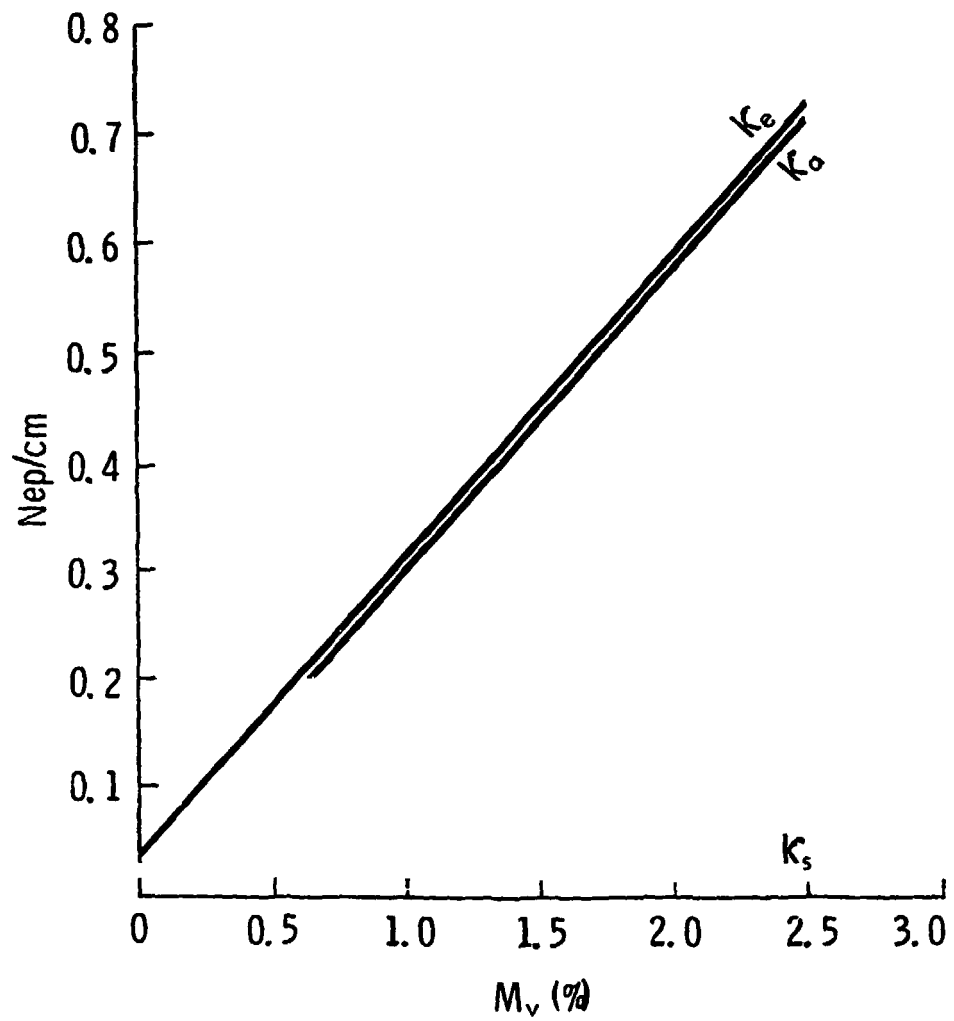


Figure 4-8 κ_a , κ_s and κ_e as a Function of Snow Wetness as Predicted by the Single Homogeneous Snowlayer Model.

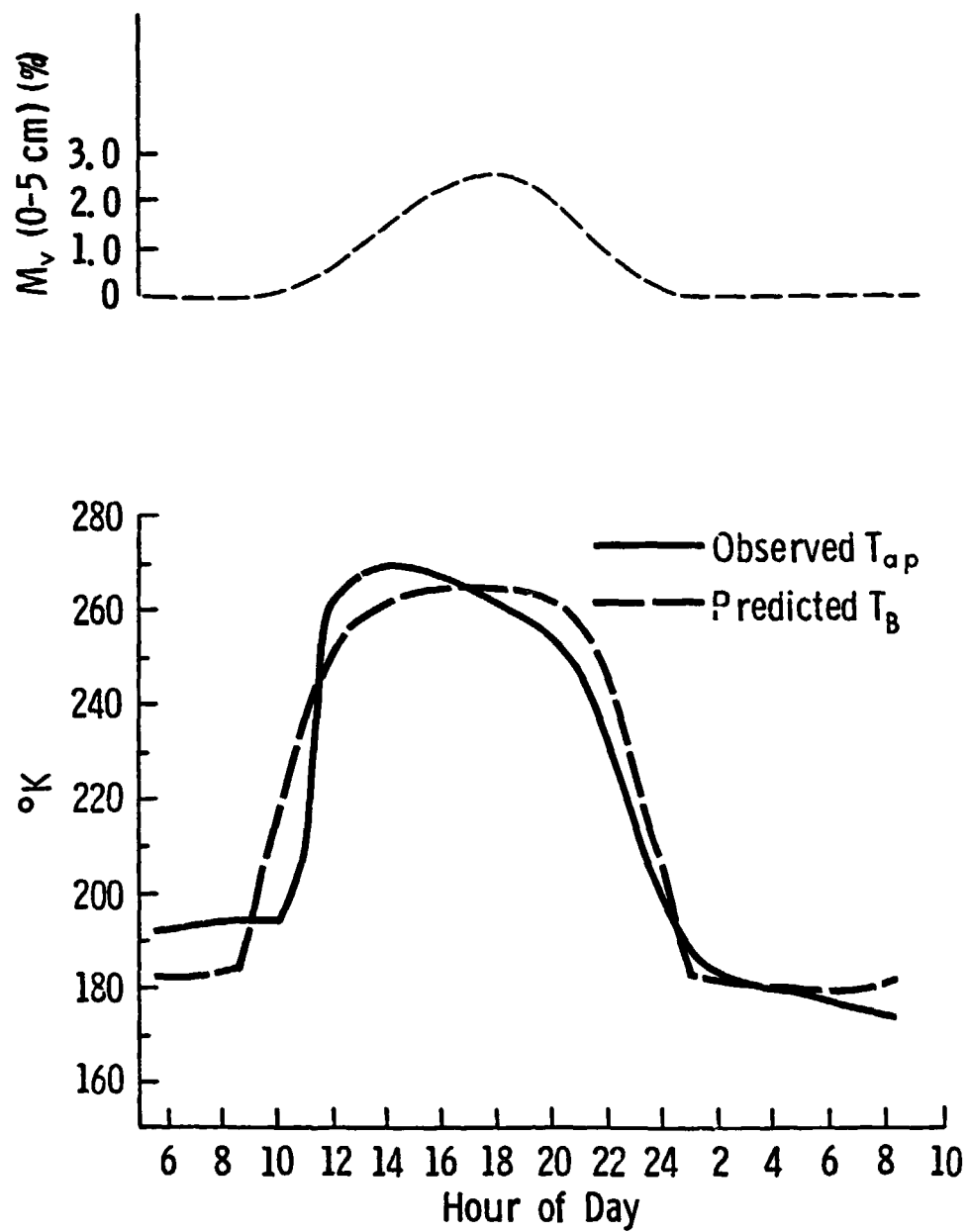


Figure 4-9 Observed T_{ap} and T_B Predicted by the Single Homogeneous Snowlayer Model as a Function of Time at $\theta = 0^{\circ}$.

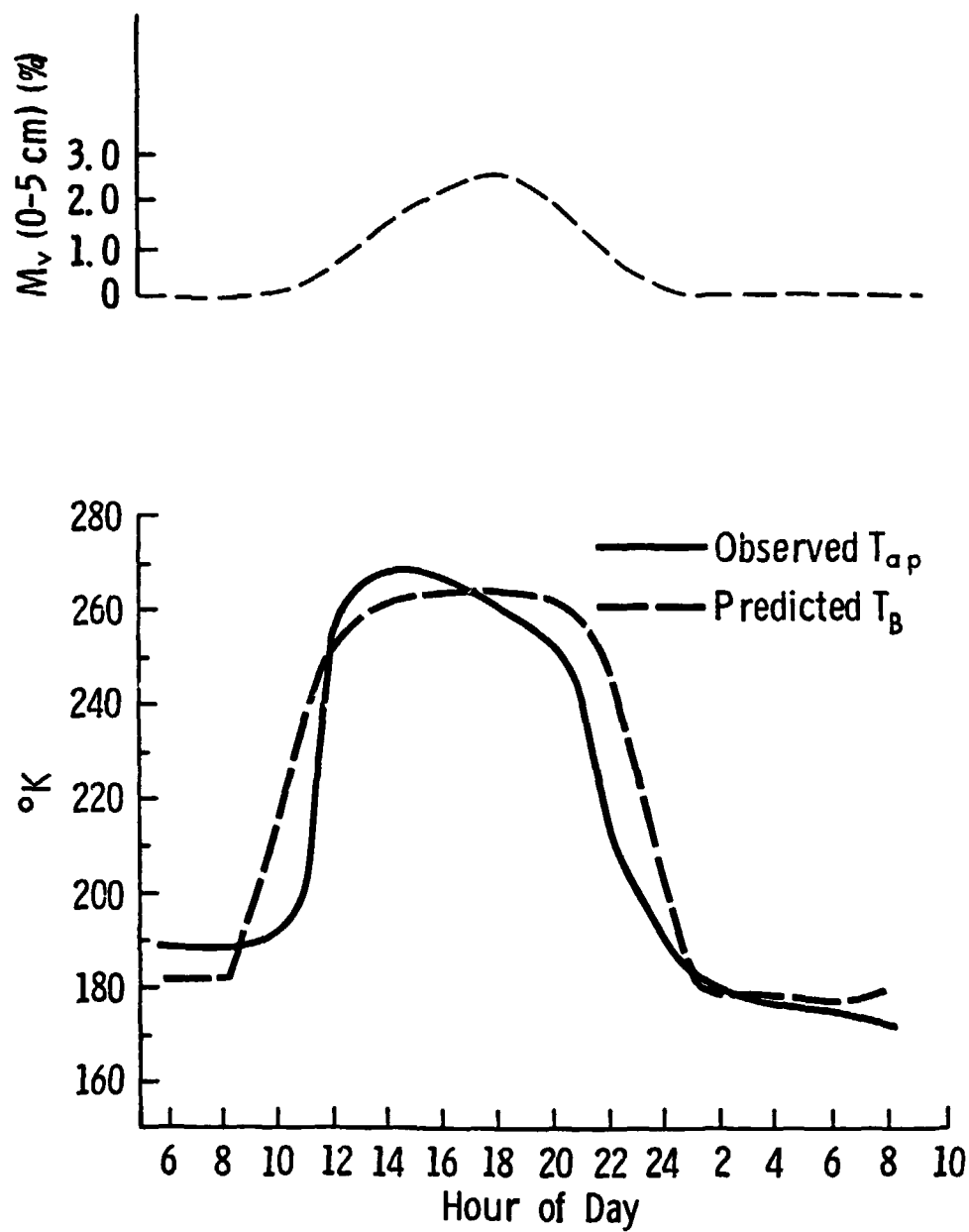


Figure 4-10 Observed T_{ap} and T_b Predicted by the Single Homogeneous Snowlayer Model as a Function of Time at $\theta = 200^{\circ}$.

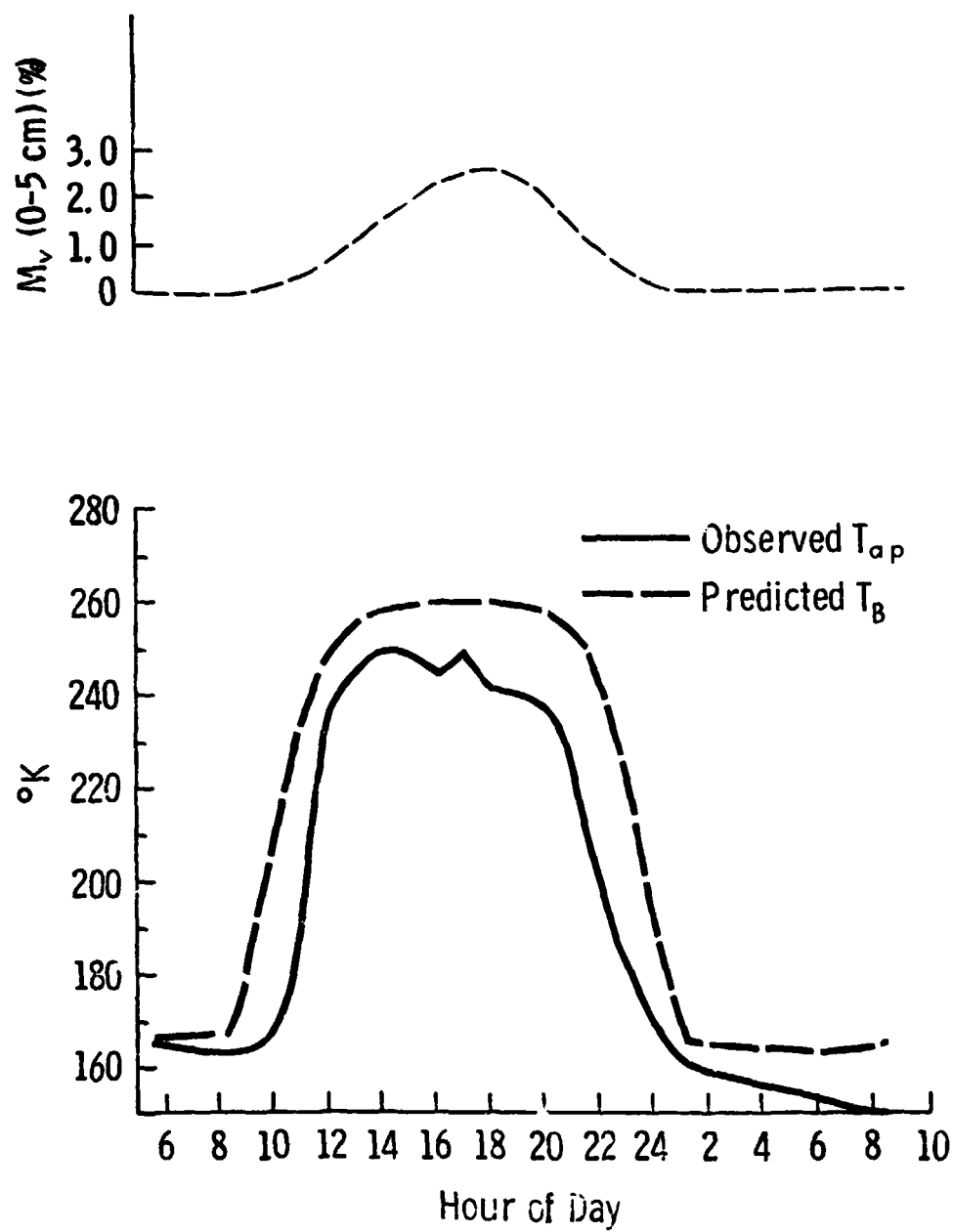


Figure 4-11: Observed T_{ap} and T_b Predicted by the Single Homogeneous Snowlayer Model as a Function of Time at $\epsilon = 50^{\circ}$.

T_B response leads that of the observed T_{ap} response when the snow is melting and lags behind it when the snow is refreezing. This is due to the fact that the response of the predicted T_B is a function of the snow wetness of the top 5 cm layer of snow. The wetness of the top 5 cm layer of snow is assumed here to be descriptive of the whole snowpack. However, the wetness of the top 5 cm layer of snow experimentally shows higher values of wetness than the rest of the sub-snow layers when the snow is melting and in turn shows lower wetness values than the rest of the sub-snow layers when the snow is refreezing.

4.4 Emission Model for a Multilayered Snowpack

As was previously mentioned in the last section, the snowpack during the 2/17 - 2/18/77 diurnal experiment had a total depth of 30 cm and ^{was} modeled to consist of four distinct snow layers. Figure 4-12 shows the thickness of each of the snow layers within the snowpack. In this analysis, Equation (4-10) describing the emission from a multilayered snowpack is used to estimate the value of κ_s and its dependence on snow wetness. The snowpack in this case is treated as consisting of four distinct snow layers.

Equation (4-10) is solved in a similar manner to that previously discussed in Section 4-3. In this case, however, the power transmission coefficients are calculated at every boundary between the snow layers, the boundary between the uppermost snow layer and the air, and the boundary between the ground and the lowermost snow layer. Similarly the propagation angles are calculated in each snow layer for the three different look angles. Values of the thermometric temperatures in each layer and the wetness M_v of each layer for the 21 different times

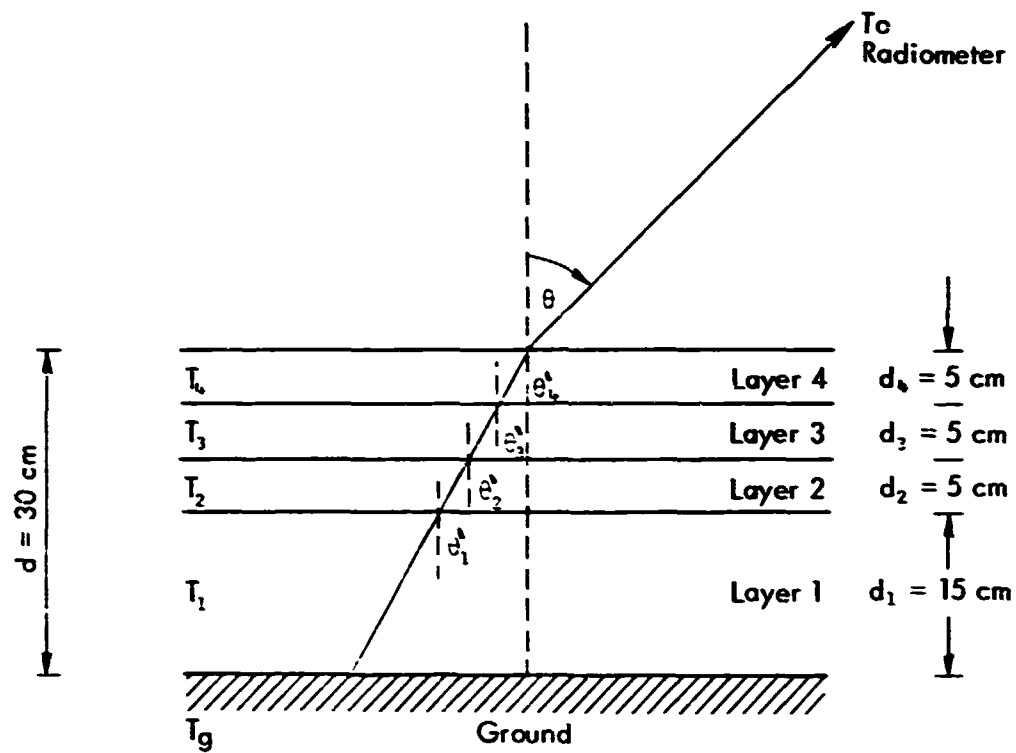


Figure 4-12 A Geometrical Presentation of the Snowpack Cross Section During the 2/17/77 - 2/18/77 Diurnal Experiment.

1-2

considered throughout the diurnal ^{a period} are shown in Table 3-1 and Figure 3-2 respectively. ρ , the density of the snow was reported equal to 0.21 g/cm³ for all the snow layers throughout the diurnal experiment. The results of this analysis gives

$$\kappa_s = 0.0175 - 0.0046 M_v \quad \text{Nep/cm} \quad (4-21)$$

That is κ_s , the scattering coefficient, is smaller in value than the absorption coefficient, κ_a , for dry snow. Also, κ_a increases linearly with increasing wetness but, κ_s decreases linearly with increasing wetness as shown in Figure 4-13. The rate of decrease of κ_s with wetness is very small as shown by Equation (4-21).

Figures 4-14, 4-15 and 4-16 show the T_{ap} observed during the diurnal experiment along with the T_B predicted by the multilayer model at $\lambda = 0^\circ$, 20° and 50° respectively. The values of T_B are calculated by substituting the values of κ_a and κ_s of every layer into Equation (4-10) along with the other parameters to give the calculated values of T_B throughout the diurnal experiment. It would be seen from Figures 4-14, 4-15 and 4-16 that T_B calculated still leads T_{ao} observed by the radiometer when the snow is melting and lags behind it when the snow is refreezing. However, the difference in values between T_{ap} observed and T_B predicted is smaller than those previously shown for the single homogeneous layer model. The fits shown by Figures 4-14, 4-15 and 4-16 are, therefore, better fits for they produce estimates of T_B that are closer in value to the T_{ap} measured by the radiometer.

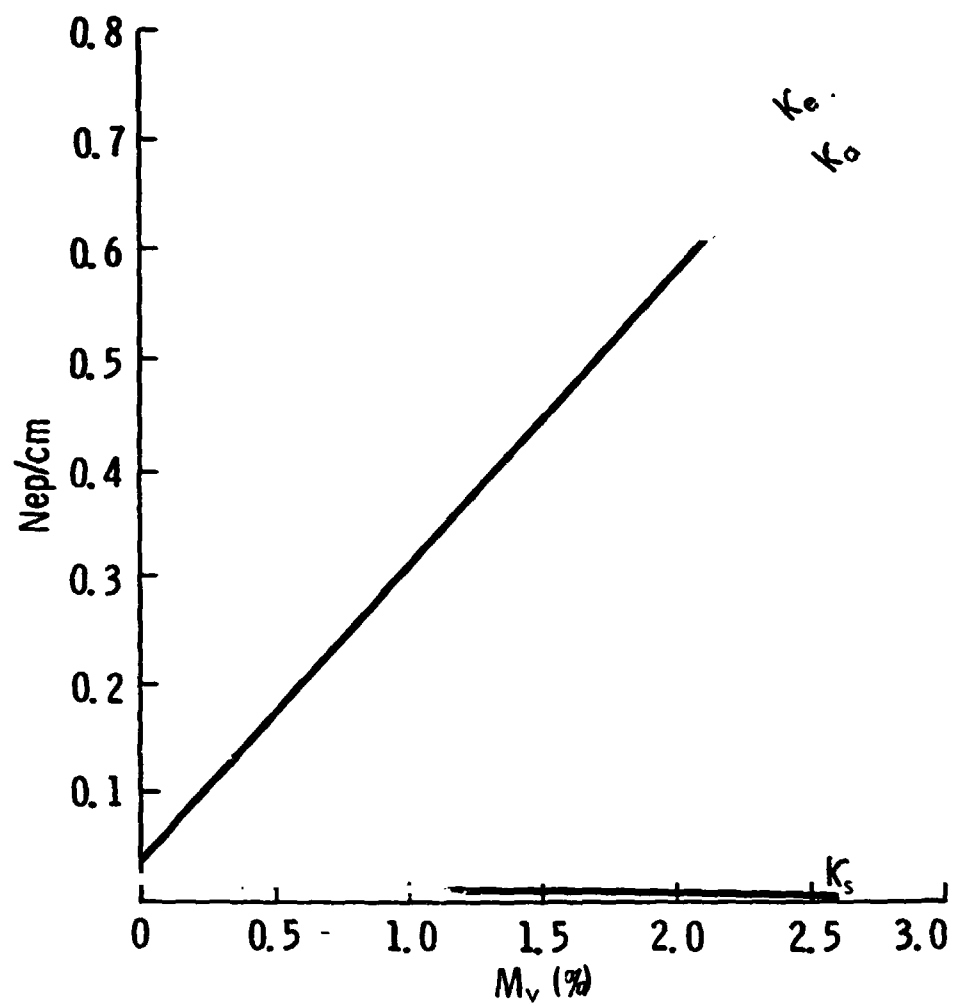


Figure 4-13 κ_a , κ_s and κ_e for Snow as a Function of Snow Wetness at 37 GHz Estimated by the Multilayered Emission Model.

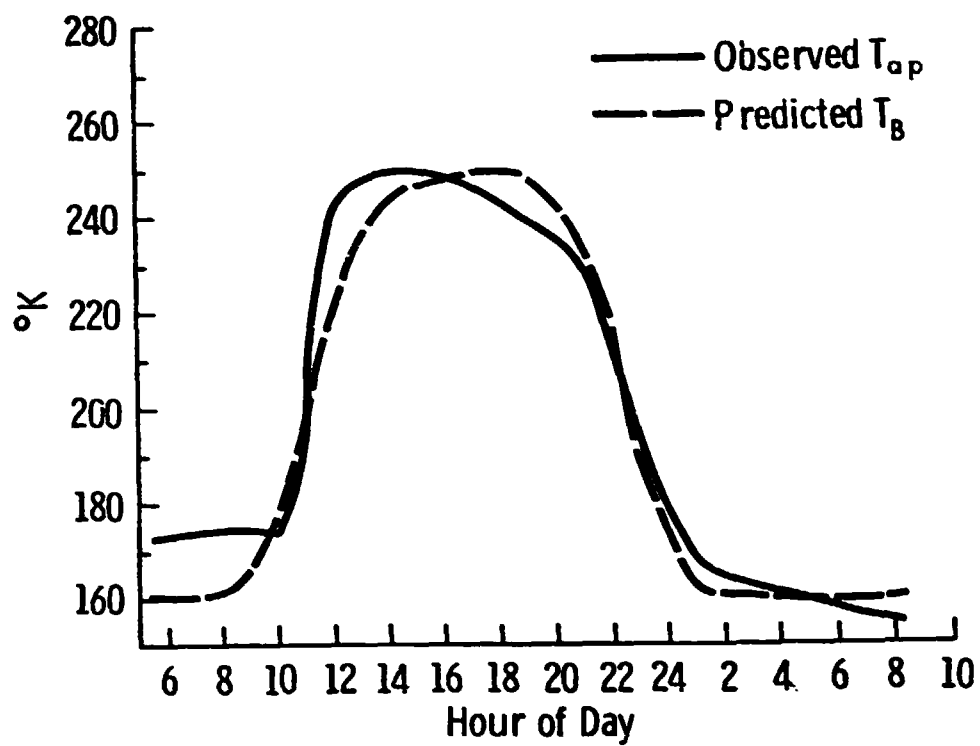


Figure 4-14 Observed T_{ap} and T_b Predicted by the Multilayered Emission Model as a Function of Time at $\theta = 0^\circ$.

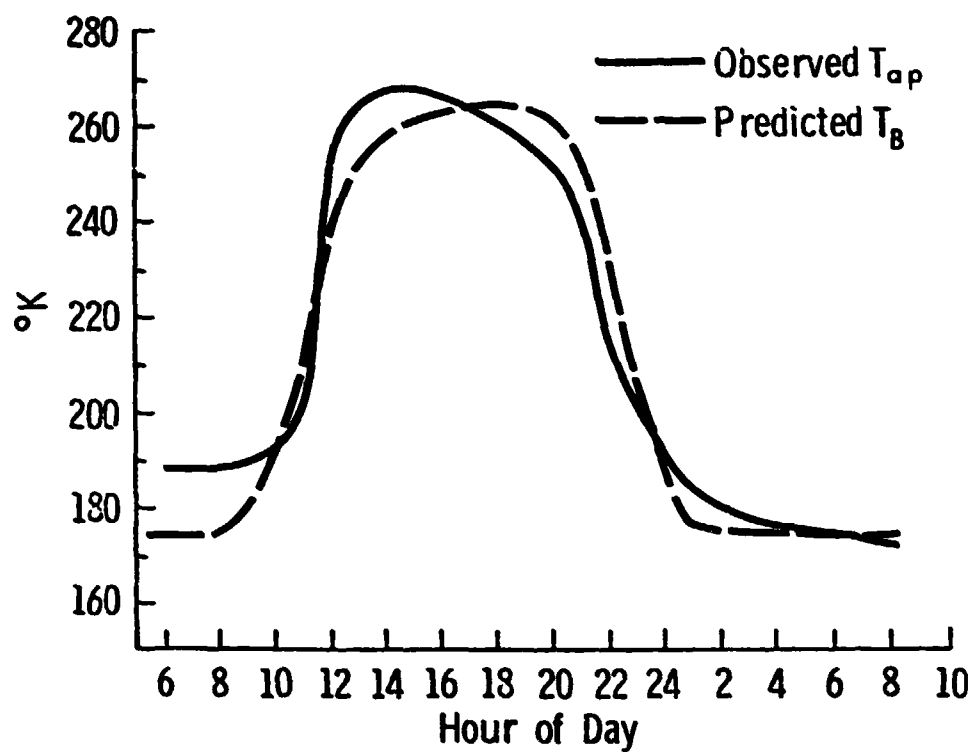


Figure 4-15 Observed T_{ap} and T_B Predicted by the Multilayered Emission Model as a Function of Time at $\theta = 20^{\circ}$.

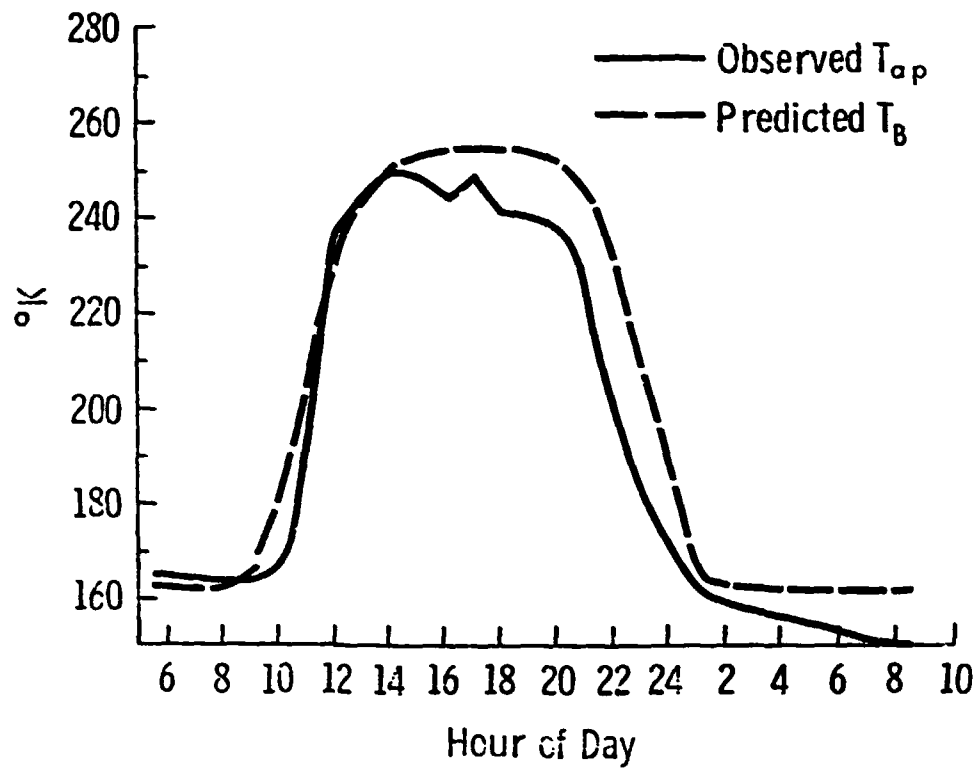
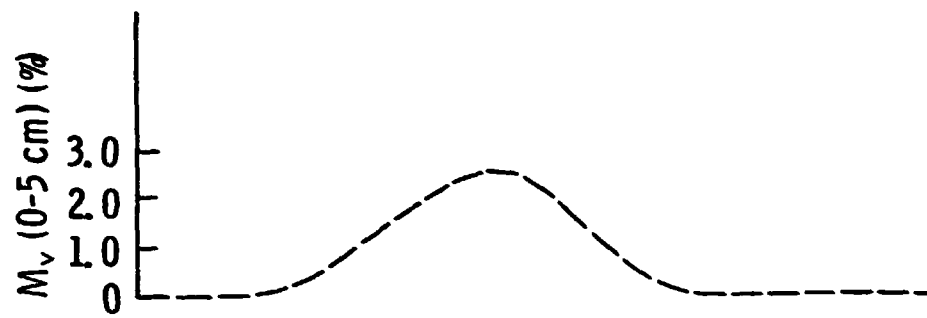


Figure 4-16 Observed T_{ap} and T_b Predicted by the Multilayered Emission Model as a Function of Time at $\theta = 50^\circ$.

4.5 Multilayered Model for Snow with Split Top Layer

In order to modify the models applied in the previous two sections to give better estimates of the observed T_{ap} , an understanding of the snow melting and refreezing process is necessary. Figures 3-3 to 3-6 along with Table 3-1 indicate that as the air temperature above the snowpack increases sufficiently above freezing combined with the radiation from the sun shining on the snowpack, the snow begins to melt. The process of melting starts on the top of the snowpack with the top 1 cm of snow or less becoming much more wet and so having a higher M_v than the rest of the snowpack below it. If the air temperature remains warm enough, the snow wetness M_v increases with time in the top few centimeters of snow, becoming wettest on the top of the snowpack and decreasing in wetness with increasing snow depth. At this time the radiometer observing the snowpack at 37 GHz is sensitive to a small snow depth on the top of the snowpack. Due to the decrease in penetration depth, this very small snow depth is responsible for the majority of the emission of microwaves from the snowpack. This top and very wet snow layer could be smaller in thickness than the top 5 cm layer of snow considered in the previous model and whose average wetness was measured by Stiles and Ulaby (1980) and is shown in Figure 3-2.

As the air temperature starts decreasing later in the afternoon to a temperature below that of freezing, the snowpack starts to refreeze. The refreezing process, similar to the melting process, starts from the top of the snowpack. A small depth of snow on the top of the snowpack, which could be 1 cm in depth or smaller, starts to refreeze and the M_v

of that depth decreases greatly. With time, the wetness, M_v , of this small depth drops to values that are less than the values of M_v of the lower depths of the snowpack. The snow in the top of the snowpack then becomes dry and its M_v drops to zero in the top few centimeters of the snowpack, while the snow in the lower layers of the snowpack remains higher in wetness. With time and continuing decrease in air temperature, the frozen layer on the top of the snowpack increases in thickness gradually down the snowpack until the whole snowpack is frozen.

The radiometer observing the snowpack at the start of the refreezing process will be sensitive at times to a snow depth that is larger than the 5 cm top layer of snow due to the increased penetration depth of the wave with the disappearance of free water from the top of the snowpack. The snow wetness measurements collected from the top 5 cm layer of snow are average values of wetness throughout the snow thickness considered and do not give the exact wetness profile in the snow thickness. This average value of wetness will, therefore, lag behind the T_{ap} observed when the snow is melting and lead the T_{ap} observed when the snow is refreezing as shown in Figure 3-1. This causes the hysteresis pattern shown in Figures 3-7, 3-8 and 3-9.

The model developed as described by Equation (4-10) needs to be modified to account for the physical behavior of snow at its melting and refreezing process. This is done by splitting the uppermost snow layer, shown in Figure 4-12 as Layer 4, into two sublayers each 2.5 cm in thickness. The thermometric temperature of these two sublayers is taken to be the same as the original 5 cm top layer. The percentage wetness by volume M_v of the top 2.5 cm layer, shown in Figure 4-17

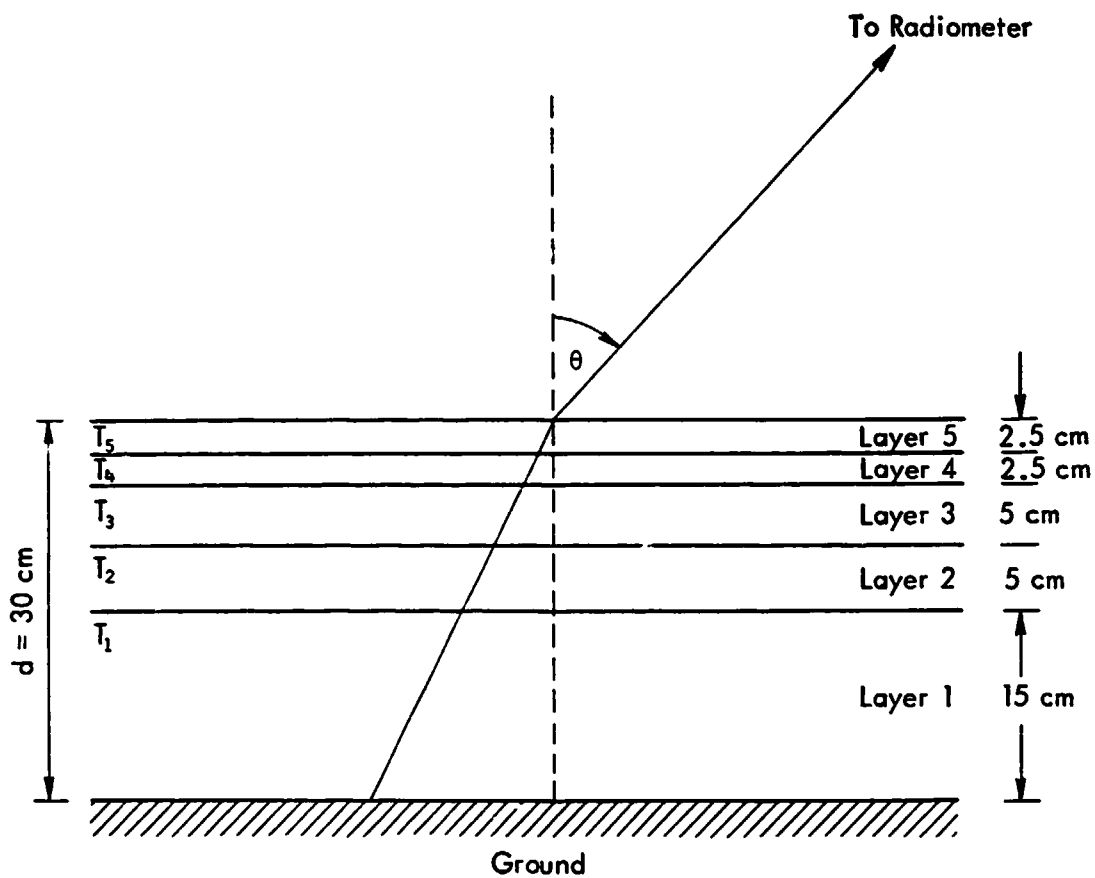


Figure 4-17 A Geometrical Presentation of the Revised Snowpack Cross Section During the 2/17/77 - 2/18/77 Diurnal Experiment. The Top 5 cm Layer is Shown Split into Two 2.5 cm Sublayers.

as Layer 5, is made seven times as wet as the original 5 cm top layer in the melting stage and then allowed to saturate at a value of $M_V = 2.53$ which was the maximum value of M_V reached by the original 5 cm top layer. The percentage wetness M_V of the lower 2.5 cm layer, shown in Figure 4-17 as Layer 4, is calculated during the melting process such that the average value of wetness M_V of both 2.5 cm snow layers is equal to that of the original 5 cm uppermost snow layer. The wetness M_V of the second 2.5 cm layer is made seven times as wet as the original 5 cm uppermost snow layer during the refreezing stage allowing it to saturate at the same value of $M_V = 2.53$. The wetness of the top 2.5 cm layer during the refreezing stage is then calculated such that the average wetness M_V of both 2.5 cm snow layers is equal to that of the original 5 cm uppermost snow layer. Figure 4-17 shows the snow layers within the snowpack and their various thicknesses. Figure 4-18 shows the calculated wetness curves of the two 2.5 cm layers that make up the original 5 cm uppermost snow layer, along with the wetness curve of the original 5 cm top layer of snow.

Equation (4-10) describing the emission from a multilayered snowpack is solved in a manner similar to that shown in the last two sections, taking into account the modifications introduced in this section. The scattering coefficient estimated by this model as modified above is the same as that estimated in the previous section and shown by Equation (4-21). Figures 4-19, 4-20 and 4-21 show the T_{ap} observed during the diurnal experiment along with the T_g predicted by the multilayered model with the split top layer at $\theta = 0^\circ$, 20° and 50° respectively. The difference between the fits shown here by Figures 4-19, 4-20 and 4-21 and those

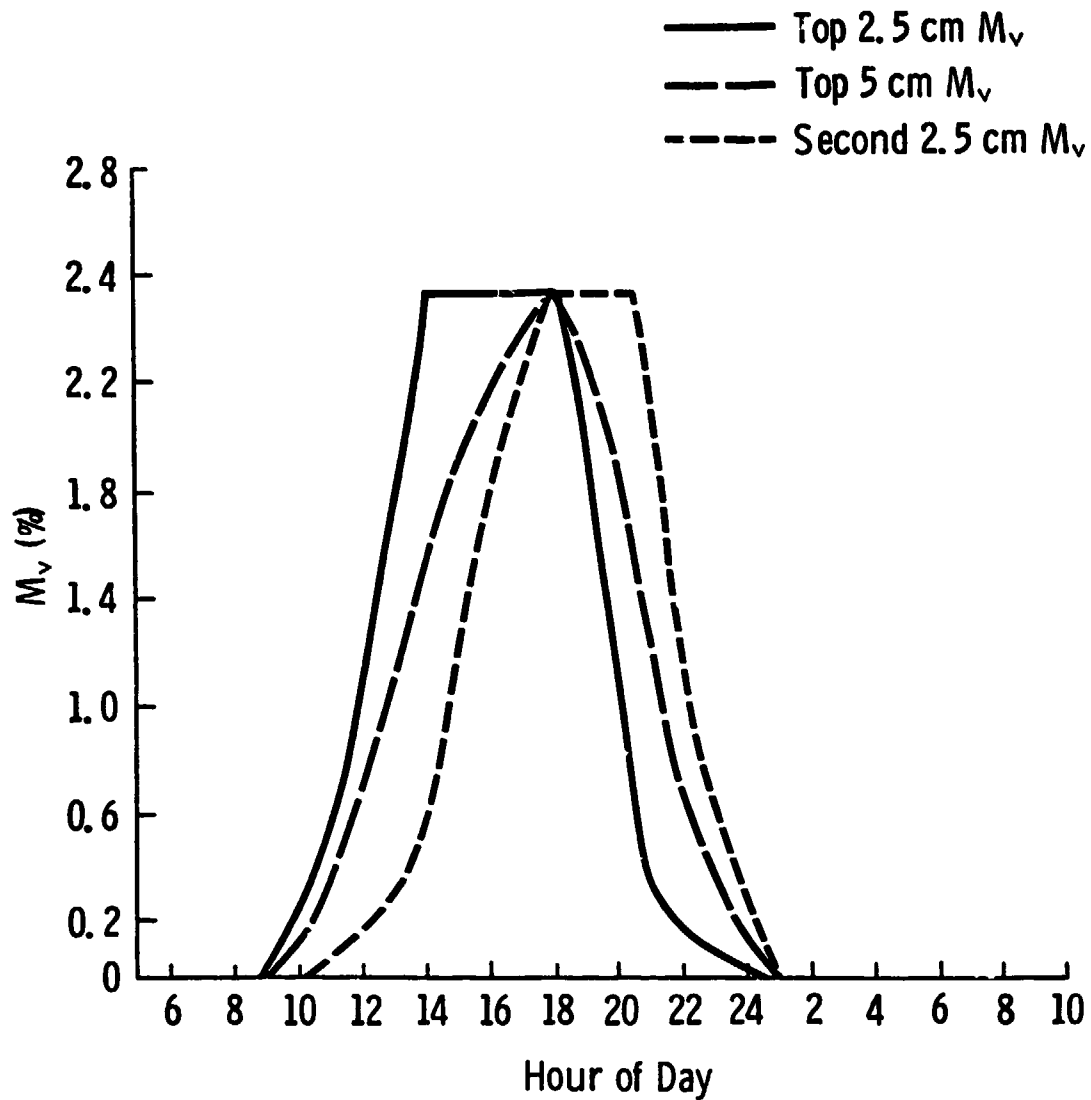


Figure 4-18

Percentage Wetness by Volume M_v Curves for the Top 2.5 cm Snow Layers Along With the Original 5 cm Snow Layer Wetness Curve of the 2/17/77 - 2/18/77 Diurnal Experiment. The Top 2.6 cm Layer is Seven Times as Wet as the Original 5 cm Layer in the Melting Stage While the Lower 2.5 cm Layer is Seven Times as Wet as the Original 5 cm Layer in the Refreezing Stage.

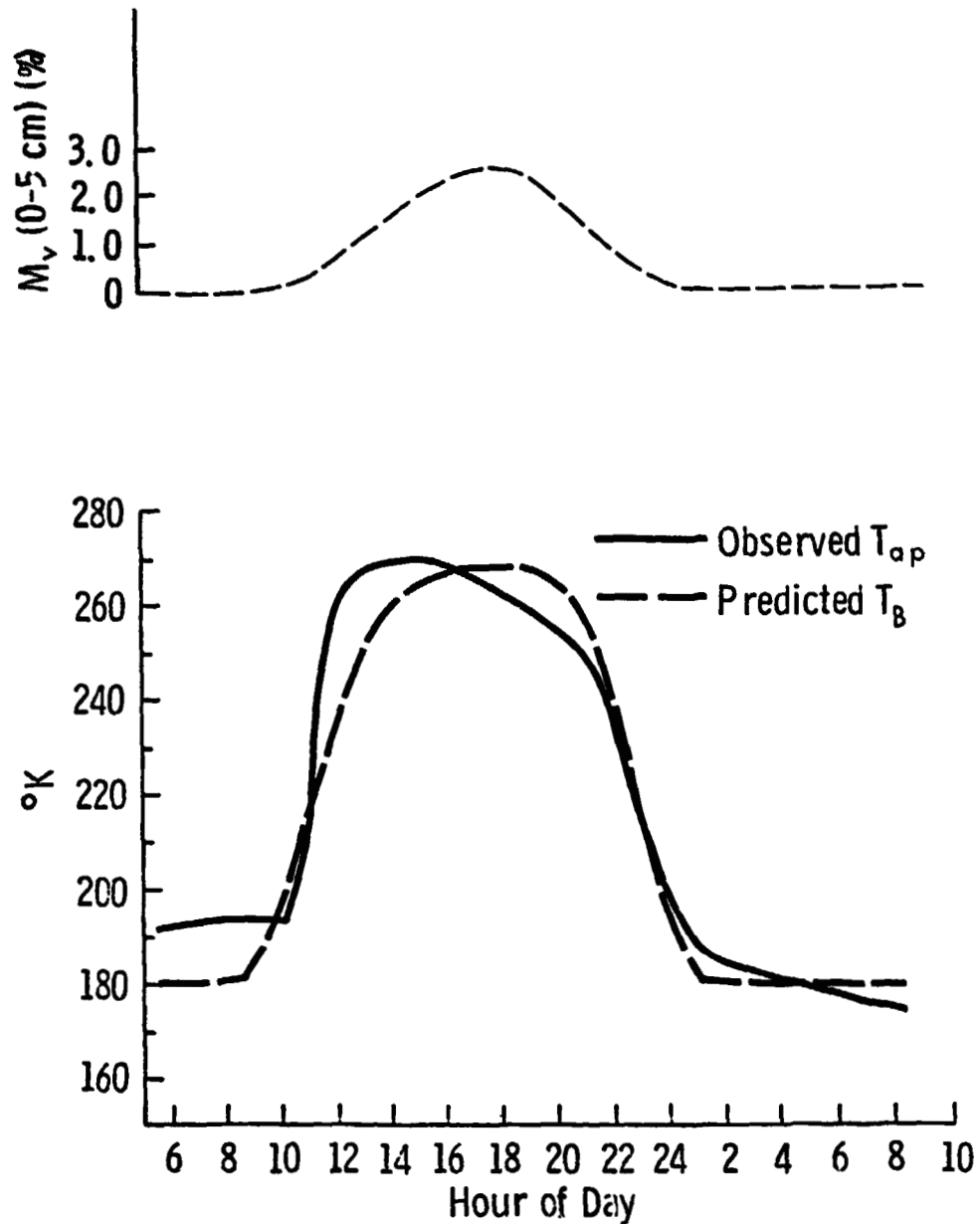


Figure 4-19 The Observed T_{ap} and the Predicted T_b as Calculated by the Multilayered Emission Model With Split Top Layer at $\theta = 0^{\circ}$. The Uppermost Sublayer is 2.5 cm Thick and Seven Times as Wet as the Original 5 cm Top Snow Layer.

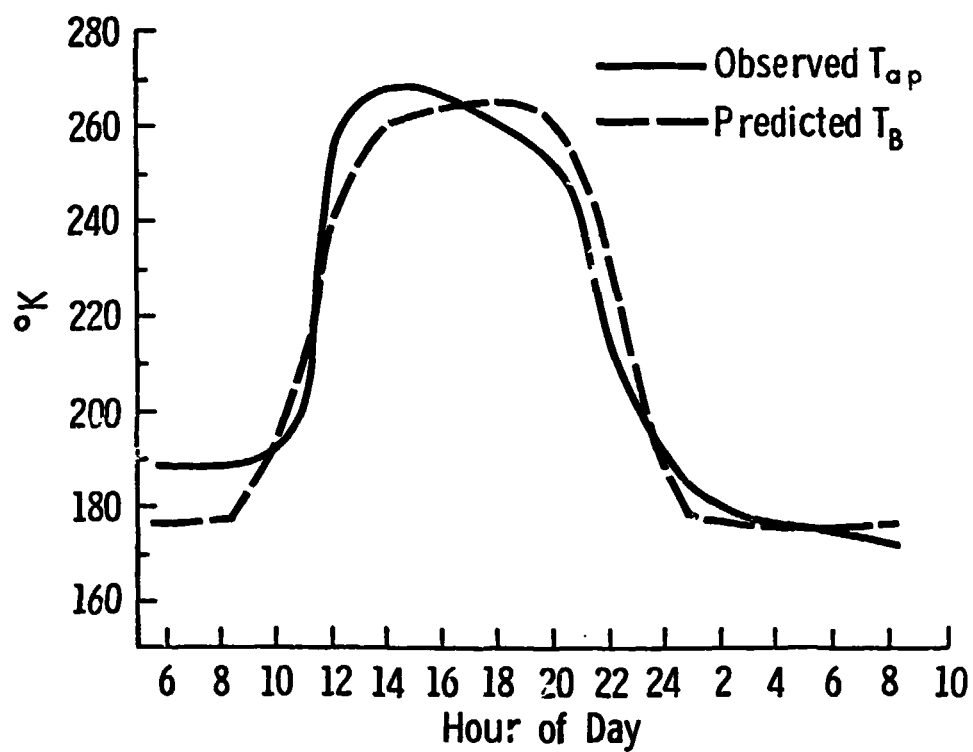


Figure 4-20 The Observed T_{ap} and the Predicted T_b as Calculated by the Multilayered Emission Model with Split Top Layer at $\theta = 20^\circ$. The Uppermost Sublayer is 2.5 cm Thick and Seven Times as Wet as the Original 5 cm Top Snowlayer

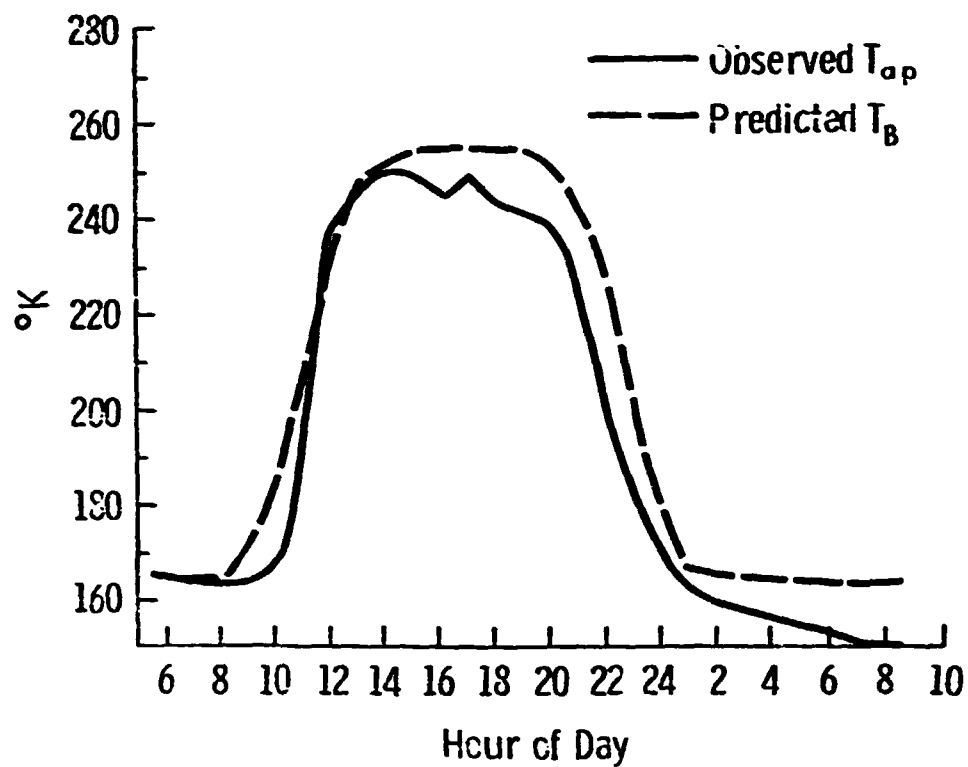


Figure 4-21 The Observed T_{ap} and the Predicted T_b as Calculated by the Multilayered Emission Model with Split Top Layer at $\theta = 50^\circ$. The Uppermost Sublayer is 2.5 cm Thick and Seven Times as Wet as the Original 5 cm Top Snowlayer.

calculated previously and shown by Figures 4-14, 4-15 and 4-16, for $\theta = 0^\circ$, 20° and 50° respectively, for T_g are very small.

The uppermost 2.5 cm snow layer was made eight, 12 and 15 times as wet as the original 5 cm uppermost layer of snow. The original top 5 cm layer of snow was split into two sublayers. The thickness of the top layer was made 1 cm and that of the second layer 4 cm in thickness and the analysis repeated again for the different wetnesses considered. However, the fits produced by the different thickness of the snow sub-layers or the different wetnesses considered were not much different from those shown by Figures 4-19, 4-20 and 4-21 and are, therefore, not shown here.

5.0 EVALUATION OF THE EMISSION MODELS AND THEIR RESULTS

In this chapter, all of the emission models developed and applied in Chapter 4 to describe the emission from a snowpack are evaluated. The model that predicts the best estimates of the T_{ap} observed by the 37 GHz radiometer throughout the diurnal experiment is considered the superior model. The values of κ_a , the absorption coefficient and κ_s , the scattering coefficient estimated by the superior model chosen are compared to similar values reported in the literature and are used to calculate the percentage contribution from each layer of the snowpack throughout the diurnal experiment.

5.1 Evaluation of the Models

Two methods are used to evaluate the models developed in Chapter 4. The first is a residual sum of squares analysis in which the sum of the squares of residuals occurring between $T_B(N^+)$ predicted by the model and T_{ap} observed is calculated for each model. The model that shows the least residual sum of squares at all of the radiometer's look angles is therefore considered a better model for it gives the best estimates of T_{ap} observed. Table 5-1 shows the results of such an analysis conducted on all the models developed. The model describing a multilayered snowpack with split uppermost layer of snow and whose 2.5 cm top layer is seven times as wet as the original 5 cm uppermost layer of snow shows the least residual sum of squares for all θ .

The second evaluation method conducted, is a linear correlation analysis between the values of the $T_B(N^+)$ predicted by each model and the T_{ap} observed by the radiometer. Figures 5-1 to 5-9 show the results

TABLE 5-1

The Residual Sum of Squares Analysis
Conducted for all the Models Developed and
at $\theta = 0^\circ, 20^\circ$ and 50° .

Model	0°	20°	50°
Single homogenous layer Snowpack	2044.23	3732.51	9022.11
Multilayered Snowpack	1690.29	2077.31	3220.84
Multilayered Snowpack with Split Top Layer	1380.06	1598.42	3148.98

$$T_B (\text{Pred}) = 0.940 T_{ap} (\text{Obs}) + 16.150$$

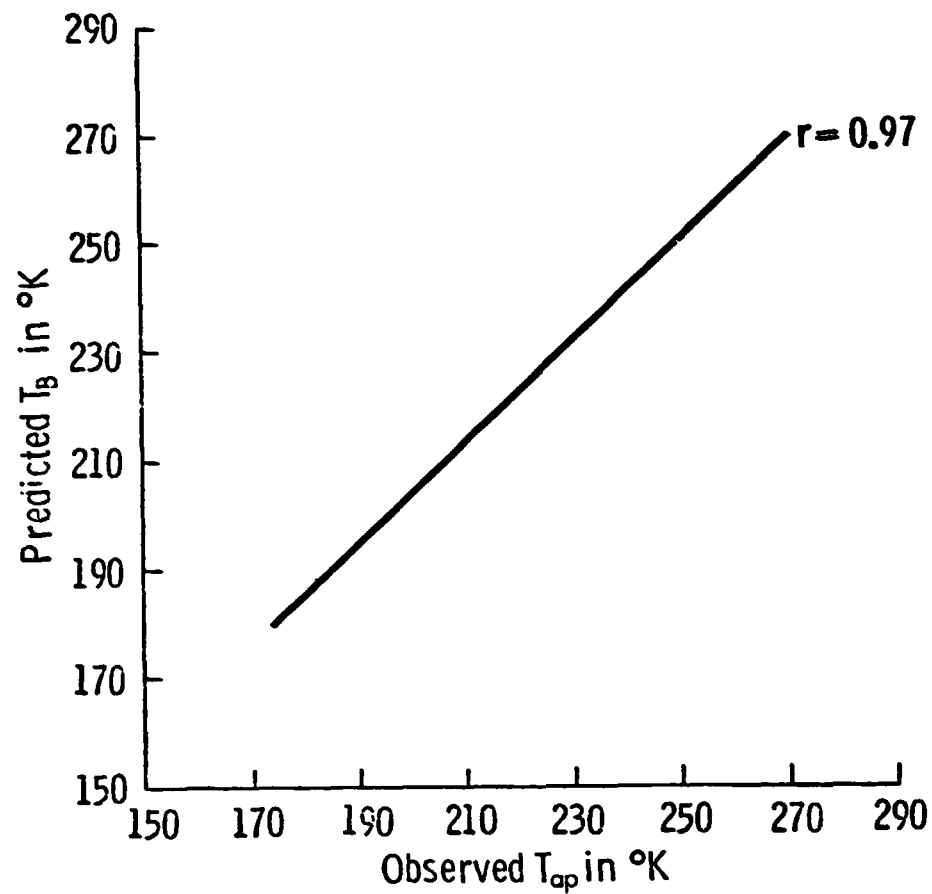


Figure 5-1 Linear Correlation Coefficient Between the Predicted T_B as Calculated by the Single Homogeneous Layer Snow-pack Model at $\theta = 00$ and the T_{ap} Observed.

$$T_B (\text{Pred}) = 0.936 T_{ap} (\text{Obs}) + 19.325$$

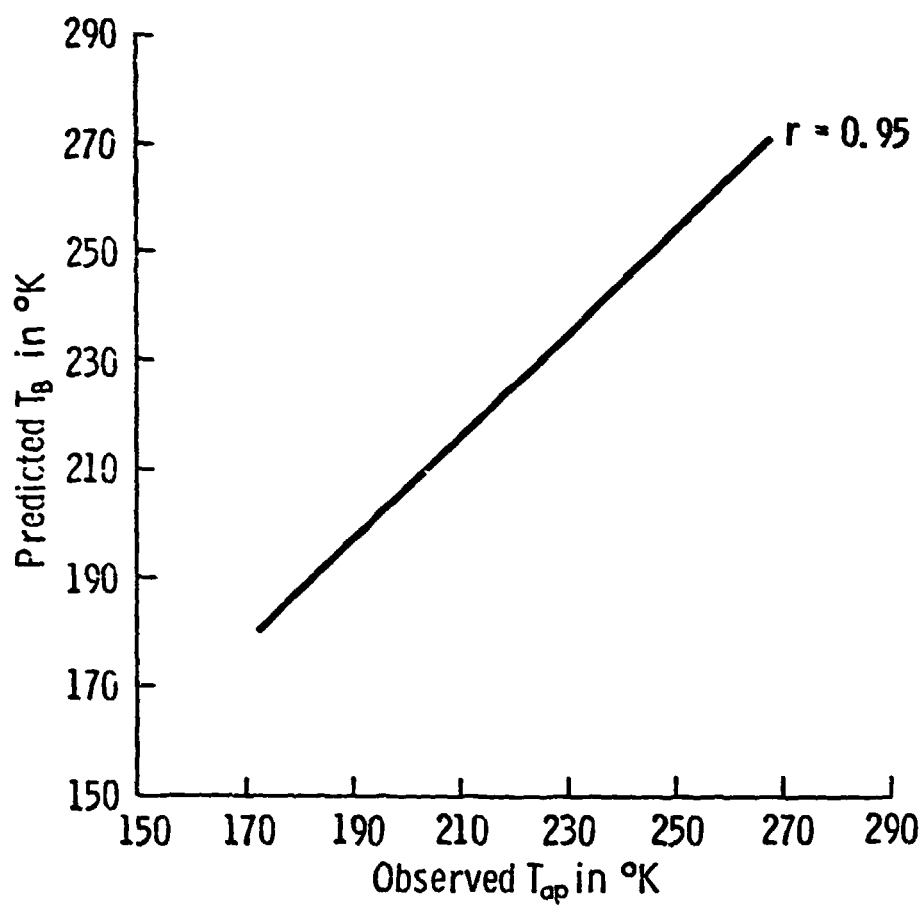


Figure 5-2 Linear Correlation Coefficient Between the Predicted T_B as Calculated by the Single Homogeneous Layer Snowpack Model at $\theta = 20^\circ$ and the T_{ap} Observed.

$$T_B \text{ (Pred)} = 1.010 T_{ap} \text{ (Obs)} + 14.751$$

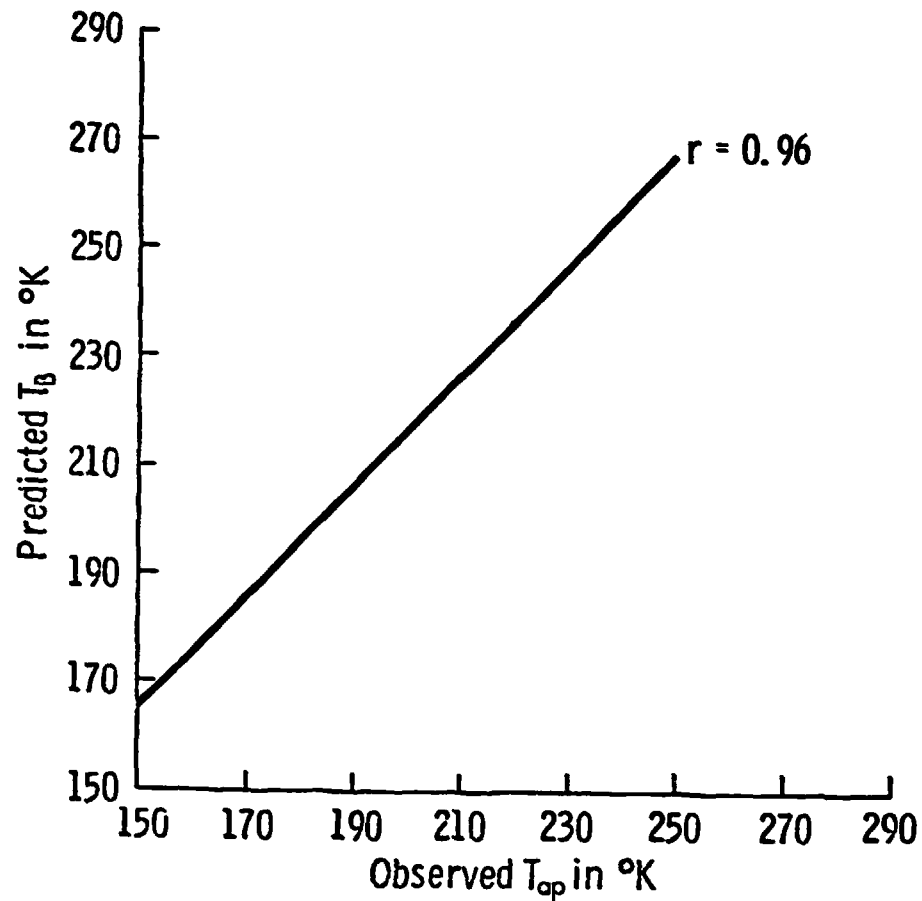


Figure 5-3 Linear Correlation Coefficient Between the Predicted T_B as Calculated by the Single Homogeneous Layer Snowpack Model at $e = 50^\circ$ and the T_{ap} Observed.

$$T_B \text{ (Pred)} = 0.979 T_{ap} \text{ (Obs)} + 3.692$$

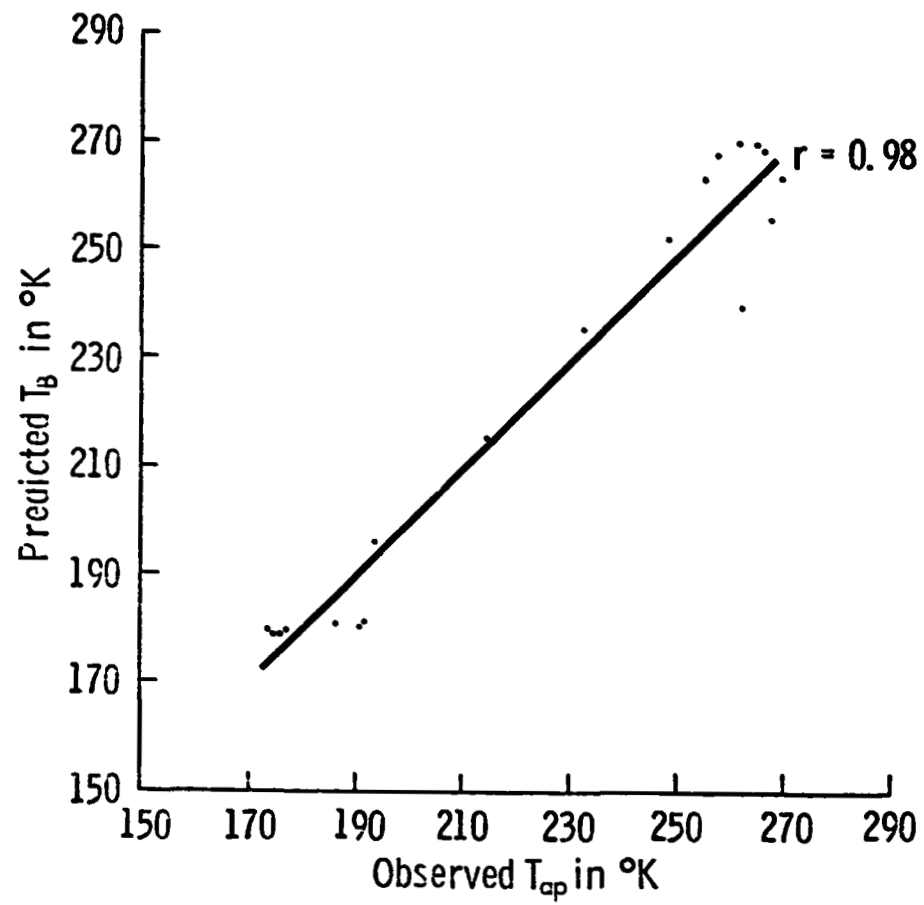


Figure 5-4 Linear Correlation Coefficient Between the Predicted T_B as Calculated by the Multilayered Snowpack Model at $\theta = 0^\circ$ and the T_{ap} Observed.

$$T_B (\text{Pred}) = 0.979 T_{ap}(\text{Obs}) + 3.004$$

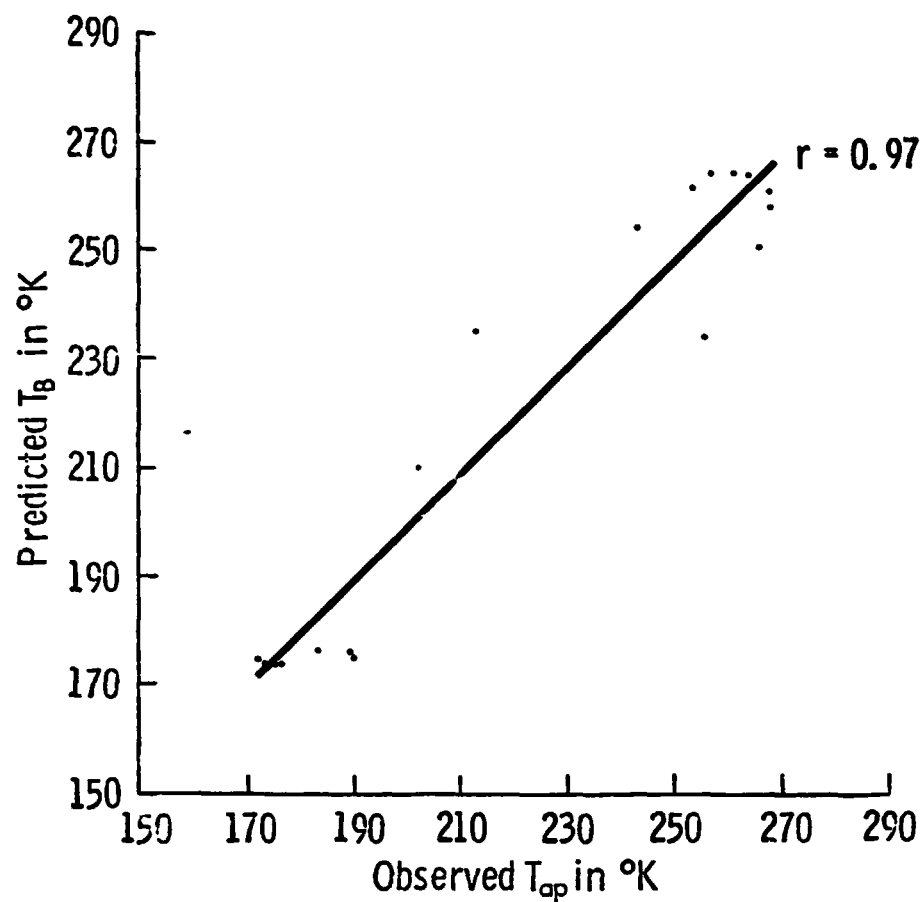


Figure 5-5 Linear Correlation Coefficient Between the Predicted T_B as Calculated by the Multilayered Snowpack Model at $\theta = 20^\circ$ and the T_{ap} Observed.

$$i_B (\text{Pred}) = 0.987 T_{ap} (\text{Obs}) + 11.640$$

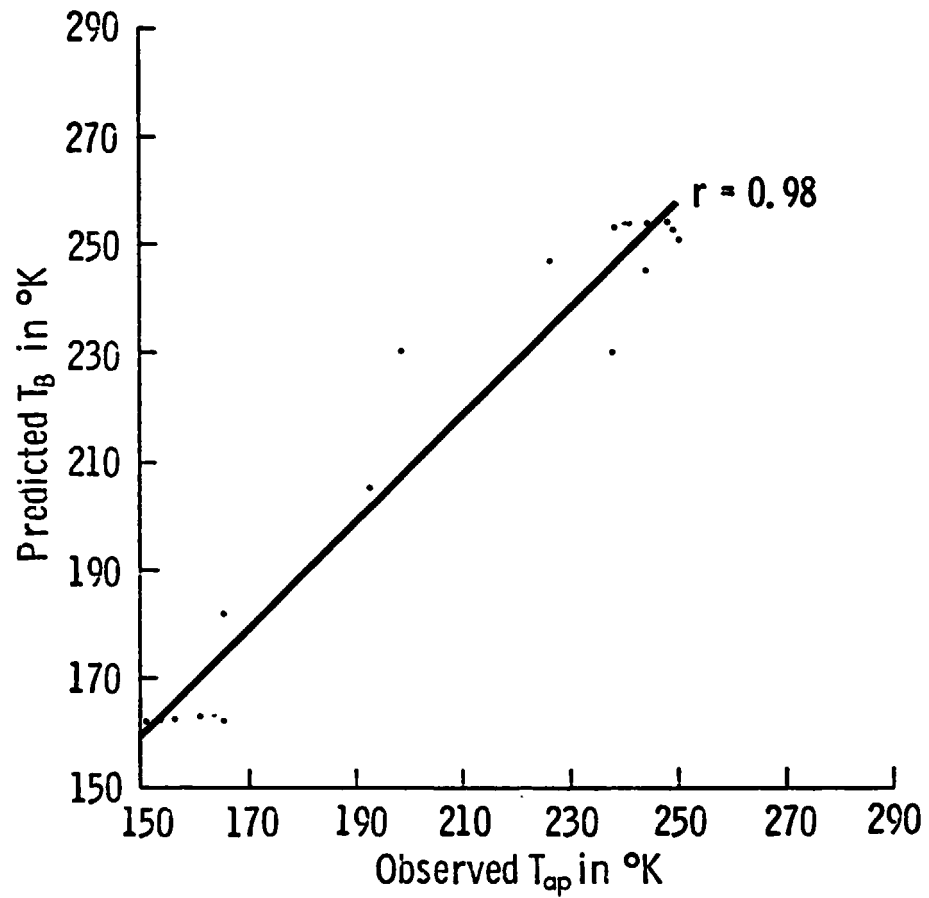


Figure 5-6 Linear Correlation Coefficient Between the Predicted T_B as Calculated by the Multilayered Snowpack Model at $\theta = 50^{\circ}$ and the T_{ap} Observed.

$$T_B (\text{Pred}) = 0.970 T_{ap} (\text{Obs}) + 5.560$$

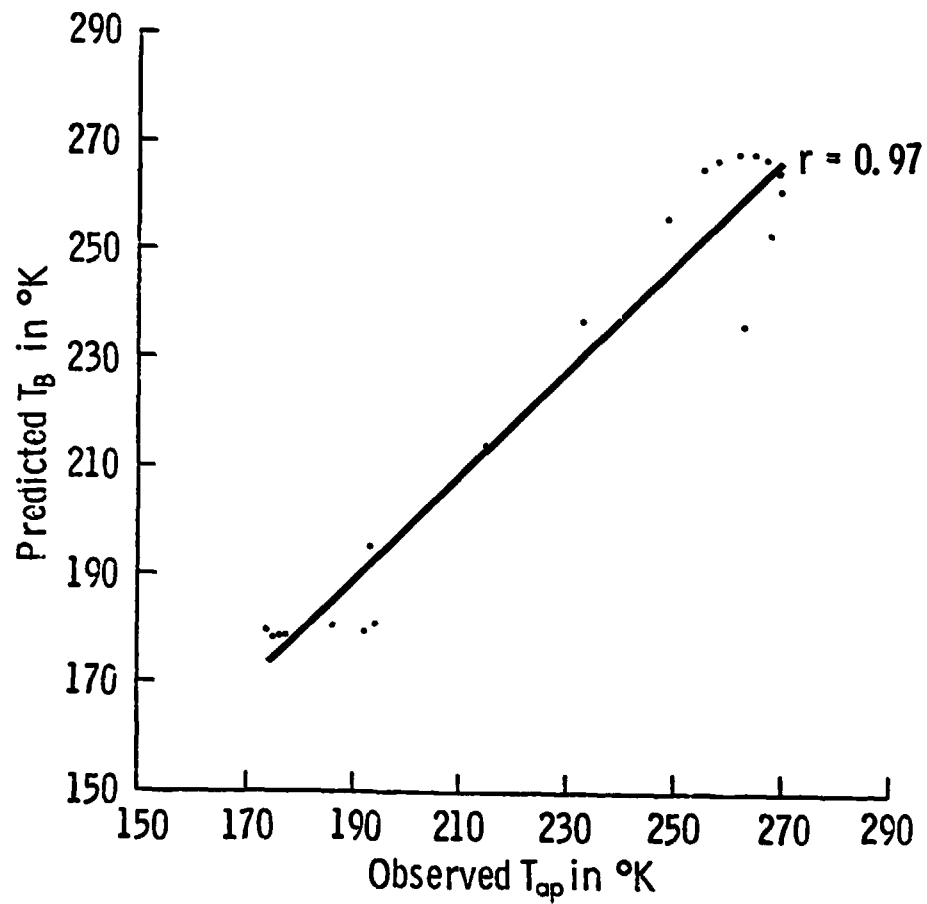


Figure 5-7 Linear Correlation Coefficient Between the Predicted T_B as Calculated by the Multilayered Snowpack with the Split Top Layer and the T_{ap} Observed at $\theta = 00$. New Uppermost Layer is 2.5 cm in Thickness and Seven Times as Wet as the Original 5 cm Top Snow Layer.

$$T_B (\text{Pred}) = 0.957 T_{ap} (\text{Obs}) + 9.215$$

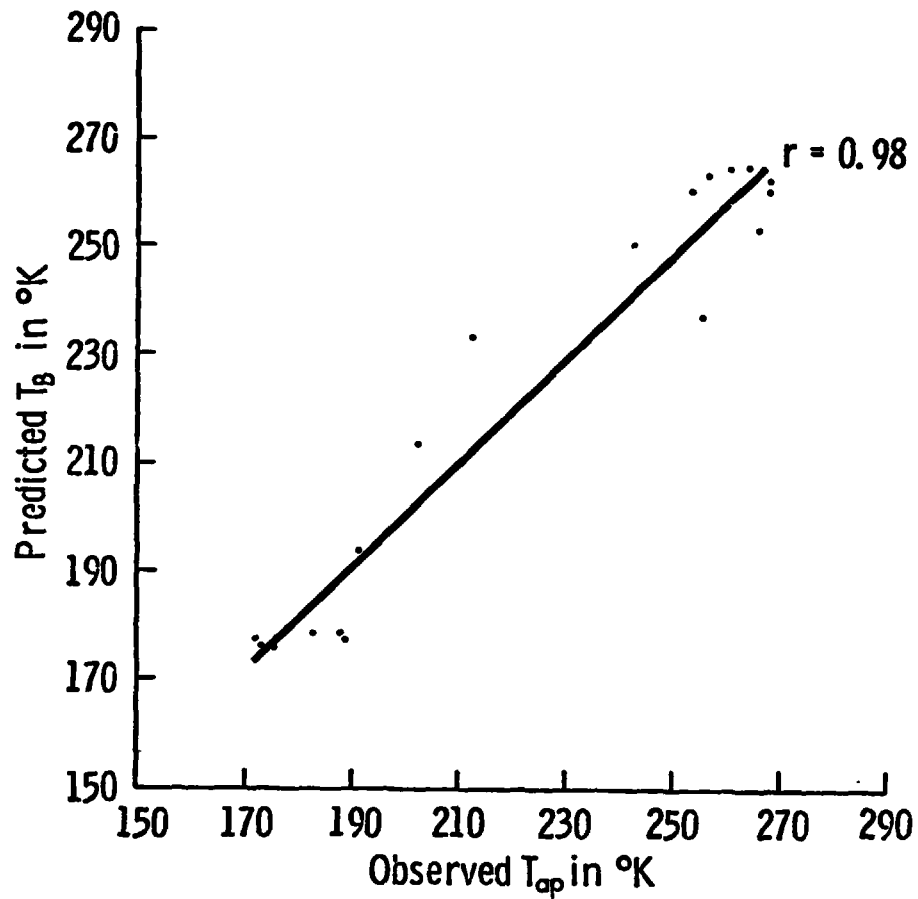


Figure 5-8 Linear Correlation Coefficient Between the Predicted T_B as Calculated by the Multilayered Snowpack with the Split Top Layer and the T_{ap} Observed at $\theta = 20^\circ$. New Uppermost Layer is 2.5 cm in Thickness and Seven Times as Wet as the Original 5 cm Top Snow Layer.

$$T_B (\text{Pred}) = 0.966 T_{ap} (\text{Obs}) + 16.494$$

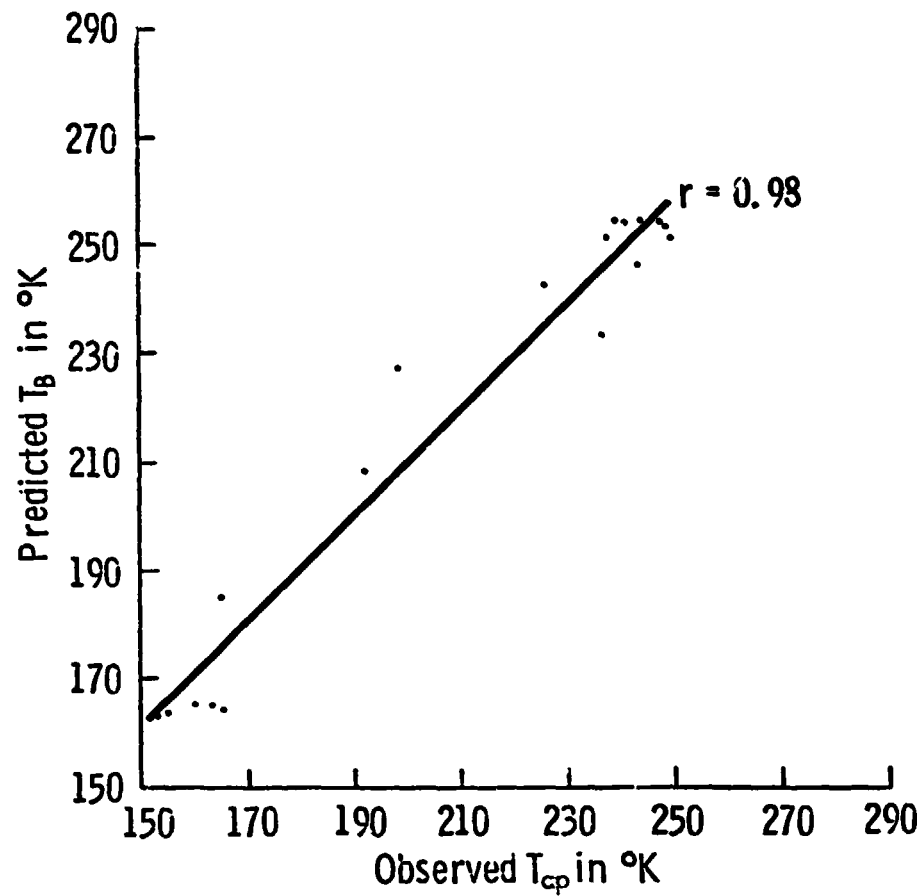


Figure 5-9 Linear Correlation Coefficient Between the Predicted T_B as Calculated by the Multilayered Snowpack with the Split Top Layer and the T_{ap} Observed at $\theta = 50^\circ$. New Uppermost Layer is 2.5 cm in Thickness and Seven Times as Wet as the Original 5 cm Top Snow Layer.

of such an analysis carried out on all the results of the models developed at $\theta = 0^\circ$, 20° and 50° . Figures 5-1, 5-2 and 5-3 show the linear correlation between the T_B predicted by the single homogeneous layered snowpack and the T_{ap} observed at $\theta = 0^\circ$, 20° and 50° respectively. Figures 5-4, 5-5 and 5-6 show the linear correlation between the T_B predicted by the multilayered snowpack and the T_{ap} observed at $\theta = 0^\circ$, 20° and 50° respectively. Figures 5-7, 5-8 and 5-9 show the linear correlation between the T_B , predicted by the multilayered snowpack model with the original uppermost snow layer split into two sublayers, each 2.5 cm in thickness, and the T_{ap} observed at $\theta = 0^\circ$, 20° and 50° respectively. Both multilayered emission models show superior estimates of T_B than the single homogeneous layer model. However, there is little difference in the correlation coefficient between the values of T_B predicted by both multilayered models and the T_{ap} observed. On this basis the multilayered snowpack model, with the uppermost layer split into two sublayers each 2.5 cm in thickness and the top sublayer is made seven times as wet as the original 5 cm uppermost snowlayer is considered the best model of the three developed.

5.2 Evaluation of the Values of κ_a and κ_s Estimated by the Multilayered Snowpack Model

Equations 4-13 and 4-21 show the absorption coefficient calculated by the Tinga et al. (1973) mixing formula and the scattering coefficient estimated by the multilayered emission model of snow as a function of snow wetness. The values of κ_a , κ_s and κ_e calculated in this study for dry snow are compared to those previously reported in the literature

as shown in Table 5-2. The values of κ_a , κ_s and κ_e calculated for dry snow in this study are greater in value than those reported by both Stiles and Ulaby (1980) and Hofer and Matzler (1980). This is due to the following reasons:

(a) The difference in the snow depth, snow density, snow temperature, and snow crystal structure in all the experiments conducted. There were also differences in air temperature and other environmental conditions which could have caused the differences seen in the values of κ_a , κ_s and κ_e .

(b) The values of κ_a , κ_s and κ_e estimated by Stiles and Ulaby (1980) are obtained from the results of the snow pile experiment shown in Figure 3-10. In their experiment, the snow was piled up to a depth of 170 cm and the apparent temperature of the snow pile at 37 GHz was measured for different depths. At the same time, T_{ap} was measured from the undisturbed snowpack around the snow pile to see the difference in the T_{ap} measurement for the same depth. Figure 3-10 shows that for a snow depth, above the ground, of 30 cm or for a 6.3 cm water equivalent at $\theta = 27^\circ$, the T_{ap} measured from the snow pile was 260°K whereas the T_{ap} measured from the undisturbed snow was 200°K . Similarly for $\theta = 57^\circ$ and a water equivalent of 15 cm, T_{ap} measured from the snow pile was 200°K whereas T_{ap} measured from the undisturbed snow was 175°K . That is the values of T_{ap} measured from the snow pile are higher than those measured from the undisturbed snow. This difference is due to the alteration in the crystal structure of the snow as it was piled causing the scattering coefficient to become smaller in the snow pile than it is for the undisturbed snow and, therefore, giving higher

TABLE 5-2

Values of κ_a , κ_s , κ_e for Dry Snow
as a Function of θ Calculated Using Stiles and Ulaby (1980) Model,
the Multilayered Snowpack Emission Model
and the Hofer and Matzler (1980) Model.

Model	θ In Degrees	κ_a dB/cm	κ_s dB/cm	κ_a/κ_e	κ_e dB/cm
Stiles and Ulaby (1980)	27°	0.04	0.04	0.52	0.08
Stiles and Ulaby (1980)	57°	0.07	0.05	0.59	0.12
Multilayered Emission Model	0°, 20° & 50°	0.18	0.15	0.55	0.33
Hofer & Matzler (1980) (High Winter)	0°-60°	0.02	0.03	0.40	0.05
Hofer & Matzler (1980) (Spring)	0°-60°	0.02	0.04	0.33	0.06

values of T_{ap} from the snow pile than undisturbed snow. Since the values of κ_a , κ_s and κ_e calculated in this study are those of undisturbed snow while those calculated by Stiles and Ulaby (1980) are those for the snow pile, the larger values of κ_a , κ_s and κ_e calculated here are, therefore, explainable. Figures 5-10 and 5-11 show the brightness temperature calculated using Equation (4-14) for a snowpack made up of one homogeneous layer of snow as a function of water equivalent at $\theta = 27^\circ$ and 57° respectively. These figures are calculated by substituting the values of κ_a , κ_s and κ_e obtained in this study for undisturbed snow into Equation (4-14). The figures also show the measurements of Stiles and Ulaby (1980) for undisturbed snow at $\theta = 27^\circ$ and 57° of Figure 3-10. Notice the small difference in T_B calculated here and that measured by Stiles and Ulaby (1980) at the two angles considered.

(c) The ratio of κ_a/κ_e is very similar in all the measurements shown in Table 5-2, however the value of κ_e tends to be much different. The dependence of T_B on κ_e' is shown in Figure 5-12. In this figure, T_B is plotted versus κ_e' for a snowpack made up of one homogeneous layer and 30 cm in depth and a snow temperature of 262.33°K . κ_e calculated in the study is comparable in value to the total loss measured by Stiles and Ulaby (1980) for dry snow as shown in Figure 2-10. This adds to the credibility of the value of κ_e calculated here.

5.3 Total Emission from Each Snow Layer

The emission from each snow layer within the snowpack, shown in Figure 4-9 is calculated using the values of κ_a and κ_s given by

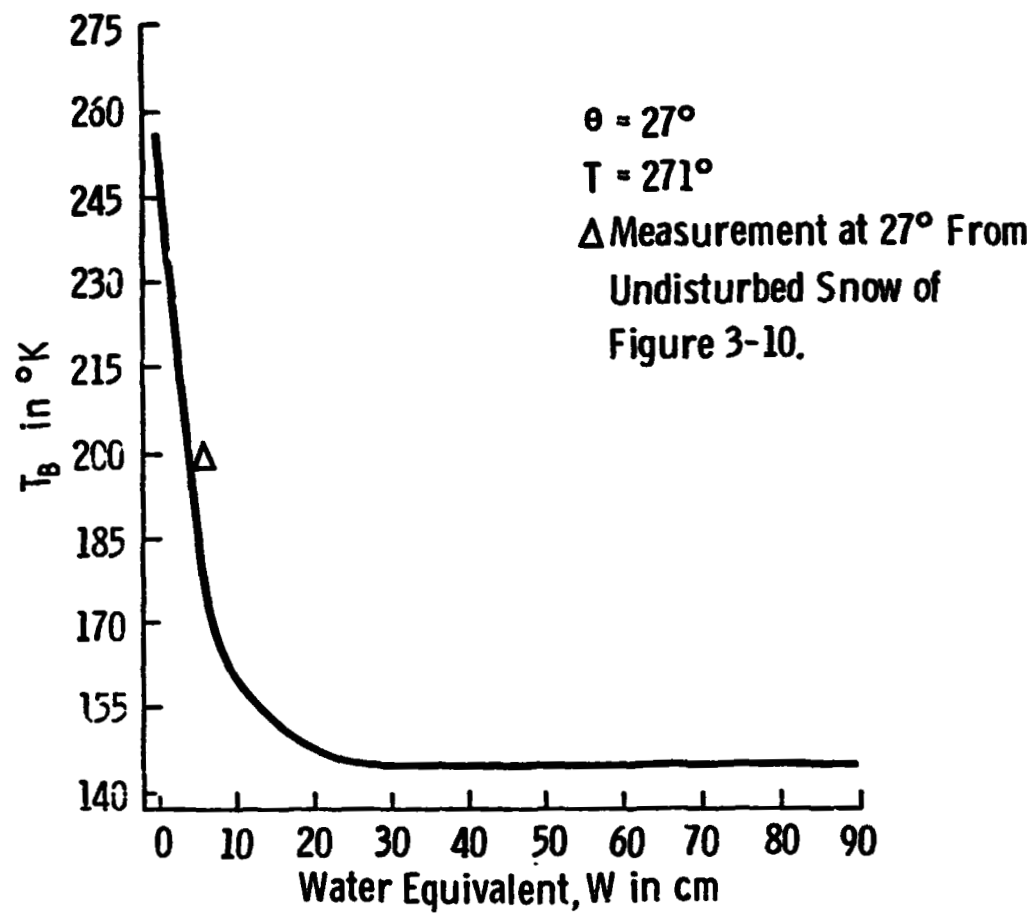


Figure 5-10 T_B Calculated From an Undisturbed Snowpack as a Function of W for One Layered Snowpack at $\theta = 27^\circ$ Using the κ_a , κ_s and κ_e Calculated in This Study.

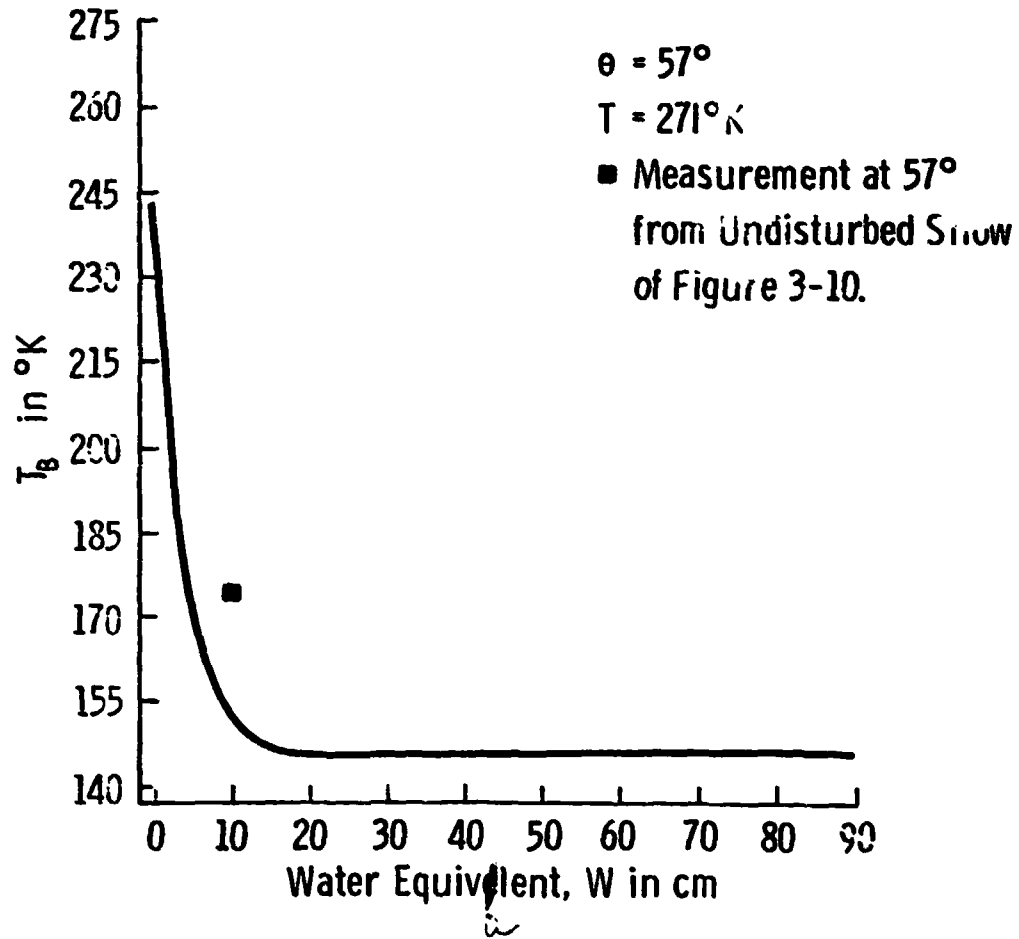


Figure 5-11 T_b Calculated From an Undisturbed Snowpack as a Function of W for a Single Layer Snowpack at $\theta = 57^\circ$ Using the κ_a , κ_s and κ_e Calculated in the Study.

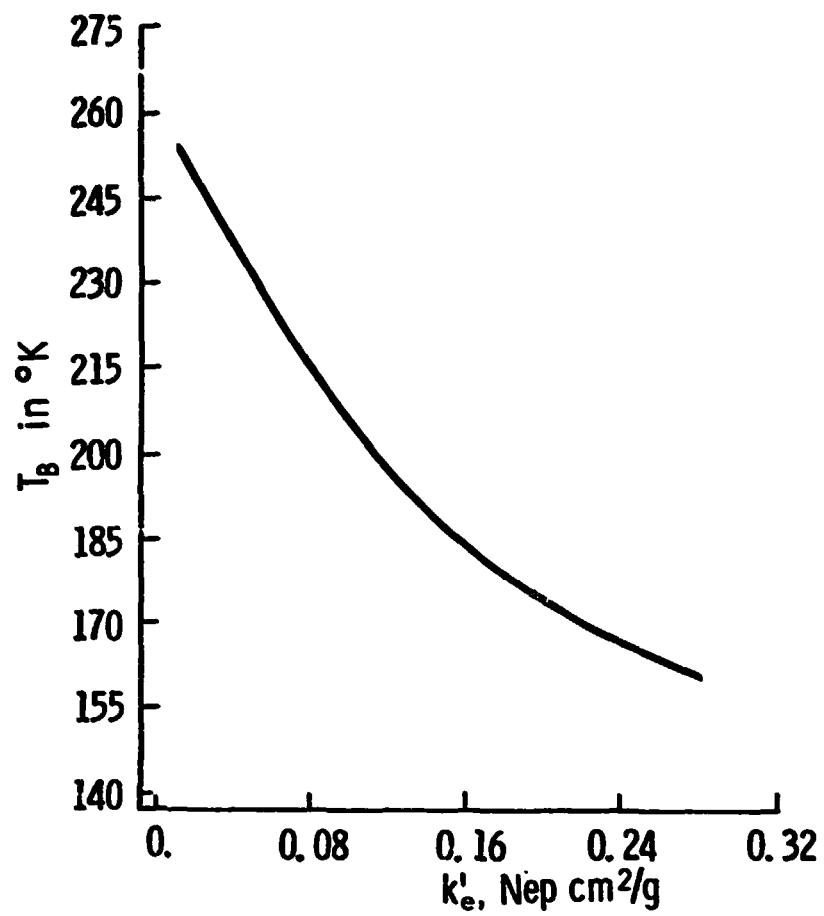


Figure 5-12 T_B as a Function of κ'_e for a Snowpack of One Homogeneous Layer at Nadiř. The Snow Depth is 30 cm and Snow Temperature is 262.330K.

Equations 4-13 and 4-21 respectively, and Equation (4-10). Figure 5-13 shows the percentage contribution of each layer within the snowpack as a function of time throughout the diurnal experiment. It is seen that for dry snow, the ground contributes the most to the total microwave emission measured by the radiometer. The contribution from the ground underneath a totally dry snowpack is above 45% of the total emission measured. As the topmost snow layer of the snowpack increases in wetness, its percentage contribution to the total emission increases as well. When the wetness of the top 5 cm layer is 1% by volume it contributes almost 80% of the total emission. When the snow wetness of the top 5 cm layer of snow is 2% by volume, it contributes 90% of the total emission. For dry snow, therefore, the emission from the snowpack and the ground underneath it is a volume emission stemming from each layer within the snowpack and the ground underneath it. However, this volume emission changes rapidly with the appearance of free water in the uppermost layer of the snowpack to become a surface emission stemming almost totally from the surface layer of the snowpack.

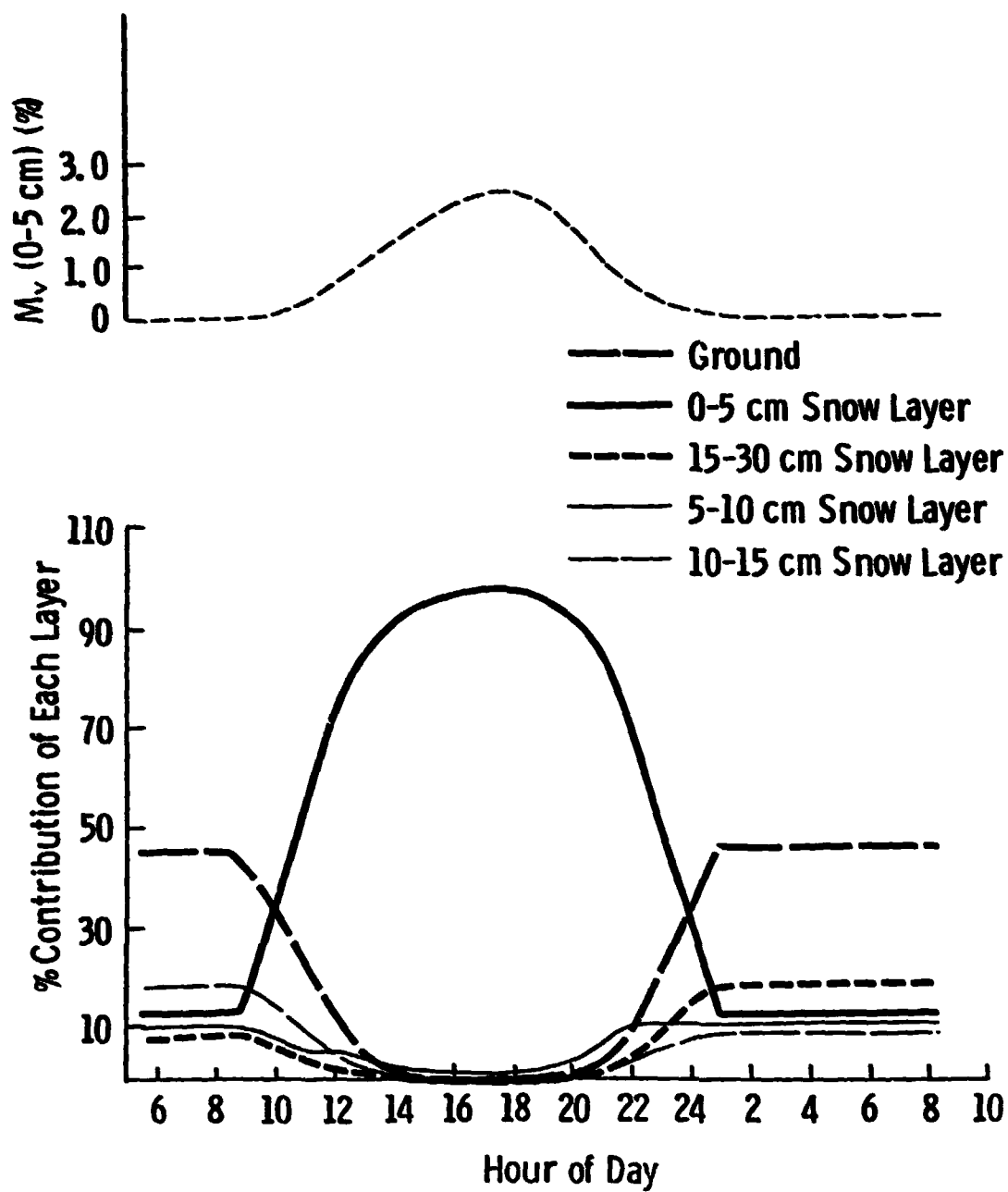


Figure 5-13 The Percentage Contribution of Each Layer Within the Snowpack as a Function of Time.

6.0 CONCLUDING REMARKS

In this paper a model describing the microwave emission from snow at 37 GHz was developed as a function of the physical and dielectric parameters of the snowpack. These parameters included the consideration of a snowpack consisting of different layers. The model provided information on the contribution of each snow layer and the ground to the total emission, for both wet and dry snow conditions. The model also provided solutions of the scattering, absorption and extinction coefficients for both wet and dry snow. The errors that exist in this model are due to the following:

(a) The model developed predicted the brightness temperature of the snow and not the apparent temperature actually measured. It, therefore, did not take into account the contribution of the downward emitted sky radiation scattered by the scene in the direction of the radiometer antenna.

(b) The lack of information of the dielectric constant of wet snow at 37 GHz, and of the dielectric constant of each snow layer considered throughout the experiment.

(c) The lack of wetness profiles that provide the wetness of the snowpack accurately and for every 1 cm thickness of the snowpack.

(d) Lack of information on the exact contribution of the ground to the apparent temperature measured by radiometer, since no T_{ap} measurements were conducted for the frozen ground of the scene during the experiment.

The model is the first to calculate values of κ_a , κ_s and κ_e as a function of snow wetness. The model is also the first to show the contribution of each snow layer to the total emission from snow and ground as a function of snow wetness.

REFERENCES

- [1] Battles, J. W. and D. E. Crane, "Millimeter Wave Attenuation Through Snow," U. S. Naval Ordnance Lab., NAVNEPS Report 8816, Corona, California, July 1965.
- [2] Battles, J. W. and D. E. Crane, "Attenuation of κ_a -Band Energy by Snow and Ice," U. S. Naval Ordnance Lab. NOLC Report 670, Corona, California, August 1966. (AD 638303)
- [3] Currie, N. C., F. B. Dyer and G. W. Ewell, "Radar Millimeter Backscatter Measurements from Snow," Final Report, Engineering Experiment Station, Georgia Tech., Atlanta, Georgia, January 1977.
- [4] Dixon, W. J. ed., BMDP - Biomedical Computer Programs, University of California Press, Berkeley, California, 880 pp., 1977.
- [5] Edgerton, A. T., A. Stogryn and G. Poe, "Microwave Radiometric Investigations of Snowpacks," Final Report No. 1285 R-4 for U. S. G. S. Contract No. 14-08-001-11828, Aerojet - General Corporation, Microwave Division, El Monte, California, July 1971.
- [6] Evans, S., "Dielectric Properties of Ice and Snow: A Review," Journal of Glaciology, v. 5, pp. 773, 1965.
- [7] Gough, S. R., "Comment on the Microwave 'Dielectric Constant' of Ice," J. Appl. Phys., 43(10):4251, October 1972.
- [8] Hallikainen, M., "Dielectric Properties of Sea Ice at Microwave Frequencies," Helsinki University of Technology Radio Laboratory Report S, 107, 1977.
- [9] Hofer, R. and C. Matzler, "Investigations on Snow Parameters by Radiometry in the 3- to 60-mm Wavelength Region," Journal of Geophysical Research, v. 85, n. C1, pp. 453-460, January 1980.
- [10] Lamb, J. and A. Turney, "The Dielectric Properties of Ice at 1.25 cm Wavelength," Proc. Phys. Soc., B 62, pp. 272, London, England, 1949.
- [11] Linlor, W. I., "Permittivity and Attenuation of Wet Snow between 4 and 12 GHz," Journal of Applied Physics, May 1980.

- [12] Perry, J. W. and A. W. Straiton, "Dielectric Constant of Ice at 35.3 and 94.5 GHz," Journal of Applied Physics, 43(2), February 1972.
- [13] Poe, G., "Remote Sensing of the Near-Surface Moisture Profile of Specular Soils with Multifrequency Microwave Radiometry," in Remote Sensing of Earth Resources and the Environment, ed. by Y. H. Katz, Proc. of the Society of Photo-optical Instrumentation Engineers, Palo Alto, California, November 1971.
- [14] Royer, G. M., "The Dielectric Properties of Ice, Snow, and Water at Microwave Frequencies and the Measurement of the Thickness of Ice and Snow Layers with Radar," Communications Research Centre. Technical Report No. 1242, Ottawa, Canada, 1973.
- [15] Stiles, W. H., and F. T. Ulaby, "Microwave Remote Sensing of Snowpacks," NASA Contractor Report 3263 Contract NAS5-23777, June 1980.
- [16] Sweeney, B. D. and S. C. Colbeck, "Measurements of the Dielectric Properties of Wet Snow Using a Microwave Technique," Research Report 325, U. S. Army Cold Regions Research and Engineering Lab., Hanover, New Hampshire, October 1974.
- [17] Tinga, W. R., W. A. Voss and D. F. Blossey, "Generalized Approach to Multiphase Dielectric Mixture Theory," Journal of Applied Physics, v. 44, n. 9, pp. 3897-3902, September 1973.
- [18] Tiuri, M. and H. Schultz, "Theoretical and Experimental Studies of Microwave Radiation," Proc. of the Workshop on the Microwave Remote Sensing of Snowpack Properties, Fort Collins, May 1980.